

The Nuclear Overhauser Effect from a Quantitative Perspective

Habilitation Thesis

Author(s):

Vögeli, Beat

Publication date:

2013

Permanent link:

<https://doi.org/10.3929/ethz-a-010061835>

Rights / license:

[In Copyright - Non-Commercial Use Permitted](#)

The Nuclear Overhauser Effect from a Quantitative Perspective

HABILITATIONSSCHRIFT

Submitted to

Department of Chemistry and Applied Biosciences

ETH Zürich (Swiss Federal Institute of Technology)

Beat Vögeli, PhD
Laboratory of Physical Chemistry
ETH-Hönggerberg
8093 Zürich
Switzerland

Zürich, February 2013

Abstract

The nuclear Overhauser enhancement or effect (NOE) is the most important measure in liquid-state NMR. Thus, the NOE is the subject of numerous reviews and books. Here, the NOE is revisited in light of our recently introduced measurements of exact nuclear Overhauser enhancements (eNOEs), which enabled the determination of multiple-state 3D protein structures. This review encompasses all relevant facets from the theoretical considerations to the use of eNOEs in multiple-state structure calculation. Important aspects include a detailed presentation of the relaxation theory relevant for the nuclear Overhauser effect, the estimation of the correction for spin diffusion, the experimental determination of the eNOEs, the conversion of eNOE rates into distances and validation of their quality, the distance-restraint classification and the protocols for calculation of structures and ensembles.

Acknowledgement

I would like to express my gratitude to Prof. Roland Riek, who gave me the opportunity, support and freedom to follow my research interests which ultimately lead up to this work. I also thank the researchers who participated in the exact NOE projects, namely Dr. Dominik Leitz, Dr. Takuya Segawa, Dr. Alexander Sobol, Michael Friedmann, Dr. Julien Orts, Prof. Peter Güntert, Sina Kazemi, Philipp Pauli, Jethro Hemmann and Dean Strotz. I would like to give further thanks to Prof. Matthias Ernst for fruitful discussions and Misti Vögeli for careful reading of the manuscript.

I would like to dedicate this work to my sons, Tyler and Bailey, who were born during these projects, and my wife, Misti.

"... es ist ein gross Ergetzen,
Sich in den Geist der Zeiten zu versetzen;
Zu schauen, wie vor uns ein weiser Mann gedacht,
Und wie wir's dann zuletzt so herrlich weit gebracht."

Wagner in *Faust. Eine Tragödie*, Johann Wolfgang von Goethe

Contents

1. Introduction.....	8
1.1. The NOE.....	8
1.2. Back to the future: The eNOE.....	9
2. Theoretical background.....	11
2.1. The Master equation.....	11
2.2. The relaxation matrix for NOESY analysis.....	15
2.2.1. Non-degenerate transitions.....	15
2.2.2. Like spins.....	20
2.2.3. Near-degenerate transitions.....	22
2.3. The Solomon equations.....	26
2.4. Conformational/chemical exchange.....	27
2.5. The spectral density function.....	29
2.5.1. Simplifications.....	32
2.5.2. Simplifications for methyl groups.....	34
2.6. Lipari-Szabo approximations.....	36
2.7. Experimental order parameters.....	38
2.8. Practical expressions.....	40
2.8.1. NOEs and distances between single spins.....	40
2.8.2. NOEs and distances between groups of equivalent spins.....	43
2.8.3. Autorelaxation rate constants.....	47
2.8.4. Continuous distance distribution.....	48
2.8.5. Expressions for molecular dynamics simulations.....	50

3. Extraction of exact NOE rates	52
3.1. Spin diffusion.....	52
3.2. Full relaxation-matrix approach.....	56
3.2.1. Iterative hybrid relaxation matrix approach with MD/DG.....	58
3.2.2. Direct iterative hybrid relaxation-matrix approach.....	59
3.2.3. Other programs.....	59
3.2.4. Inclusion of intermolecular exchange.....	60
3.3. Structure refinement against NOESY intensities.....	61
3.4. Non-linear ISPA with correction for spin diffusion.....	63
3.4.1. Correction for spin diffusion.....	67
3.4.2. Transfer function in the presence of conformational exchange.....	74
3.4.3. Validation and selection of experimental buildups.....	76
3.4.4. Practical aspects, NMR spectroscopy.....	78
3.4.5. Impact of motion.....	87
3.4.6. Validation of experimental distances.....	92
3.4.7. Temperature dependence of amide proton-amide proton eNOEs.....	99
4. Structure calculation.....	102
4.1. Structure calculation using the full matrix approach.....	102
4.1.1. Nucleic acids.....	103
4.1.2. From peptides to proteins.....	105
4.2. Ensemble calculation using conventional NOE-distance restraints.....	108
4.2.1. Restrained molecular dynamics (rMD) simulation.....	108
4.2.2. Direct structural ensemble calculation.....	109
4.2.3. Continuous distance distribution.....	116

4.3. Multiple-state structural ensemble calculation using eNOEs.....	116
4.3.1. Conventional structure calculation.....	117
4.3.2. Multiple-state structure calculation protocol.....	118
4.3.3. Cross-validation of the ensemble.....	122
5. Outlook.....	125
5.1. Future challenges: 14 questions.....	125
5.1.1. Experimental.....	125
5.1.2. Ensemble calculation.....	130
6. Appendix.....	134
7. References.....	156
8. Curriculum vitae.....	169

1. Introduction

1.1. *The NOE*

The dipolar interaction between two spins, named for its discoverer, the nuclear Overhauser enhancement or effect (NOE) [1], has arguably become the most important phenomenon in nuclear magnetic resonance (NMR) spectroscopy. Two of the most popular and important books in the field stand for two important development stages of the NOE and NMR as a whole. The monolog by Noggle and Schirmer summarizes the state of the 1970s [2] when NMR was recorded in one dimension and the NOE was used to characterize small molecules. The second one by Wüthrich represents the leap in the 1980s when two-dimensional spectroscopy allowed protein and nucleic acid structure calculation from NOEs [3].

Since these groundbreaking discoveries, the application of the NOEs branched into many dedicated fields. This may be mirrored by a list of reviews in the *Progress of Nuclear Magnetic Resonance Spectroscopy* in which the NOE is the main subject from 1990 onward (making no claim to be complete): Reference [4,1990] covers the full relaxation matrix approach for structural studies; reference [5,1994] reviews NOE and rotating-frame Overhauser enhancement (ROE) theory and models for the description of motions; references [6,1994] and [7,1997] review the intermolecular interactions observed by NOEs; reference [8,1998] presents the theory of dipolar interaction in liquid- and solid-state NMR; reference [9,1998] reviews the use of ambiguous NOE restraints in structure calculation, and finally references [10,2005] and [11,2006] review again the intermolecular interactions observed by NOEs.

The NOE was first described in 1953 when it was observed that saturation of the electron spin resonance causes a polarization of nuclear spins to an extent given by the ratio of the

gyromagnetic ratios of the two spins [1,12,13]. Although later extended, the simple theoretical description known as the Solomon equations formulated two years later remains the most practical formulation of the NOE [14]. It took another ten years until the dependence of the NOE on the distance between the two nuclear spins was used for conformational studies of small molecules in solution [15]. In 1972, it was observed that the NOE also transfers magnetization between molecules [16] and thus may serve as a tool to study bound ligand conformations [17].

The subject of this review is mostly the transient nuclear Overhauser effect as observed in two proton dimensions [3,18-22] or more. A quantitative analysis of the NOE is also key in techniques such as the saturated NOE (usually one-dimensional experiments with selective irradiation) [23,24] or the transferred NOE (trNOE) [6,25,26] but these topics are beyond the scope of the present work. As this review addresses the extraction of very accurate distances [27,28] and motional effects [29], strong focus is laid on the impact of dynamics on the spectral density function and exact understanding of the approximations that are employed.

1.2. Back to the future: the eNOE

What started out as "a new method for polarizing nuclei, applicable only to metals" 60 years ago [1] lead to the recent characterization of structural ensembles indicating the presence of correlated motion in a protein by the collection of many exact NOEs (eNOE) [30-32].

Standard structure determination by NMR spectroscopy makes use of a large number of experimentally accessible NOE rates – typically up to 20 per residue in small proteins [3]. Since the NOE rate is inversely proportional to the sixth power of the distance between the two dipolar interacting spins, the strength of the NOE lies in the supply of a large number of through-space

distance restraints. Usually, these restraints are employed in a semi-quantitative manner at most because the measurement of NOEs is flawed by mobility, spin diffusion, low signal-to-noise ratio and technical limitations.

In spite of all the progress in the NOE methodology, it seems that the tools employed today to measure and interpret NOEs are barely more sophisticated than those established in the 1980s. However, modern spectrometers and computer hardware and software open up new possibilities. We have recently demonstrated that it is possible to obtain exact amide proton/amide proton NOEs (eNOEs) both in deuterated [33] and protonated protein samples [34]. To this purpose, we measured NOE buildups as a function of the NOESY mixing time and converted the NOEs into precise distances. For example, distances up to 5 Å obtained from a perdeuterated ubiquitin sample have an experimental random error of only ≈ 0.07 Å. Since the eNOE is a time- and ensemble-averaged observable, it contains both structural and dynamical information. The collection of potentially thousands of eNOEs throughout a biomacromolecule may serve as an excellent probe towards a more complete representation of both its structure and dynamics. Assignments can be performed with the same well-established methods as for conventional NOEs. In addition, the NOE is among the few observables that are measurable even for high molecular weight systems such as large proteins, protein complexes, or membrane proteins substituted in membrane-mimicking environments.

We also established a new CYANA protocol which calculates multiple-state ensembles of structures in which the conformational restraints are required to be fulfilled on average over all members of the ensemble rather than for each individual conformer.

2. Theoretical background

Most text books introduce the nuclear Overhauser effect and the differential equations describing the NOESY process (the Solomon equations) classically [35]. It is recommended to study this approach to obtain initial insight. Here the derivation is based on the quantum-chemical approach in combination with a classical treatment of the lattice. Only this approach provides the more subtle mechanisms that are also active. A detailed understanding of these effects and the conditions for their neglect is important in the view of exact quantitative evaluation of NOEs.

2.1. The Master equation

The time evolution of a spin system is described by the Liouville-von Neumann equation [36,37].

$$\frac{d}{dt}\rho(t) = -i[H_0 + H_1(t), \rho(t)] \quad (1)$$

$\rho(t)$ is the density operator, H_0 is the stationary Hamiltonian and $H_1(t)$ is the stochastic Hamiltonian which couples the spins to the lattice. The equation may be expressed in the interaction frame by transformation of any operator K :

$$K^{\text{int}}(t) = e^{iH_0 t} K e^{-iH_0 t} \quad (2)$$

Quantum mechanical and classical treatments of the nuclear spin system and the lattice, respectively, have proven most practical for NMR descriptions [38]. A quantum description of

the lattice has been presented by Goldman [39]. The semi-classical Master equation in the interaction frame is a solution to the Liouville-von Neumann equation:

$$\frac{d}{dt} \langle \rho^{\text{int}}(t) - \rho_0 \rangle = - \int_0^{t_{\text{mix}}} \left\langle \left[H_1^{\text{int}}(t), \left[H_1^{\text{int}}(t-\tau), \rho^{\text{int}}(t) - \rho_0 \right] \right] \right\rangle d\tau \quad (3)$$

As NMR experiments deal with a large number of molecules, ensemble averaging over all stochastic Hamiltonians is used. The equilibrium density operator ρ_0 is introduced *ad hoc* since in the semi-classical approach the Boltzmann equilibrium is not re-established. Additional assumptions used to obtain equation 3 may be looked up in the literature [36,37,39-41]. One common assumption, however, is not made here. The upper limit of the integral is usually replaced by infinity. In experiment, however, it is only carried out for the length of the mixing time t_{mix} (typically 100 ms in a NOESY).

The stochastic Hamiltonian can be decomposed into products of spin operators given by irreducible tensor operators of rank 2, T_m , and stationary random functions given by second order spherical harmonics, F_m , where m are coherence levels:

$$H_1(t) = \sum_{m=-2}^2 T_m F_m(t) \quad (4.1)$$

The conventions of reference [41] are used. Transformation of $H_1(t)$ into the interaction frame gives:

$$H_1^{\text{int}}(t) = \sum_{m,n} T_m^n F_m(t) e^{i\omega_m^n t} \quad (4.2)$$

The T_m operators are split into contributions corresponding to the differences between the eigenfrequencies of H_0 . More details are shown in equations A1-A18 in the Appendix. When

$H_1^{\text{int}}(t)$ for all interactions a are inserted into equation 3, it takes the form:

$$\frac{d}{dt} \langle \rho^{\text{int}}(t) - \rho_0 \rangle = - \sum_{m,m',n,n',a,a'} (-1)^{m'} e^{i(\omega_m^{n,a} + \omega_{m'}^{n',a})t} \left[T_m^{n',a'}, \left[T_m^{n,a}, \langle \rho^{\text{int}}(t) - \rho_0 \rangle \right] \right] \int_0^{t_{\text{mix}}} \langle F_{-m}^{a'*}(t+\tau) F_m^a(t) \rangle e^{-i\omega_m^{n,a}\tau} d\tau \quad (5)$$

In the secular approximation only terms with $\omega_m^{n,a} \approx -\omega_{m'}^{n',a'}$ are retained. All other terms contain a rapidly oscillating component that averages them to zero. It is shown in the Appendix that m' can be replaced by $-m$ (see equation A13). Back-transformation into the laboratory frame leads to the semi-classical Master equation for the expectation value of the operator B , $\langle B \rangle = \text{Trace}(B \langle \rho \rangle)$:

$$\frac{d}{dt} \langle B \rangle(t) = \langle -i[B, H_0] \rangle(t) - \langle \hat{\Gamma}(B) \rangle(t) - \langle \hat{\Gamma}(B) \rangle_0 \quad (6)$$

with the relaxation superoperator for non-degenerate transitions [37]

$$\hat{\Gamma}(B) = \sum_{m,n,n^{nd},a,a'} (-1)^m J_m^{aa'}(\omega_m^{n,a}) \left[T_m^{n,a}, \left[T_{-m}^{n^{nd},a'}, B \right] \right] \quad (7.1)$$

n^{nd} are those n' that fulfill $\omega_m^{n,a} \approx -\omega_{-m}^{n',a'}$ ¹. The relaxation superoperator for degenerate transitions

is

$$\hat{\Gamma}(B) = \sum_{m,n,n^d,a,a'} (-1)^m J_m^{aa'}(\omega_m^{n,a}) \left[T_m^{n,a}, \left[T_{-m}^{n^d,a'}, B \right] \right] \quad (7.2)$$

¹ Note that in reference [41] this condition is expressed with $n = n'$. This is not true, as $\omega_0^{2,D} \approx -\omega_0^{3,D'}$ obviously also fulfills the condition (see equations A14 in the Appendix).

n^d are those n' that fulfill $\omega_m^{n,a} \approx -\omega_{-m}^{n',a'}$ with additional pathways from the fact that $\omega_i - \omega_j = 0$.

$J_m^{aa'}(\omega)$ is the spectral density function which carries the information on the fluctuating angular orientations and distances of the interaction vectors (*vide infra*).

$$J_m^{aa'}(\omega) = \int_0^{t_{\text{mix}}} \langle F_m^{a'*}(t+\tau) F_m^a(t) \rangle \cos(\omega\tau) d\tau \quad (8)$$

In a strict sense, $\cos(\omega\tau)$ must be replaced by $e^{-i\omega\tau} = \cos(\omega\tau) - i\sin(\omega\tau)$. However, the second term causes a small frequency shift and does not affect the relaxation behavior. As this effect is not relevant for the current work, the simplification is justified.

A convenient way to use the Master equation is to choose an (orthogonal) operator basis spanning the complete relevant Liouville subspace. The expectation values of these operators can be arranged in vector form $\langle \vec{b} \rangle$, such that the Master equation is written in matrix form:

$$\frac{d}{dt} \langle \vec{b} \rangle(t) = A \langle \vec{b} \rangle(t) - R \left(\langle \vec{b} \rangle(t) - \langle \vec{b} \rangle_0 \right) \quad (9)$$

R is the relaxation matrix, and A is the matrix describing the unperturbed motion of the spin system.

The complete relevant stationary and stochastic Hamiltonians for a N -proton system are:

$$H_0^N = -\gamma \vec{B}_0 \sum_{i=1}^N (1 - \Omega_i^{\text{CSI}}) \vec{I}_i + 2\pi \sum_{i<j}^N J_{ij} (\vec{I}_i \vec{I}_j) \quad (10.1)$$

$$H_1^N(t) = \gamma \vec{B}_0 \sum_{i=1}^N \Omega_i^{\text{CSA}}(t) \vec{I}_i + \frac{\mu_0}{4\pi} \sum_{i<j}^N \frac{\gamma^2 \hbar}{r_{ij}^3(t)} \left(\vec{I}_i \vec{I}_j - \frac{3}{r_{ij}^3(t)} (\vec{I}_i \vec{r}_{ij}(t)) (\vec{I}_j \vec{r}_{ij}(t)) \right) \quad (10.2)$$

γ is the gyromagnetic ratio of the proton, \vec{B}_0 the polarizing field vector, Ω_i^{CSI} and $\Omega_i^{\text{CSA}}(t)$ are the isotropic and anisotropic parts of the chemical shielding tensor of nucleus i (referred to as CSI and CSA tensors) in the laboratory frame, J_{ij} the scalar coupling constant between spins i and j , μ_0 is the permeability in vacuum, \hbar denotes Planck's constant divided by 2π , and $\vec{r}_{ij}(t)$ is the vector connecting nuclei i and j . The first term on the right-hand side of equation 10.1 integrates the isotropic chemical shielding tensor into the Zeeman Hamiltonian yielding the Larmor frequency $\omega_i = -\gamma B_0(1 - \Omega_i^{\text{CSI}})$. The second term is the electron-mediated scalar coupling Hamiltonian. The first term on the right-hand side of equation 10.2 describes the chemical shielding anisotropy Hamiltonian and the second term is the dipolar Hamiltonian which is ultimately responsible for NOEs. The stochastic Hamiltonians formulated in the form of equations 4.1 and 4.2 can be looked up in the Appendix.

2.2. The relaxation matrix for NOESY analysis

2.2.1. Non-degenerate transitions

Inspection of the Redfield Kite of the relaxation matrix R shows that in the presence of degenerate transitions cross-relaxation pathways are active within and between the longitudinal operators and zero-quantum coherences and never couple between different coherence orders [37]. In the absence of degenerate transitions (that is separated by at least the linewidth [40]), cross-relaxation is also forbidden between longitudinal and zero-quantum operators. In the ideal case, the pulse sequence prior to the NOESY mixing period creates only longitudinal magnetization away from the (macroscopic) Boltzmann equilibrium magnetization. Any residual

transverse magnetization is assumed to be dephased by a gradient and not considered further. The initial magnetization vector $\langle \vec{b}_0 \rangle$ contains only nonzero elements for the polarization operators (longitudinal single-spin order) $I_{i,z}$. For non-near-degenerate transitions, the scalar coupling is usually weak (that is $2\pi J_{ij} \ll |\omega_i - \omega_j|$). The terms proportional to $I_{i,x}I_{j,x}$ and $I_{i,y}I_{j,y}$ in H_0 can be neglected and H_0 commutes with $I_{i,z}$ and the A -driven term in equation 6 vanishes. As a consequence, zero-, single- and higher-quantum coherences are never populated in the course of the mixing time in a NOESY experiment. The two conditions (non-degenerate transition and weak scalar coupling) are usually well fulfilled for resolved NOESY cross peaks, since the strongest scalar couplings between protons are ≈ 15 Hz which does not exceed a typical linewidth. In particular, those cross peaks for which it is not valid are very close to the diagonal peaks and are usually very difficult to evaluate quantitatively. The complete Master equation for a N spin-1/2 system can now be formulated in the subspace spanned by the population operators. $\langle \vec{b} \rangle$ is then built by (Ernst notation):

$$b_{\vec{\alpha}} = \frac{1}{2} \prod_{i=1}^N (2I_{i,z})^{\alpha_i} \quad (11)$$

$\vec{\alpha}$ is a vector containing N elements α_i which are either 0 or 1 ($1 \leq i \leq N$). In total, $2^N - 1$ operators can be generated (the null vector which generates the identity operator is not included). Longitudinal multi-spin order terms are 0 at the outset of the mixing time and are subsequently created with decreasing efficiency as the order increases. For example, direct transfer from single-spin order can only occur to two- and three-spin order populations. In the following, the explicit solution of the relaxation matrix is shown if only longitudinal single-, two- and three-spin orders are considered. This subspace is sufficient to demonstrate all types of relaxation-matrix

elements. Extension to higher spin orders is straight-forward. The calculation of the matrix elements is presented in detail in the Appendix.

$$\frac{d}{dt} \begin{pmatrix} \langle I_{1,z} \rangle - I_{1,0} \\ \langle I_{2,z} \rangle - I_{2,0} \\ \langle I_{3,z} \rangle - I_{3,0} \\ \dots \\ \langle I_{N,z} \rangle - I_{N,0} \\ \langle 2I_{1,z}I_{2,z} \rangle \\ \langle 2I_{1,z}I_{3,z} \rangle \\ \dots \\ \langle 2I_{1,z}I_{N,z} \rangle \\ \langle 2I_{2,z}I_{3,z} \rangle \\ \dots \\ \langle 2I_{N-1,z}I_{N,z} \rangle \\ \langle 4I_{1,z}I_{2,z}I_{3,z} \rangle \\ \langle 4I_{1,z}I_{2,z}I_{4,z} \rangle \\ \dots \\ \langle 4I_{N-2,z}I_{N-1,z}I_{N,z} \rangle \end{pmatrix} = - \begin{pmatrix} R(A) & R(B) \\ R(C) & R(D) \end{pmatrix} \begin{pmatrix} \langle I_{1,z} \rangle - I_{1,0} \\ \langle I_{2,z} \rangle - I_{2,0} \\ \langle I_{3,z} \rangle - I_{3,0} \\ \dots \\ \langle I_{N,z} \rangle - I_{N,0} \\ \langle 2I_{1,z}I_{2,z} \rangle \\ \langle 2I_{1,z}I_{3,z} \rangle \\ \dots \\ \langle 2I_{1,z}I_{N,z} \rangle \\ \langle 2I_{2,z}I_{3,z} \rangle \\ \dots \\ \langle 2I_{N-1,z}I_{N,z} \rangle \\ \langle 4I_{1,z}I_{2,z}I_{3,z} \rangle \\ \langle 4I_{1,z}I_{2,z}I_{4,z} \rangle \\ \dots \\ \langle 4I_{N-2,z}I_{N-1,z}I_{N,z} \rangle \end{pmatrix}$$

$$R(A) = \begin{pmatrix} \rho_1 & \sigma_{12} & \sigma_{13} & \dots & \sigma_{1N} & \eta_{12}^{\text{D/CSA}} & \eta_{13}^{\text{D/CSA}} & \dots \\ \sigma_{12} & \rho_2 & \sigma_{23} & \dots & \sigma_{2N} & \eta_{21}^{\text{D/CSA}} & 0 & \dots \\ \sigma_{13} & \sigma_{23} & \rho_3 & \dots & \sigma_{3N} & 0 & \eta_{31}^{\text{D/CSA}} & \dots \\ \dots & \dots & \dots & \dots & \dots & \dots & \dots & \dots \\ \sigma_{1N} & \sigma_{2N} & \sigma_{3N} & \dots & \rho_N & 0 & 0 & \dots \\ \eta_{12}^{\text{D/CSA}} & \eta_{21}^{\text{D/CSA}} & 0 & \dots & 0 & \rho_{12} & \sigma_{23} + \eta_{1213}^{\text{D/D}} & \dots \\ \eta_{13}^{\text{D/CSA}} & 0 & \eta_{31}^{\text{D/CSA}} & \dots & 0 & \sigma_{23} + \eta_{1213}^{\text{D/D}} & \rho_{13} & \dots \\ \dots & \dots & \dots & \dots & \dots & \dots & \dots & \dots \end{pmatrix}$$

$$R(B) = \begin{pmatrix} \eta_{1N}^{\text{D/CSA}} & 0 & \dots & 0 & \eta_{1213}^{\text{D/D}} & \eta_{1214}^{\text{D/D}} & \dots & 0 \\ 0 & \eta_{23}^{\text{D/CSA}} & \dots & 0 & \eta_{2131}^{\text{D/D}} & \eta_{2124}^{\text{D/D}} & \dots & 0 \\ 0 & \eta_{32}^{\text{D/CSA}} & \dots & 0 & \eta_{3132}^{\text{D/D}} & 0 & \dots & 0 \\ \dots & \dots & \dots & \dots & \dots & \dots & \dots & \dots \\ \eta_{N1}^{\text{D/CSA}} & 0 & \dots & \eta_{NN-1}^{\text{D/CSA}} & 0 & \dots & \dots & \eta_{NN-2NN-1}^{\text{D/D}} \\ \sigma_{2N} + \eta_{121N}^{\text{D/D}} & \sigma_{13} + \eta_{2123}^{\text{D/D}} & \dots & 0 & \eta_{13}^{\text{D/CSA}} + \eta_{23}^{\text{D/CSA}} & \eta_{14}^{\text{D/CSA}} + \eta_{24}^{\text{D/CSA}} & \dots & 0 \\ \sigma_{3N} + \eta_{131N-1}^{\text{D/D}} & \sigma_{12} + \eta_{3132}^{\text{D/D}} & \dots & 0 & \eta_{12}^{\text{D/CSA}} + \eta_{32}^{\text{D/CSA}} & 0 & \dots & 0 \\ \dots & \dots & \dots & \dots & \dots & \dots & \dots & \dots \end{pmatrix}$$

$$\begin{aligned}
R(C) &= \begin{pmatrix} \eta_{1N}^{D/CSA} & 0 & 0 & \dots & \eta_{N1}^{D/CSA} & \sigma_{2N} + \eta_{121N}^{D/D} & \sigma_{3N} + \eta_{131N-1}^{D/D} & \dots \\ 0 & \eta_{23}^{D/CSA} & \eta_{32}^{D/CSA} & & 0 & \sigma_{13} + \eta_{2123}^{D/D} & \sigma_{12} + \eta_{3132}^{D/D} & \\ \dots & & & & & & & \dots \\ 0 & 0 & 0 & & \eta_{NN-1}^{D/CSA} & 0 & 0 & \\ \eta_{1213}^{D/D} & \eta_{1213}^{D/D} & \eta_{3132}^{D/D} & & 0 & \eta_{13}^{D/CSA} + \eta_{23}^{D/CSA} & \eta_{12}^{D/CSA} + \eta_{32}^{D/CSA} & \\ \eta_{1214}^{D/D} & \eta_{2124}^{D/D} & 0 & & 0 & \eta_{14}^{D/CSA} + \eta_{24}^{D/CSA} & 0 & \\ \dots & & & & & & & \dots \\ 0 & 0 & 0 & \dots & \eta_{NN-2NN-1}^{D/D} & 0 & 0 & \dots \end{pmatrix} \\
R(D) &= \begin{pmatrix} \rho_{1N} & 0 & \dots & \sigma_{1N-1} + \eta_{N1NN-1}^{D/D} & 0 & 0 & \dots & 0 \\ 0 & \rho_{23} & & 0 & \eta_{21}^{D/CSA} + \eta_{31}^{D/CSA} & & & 0 \\ \dots & & \dots & & & & & \dots \\ \sigma_{1N-1} + \eta_{N1NN-1}^{D/D} & 0 & & \rho_{N-1N} & 0 & 0 & \eta_{N-1N-2}^{D/CSA} + \eta_{NN-2}^{D/CSA} & \\ 0 & \eta_{21}^{D/CSA} + \eta_{31}^{D/CSA} & & 0 & \rho_{123} & \sigma_{24} & 0 & \\ 0 & 0 & & 0 & \sigma_{24} & \rho_{124} & 0 & \\ \dots & & & & & & & \dots \\ 0 & 0 & \dots & \eta_{N-1N-2}^{D/CSA} + \eta_{NN-2}^{D/CSA} & 0 & 0 & \dots & \rho_{N-2N-1N} \end{pmatrix}
\end{aligned} \tag{12}$$

ρ_i , ρ_{ij} and ρ_{ijk} are the autorelaxation rate constants of I_i , $2I_{i,z}I_{j,z}$ and $4I_{i,z}I_{j,z}I_{k,z}$, respectively. σ_{ij} is the cross-relaxation rate constant between spins I_i and I_j (sometimes referred to as the 'NOE rate'). $\eta_{ij}^{D/CSA}$ ($\eta_{ijk}^{D/D}$) is the longitudinal cross-correlated relaxation rate constant between chemical shift anisotropy (CSA) and dipolar interactions (two dipolar interactions) [42]. The rate constants contain the following contributions [43]:

$$\rho_i = \left(\sum_{j=1, j \neq i}^N R_{ij}^D \right) + R_i^{CSA} + (R_i^{\text{leak}}) \tag{13.1}$$

$$\rho_{ij} = \left(\sum_{k=1, k \neq i, j}^N R_{ik}^D \right) + \left(\sum_{k=1, k \neq i, j}^N R_{jk}^D \right) + \lambda_{ij}^D + R_i^{CSA} + R_j^{CSA} \tag{13.2}$$

$$\rho_{ijk} = \left(\sum_{l=1, l \neq i, j, k}^N R_{il}^D \right) + \left(\sum_{l=1, l \neq i, j, k}^N R_{jl}^D \right) + \left(\sum_{l=1, l \neq i, j, k}^N R_{kl}^D \right) + \lambda_{ij}^D + \lambda_{ik}^D + \lambda_{jk}^D + R_i^{CSA} + R_j^{CSA} + R_k^{CSA} \tag{13.3}$$

$$\sigma_{ij} = \left(\frac{\mu_0}{4\pi} \right)^2 \frac{\gamma^4 \hbar^2}{10} \frac{1}{(r_{ij}^{\text{rigid}})^6} \left[-J_{ij}^D(\omega_i - \omega_j) + 6J_{ij}^D(\omega_i + \omega_j) \right] \tag{13.4}$$

$$\eta_{ij}^{\text{D/CSA}} = -\left(\frac{\mu_0}{4\pi}\right) \frac{2\gamma^3 \hbar \mathbf{B}_0}{5} \frac{1}{(r_{ij}^{\text{rigid}})^3} \Delta\sigma_i J_{ij}^{\text{D/CSA}}(\omega_i) \quad (13.5)$$

$$\eta_{ijk}^{\text{D/D}} = \frac{3}{5} \left(\frac{\mu_0}{4\pi}\right)^2 \frac{\gamma^4 \hbar^2}{(r_{ij}^{\text{rigid}})^3 (r_{ik}^{\text{rigid}})^3} J_{ijk}^{\text{D/D}}(\omega_i) \quad (13.6)$$

with

$$R_{ij}^{\text{D}} = \left(\frac{\mu_0}{4\pi}\right)^2 \frac{\gamma^4 \hbar^2}{10} \frac{1}{(r_{ij}^{\text{rigid}})^6} \left[J_{ij}^{\text{D}}(\omega_i - \omega_j) + 3J_{ij}^{\text{D}}(\omega_i) + 6J_{ij}^{\text{D}}(\omega_i + \omega_j) \right] \quad (14.1)$$

$$R_i^{\text{CSA}} = \frac{2\gamma^2 \mathbf{B}_0^2}{15} (\Delta\sigma_i)^2 J_i^{\text{CSA}}(\omega_i) \quad (14.2)$$

$$\lambda_{ij}^{\text{D}} = \left(\frac{\mu_0}{4\pi}\right)^2 \frac{3\gamma^4 \hbar^2}{10} \frac{1}{(r_{ij}^{\text{rigid}})^6} \left[J_{ij}^{\text{D}}(\omega_i) + J_{ij}^{\text{D}}(\omega_j) \right] \quad (14.3)$$

R_i^{leak} is the leakage rate caused by additional relaxation processes such as interaction with the solvent, paramagnetic reagents, NMR-active heteronuclei, etc. r_{ij}^{rigid} is the internuclear i - j distance in a hypothetically rigid structure. $\Delta\sigma_i$ is the difference between the parallel and perpendicular main components of Ω_i^a of nucleus i . $J(\omega)$ is the spectral density function at spectral frequency ω as defined in equation 8. It depends on the exact nature of the vectors connecting spins I_i , I_j , and I_k (and CSA main axes), and is described below. It is noted that the cross-correlation terms usually contain an additional factor $P_2(\cos\theta)$ which describes the angle θ between the two interaction axes. Here this dependence is included in the spectral density function. In doing so, the assumption of isotropic molecular tumbling is released.

2.2.2. Like spins

If the transitions are degenerate, diagonal and cross peaks appear at identical frequencies and can obviously not be evaluated separately in a spectrum. They may still be used by interpreting the sum of the single peaks. The relaxation rate constants are now calculated from equation 7.2 rather than from 7.1. One way to treat them is to allocate an individual magnetization in $\langle \vec{b} \rangle$ to each proton and include the according relaxation rates for degenerate transitions [44,45]. In addition, exchange rates between the protons can also be included (*vide infra*).

However, the subspace chosen here is not sufficient to exactly express the relaxation of magnetically equivalent spins. It is convenient to formally treat a group of N spins like one spin with N -fold spectral intensity [46]. This approach is most prominently applied to methyl groups and aromatic protons. The magnetization is written as

$$I_{\vec{i},z} = \sum_{\kappa=1}^N I_{i_{\kappa},z} \quad (15)$$

\vec{i} is a pseudo proton number in vector form including the protons i_1 to i_N . A corresponding spectral peak is N times more intense than one expected from a single proton.

For a methyl group, the dipolar auto-relaxation rate is calculated by summation of the contributions listed in Tables A1 and A2 under consideration of both other protons resulting in a modified $R_{i_{\kappa}i_{\lambda}}^D$.

$$R_{\vec{i}}^{D,\text{methyl}} = \left(\frac{\mu_0}{4\pi} \right)^2 \frac{\gamma^4 \hbar^2}{10} \frac{1}{(r_{\text{methyl}})^6} \left[6J_{\vec{i}}^{D,\text{methyl}}(\omega_{\vec{i}}) + 24J_{\vec{i}}^{D,\text{methyl}}(2\omega_{\vec{i}}) \right] \quad (16)$$

This equation can also be understood from the fact that cross-relaxation between the methyl protons does not alter the overall methyl magnetization. Therefore, expression 16 is a sum of $R_{i_{\kappa}i_{\lambda}}^D$.

and $\sigma_{i_k i_h}$ (equations 13.4 and 14.1). The intramethyl distances $r_{i_k i_h} = r_{\text{methyl}}$ do not fluctuate and can be factored out of the spectral density function. The CSA-induced relaxation rate is

$$R_{\vec{i}}^{\text{CSA,methyl}} = \frac{2\gamma^2 B_0^2}{15} (\Delta\sigma_{\vec{i}}^{\text{methyl}})^2 J_{\vec{i}}^{\text{CSA,methyl}}(\omega_{\vec{i}}) \quad (17)$$

$\Delta\sigma_{\vec{i}}^{\text{methyl}}$ is an effective value whose directionality is parallel to the c3 symmetry axis due to fast methyl rotation as proposed in reference [47].

The cross relaxation rate constant between $N_{\vec{i}}$ and $N_{\vec{j}}$ magnetically equivalent spins is

$$\sigma_{\vec{i}\vec{j}} = \sum_{\kappa=1}^{N_i} \frac{1}{N_j} \sum_{\iota=1}^{N_j} \left(\frac{\mu_0}{4\pi} \right)^2 \frac{\gamma^4 \hbar^2}{10} \frac{1}{(r_{i_\kappa j_\iota}^{\text{rigid}})^6} \left[-J_{i_\kappa j_\iota}^{\text{D}}(\omega_{\vec{i}} - \omega_{\vec{j}}) + 6J_{i_\kappa j_\iota}^{\text{D}}(\omega_{\vec{i}} + \omega_{\vec{j}}) \right] \quad (18)$$

$\sigma_{\vec{i}\vec{j}}$ is $N_{\vec{i}}$ times larger than expected for a single transfer pathway $\sigma_{i_k i_h}$. The summation can be absorbed into the spectral density functions.

$$\sigma_{\vec{i}\vec{j}} = \left(\frac{\mu_0}{4\pi} \right)^2 \frac{\gamma^4 \hbar^2}{10} \frac{N_{\vec{i}}}{(r_{\vec{i}\vec{j}}^{\text{rigid}})^6} \left[-J_{\vec{i}\vec{j}}^{\text{D}}(\omega_{\vec{i}} - \omega_{\vec{j}}) + 6J_{\vec{i}\vec{j}}^{\text{D}}(\omega_{\vec{i}} + \omega_{\vec{j}}) \right] \quad (19)$$

The distance $r_{\vec{i}\vec{j}}^{\text{rigid}}$ is the distance between the pseudoatoms representing the groups \vec{i} and \vec{j} .

It is stressed again that there are also pathways due to cross-correlated relaxation that convert single into two- and three spin order terms and other non-observable irreducible modes within a methyl group [43,47,48]. These lead to non-exponential autorelaxation which cannot be accounted for in this simple model. An additional complication arises from the lost symmetry of the relaxation matrix R as $N_j \sigma_{\vec{i}\vec{j}} = N_i \sigma_{\vec{j}\vec{i}}$ and thus in general $\sigma_{\vec{i}\vec{j}} \neq \sigma_{\vec{j}\vec{i}}$. A solution has been proposed for symmetrization [49].

It is worthy to note that explicit consideration of each individual atom with equal peak intensity treats spin diffusion mediated by such a spin group more realistically than a pseudo atom. For example, only this approach reveals that protons separated by 8 Å may appear to be

separated by 4 - 5 Å if an aromatic ring is located between them [45]. A simplified approach can be used for fast multiple-site exchange where one magnetization intensity (the sum) is used and the relaxation rate is the population-weighted average of the individual relaxation matrices [50]. A more general solution has been presented by [51].

2.2.3. Near-degenerate transitions

The situation is different if the peaks are barely resolved. Then the transitions may be near-degenerate. Remarkably, auto-correlated contributions to R are identical for degenerate and non-degenerate transitions in the specific case of NOESY (see Appendix Table A2). There are, however, pathways to zero-quantum coherence between degenerate transitions mediated by cross-correlated relaxation (see Tables A5, A7 and A8). This implies that the formulae for non-degenerate transitions can be used if the cross-correlation relaxation is sufficiently small. As a rule-of-thumb, it has to be taken into account if $\omega_m^n + \omega_m^{n'} \approx \langle |H_1^{\text{int}}(t)| \rangle^2 \tau_c$ holds, where τ_c is the effective molecular tumbling time (*vide infra*) [41]. In practice, this is relevant for spectral frequencies separated by no more than 2 to 20 s⁻¹. This range is typically less than the line width for macromolecules.

An additional complication arises if the spins are strongly scalar coupled [52-55], which can occur for protons if they have non- or near-degenerate transitions (for example, methylene protons). Then the basis chosen in equation 11 is no longer appropriate. Instead, the eigenfunctions of H_0 are linear combinations of the wavefunctions of the strongly coupled spins and the eigenvalues also depend on the scalar coupling constant. If the multiplets due to scalar coupling between spins i and j are not resolved, but the peaks still are (in the weak coupling limit

positioned at the frequencies of spin i and j , and for strong coupling increasingly intermixed with the frequencies of the coupling partner), the spectra can be analyzed by using equation 12 with modified terms. A derivation is provided in the Appendix. If the relaxation rate constants are dominated by the contributions from the spectral density function sampled at $|\omega_i - \omega_j|$, the following modifications may be used:

$$R_{ij}^D \rightarrow R_{ij}^{D,J\text{strong}} \approx (1 - \sin^2(2\theta_{ij}^J)) R_{ij}^D \quad (20)$$

$$\sigma_{ij} \rightarrow \sigma_{ij}^{J\text{strong}} \approx (1 - \sin^2(2\theta_{ij}^J)) \sigma_{ij} \quad (21)$$

with

$$\tan(2\theta_{ij}^J) = \frac{2\pi J_{ij}}{\omega_i - \omega_j} \quad (22)$$

The scaling factor $(1 - \sin^2(2\theta_{ij}^J))$ is plotted versus $(\omega_i - \omega_j)/(2\pi J_{ij})$ in the top panel of Figure 1. As shown in the bottom panel, the apparent peak separation (assuming the J coupling is not resolved) is nearly identical to the chemical shift difference for resolved peaks. This difference may then be used to estimate the scaling factor plotted in red. In methylene groups, J_{ij} is typically -15 Hz, and the line widths in the study on GB3 presented in this review are typically 35 Hz and 55 Hz in the direct and indirect ^1H dimensions. An appreciable scaling can be active for resolved peaks. If they are separated by 35 Hz, the scaling factor is 0.85. If they are also resolved in the indirect dimension, the factor is still 0.9. A scaling by 99 % is obtained if the shift difference is ten times larger than the scalar coupling constant. In practice, however, the cross peaks appear larger than expected for weak coupling due to a second efficient mechanism of magnetization transfer depending purely on the strong scalar coupling. It arises from unequal conversion of transverse into longitudinal magnetization by the pulse sequence elements typically preceding the mixing period [55]. For example, it has been estimated that after a 3-second mixing period 70 %

of the intensities of the cross-peaks between the H(3) and H(4) protons in 2,6 dicarboxynaphthalene stems from this effect, where $(\omega_i - \omega_j)/(2\pi J_{ij}) \approx 2$ and the internuclear distance is 2.44 Å [52].

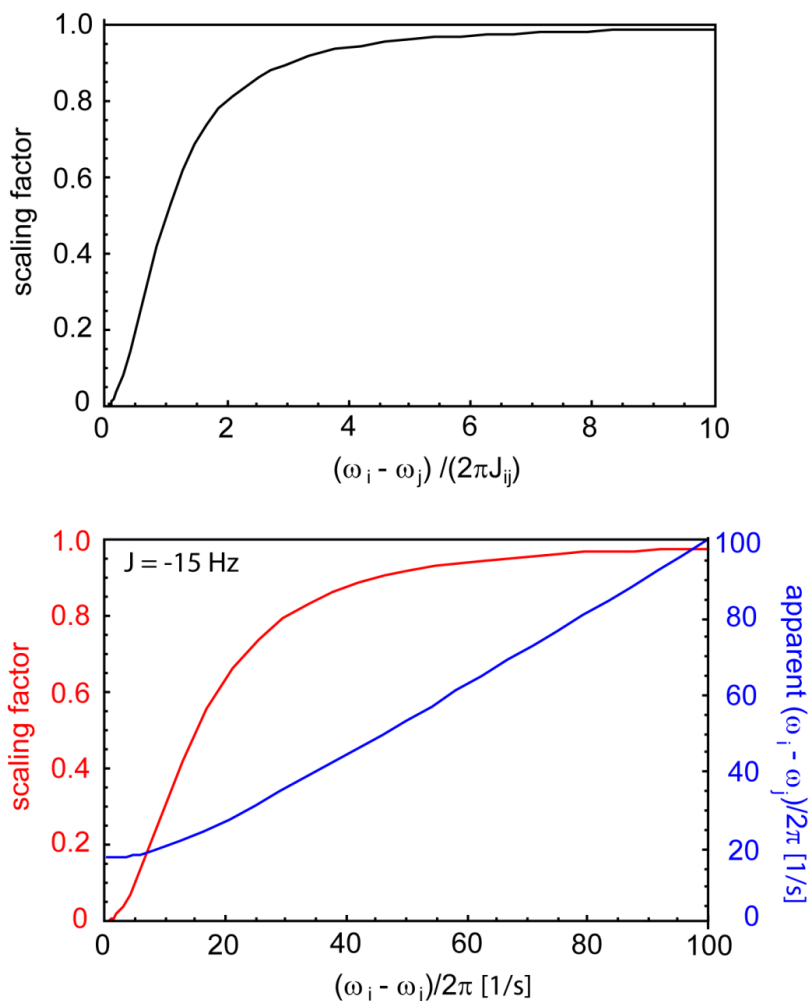


Figure 1. The effect of strong scalar coupling on the cross-relaxation rate. The scaling factor $(1 - \sin^2(2\theta_{ij}))$ is shown versus $(\omega_i - \omega_j)/(2\pi J_{ij})$ (top panel) and versus $(\omega_i - \omega_j)/2\pi$ for $J_{ij} = -15$ Hz (bottom panel, red curve). The apparent peak separation is calculated as the chemical shift difference between the centers of the doublets $\{\omega(12), \omega(34)\}$ and $\{\omega(13), \omega(24)\}$ as provided in equation A28 in the Appendix (bottom panel, blue curve). Note that the apparent peak separation actually becomes zero as the shifts become identical because the outer lines approach zero intensity.

For the current purpose the most relevant manifestation is the one observed in a ABX-type system $i-j-k$, where spins i and j are strongly coupled, and NOEs are determined for the spin pairs $i-k$ or $j-k$. In addition to the strong spin diffusion effect via j or i , respectively, both NOEs are altered by the partial mixing with the second strong coupling partner [50,53]. The cross-relaxation rate between k and the atom of the pair $i-j$ which is closer to k is reduced and the one further away is enhanced. For $|J_{ik} - J_{jk}| \ll |\omega_i - \omega_j|$ one obtains

$$\sigma_{ik} \rightarrow \sigma_{ik}^{\text{Jstrong}} = \cos^2(\theta_{ij}^J) \sigma_{ik} + \sin^2(\theta_{ij}^J) \sigma_{jk} \quad (23.1)$$

$$\sigma_{jk} \rightarrow \sigma_{jk}^{\text{Jstrong}} = \cos^2(\theta_{ij}^J) \sigma_{jk} + \sin^2(\theta_{ij}^J) \sigma_{ik} \quad (23.2)$$

The scaling factors are plotted versus $(\omega_i - \omega_j)/(2\pi J_{ij})$ in Figure 2. For a NOE between a spin i located in a methylene group $i-j$ ($J_{ij} = -15$ Hz) and an isolated spin k which is assumed to be infinitely distant from j , the scaling of the cross-relaxation rate constant is 0.96 and 0.98 if the methylene peaks are separated by 35 Hz and 55 Hz, respectively. On the other hand, the cross-relaxation rate constant between j and k is 0.04 and 0.02 times σ_{ik} instead of zero. The consequence for the practice is that spin diffusion dominates the strong coupling effect which is irrelevant for macromolecules.

In addition, during the pulse sequence elements preceding NOESY mixing antiphase terms are created that are partially converted into zero-quantum coherences by the 90° pulse which initiates the mixing process. These terms are notoriously difficult to suppress during mixing [57].

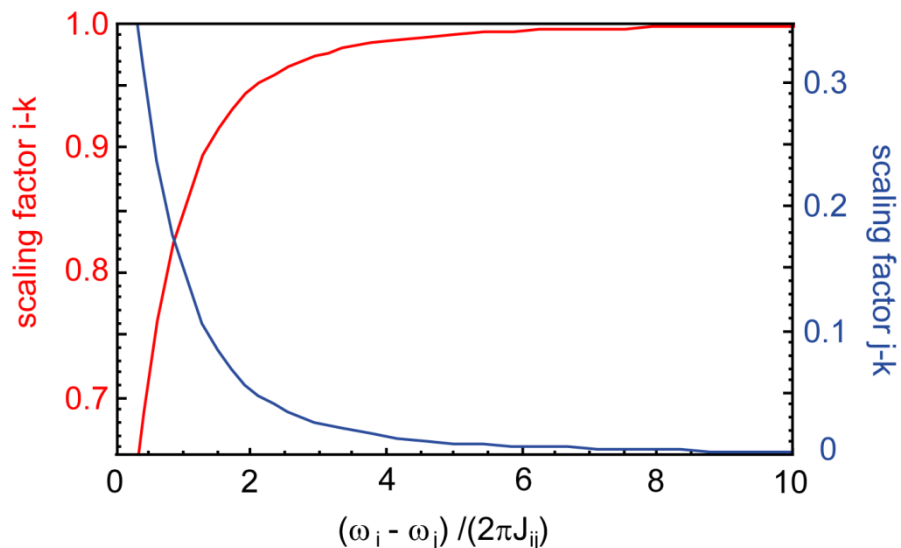


Figure 2. The effect of strong scalar coupling on the cross-relaxation rate between the weakly coupled spins $i-k$, where i is strongly coupled to a third spin j . The scaling factors $\cos^2(\theta_{ij})$ and $\sin^2(\theta_{ij})$ are shown versus $(\omega_i - \omega_j)/(2\pi J_{ij})$ in red and blue, respectively. $\cos^2(\theta_{ij})$ scales the cross-relaxation rate constant σ_{ik} , which would be expected in case of weak coupling, and $\sin^2(\theta_{ij})$ scales the contribution from σ_{jk} .

2.3. The Solomon equations

Further simplifications lead to the generalized form of the Solomon equations [14]. Bull shows that dipole/dipole cross-correlated relaxation has a rather small effect in NOESYs [58]. Cross-correlated relaxation between dipolar and CSA interactions is even smaller, since the proton $\Delta\sigma_i$ is typically only 10 ppm. Thus, there is no efficient transfer mechanism to populate two- and higher-spin orders. To a good approximation, the relevant NOESY process can be described by the Solomon equations, which are formulated in the reduced space spanned only by N single-spin order operators:

$$\frac{d}{dt} \begin{pmatrix} \langle I_{1,z} \rangle - I_{1,0} \\ \langle I_{2,z} \rangle - I_{2,0} \\ \cdot \\ \cdot \\ \cdot \\ \langle I_{N,z} \rangle - I_{N,0} \end{pmatrix} = - \begin{pmatrix} \rho_1 & \sigma_{12} & \cdot & \cdot & \cdot & \sigma_{1N} \\ \sigma_{12} & \rho_2 & \cdot & \cdot & \cdot & \sigma_{2N} \\ \cdot & \cdot & \cdot & \cdot & \cdot & \cdot \\ \cdot & \cdot & \cdot & \cdot & \cdot & \cdot \\ \cdot & \cdot & \cdot & \cdot & \cdot & \cdot \\ \sigma_{1N} & \sigma_{2N} & \cdot & \cdot & \cdot & \rho_N \end{pmatrix} \begin{pmatrix} \langle I_{1,z} \rangle - I_{1,0} \\ \langle I_{2,z} \rangle - I_{2,0} \\ \cdot \\ \cdot \\ \cdot \\ \langle I_{N,z} \rangle - I_{N,0} \end{pmatrix} \quad (24)$$

These equations are usually employed to analyze NOESY spectra.

2.4. Conformational/chemical exchange

Conformational and chemical exchange cause modulation of the Hamiltonians by shifting the Larmor frequency through the frequencies associated with each sampled conformation/state (among other changes). The Hamiltonians are then the sums over the contributions from each conformation for a specific spin. While the stationary Hamiltonian weights these contributions by the populations, the stochastic Hamiltonian uses time-modulated weights depending on the exchange rates. The effects can be derived quantum mechanically [41], but modified Bloch equations, the so-called McConnell equations are sufficient to give insight [59]. Analysis of the transverse components of the magnetization of spin i shows that peaks are not resolved in a spectrum if the difference between the chemical shifts of different states is smaller than the exchange rate ($k_{\text{ex}} \gg |\Delta\omega_i|$), which is defined as the sum of the forward and reverse reaction rate constants [37,40,41]. This situation is called fast exchange (not to be confused with fast motion). The single apparent peak shows up at a population-weighted average frequency. Motion is then described within the spectral density function (see 2.5.).

If, on the other hand, the exchange is slow ($k_{\text{ex}} \ll |\Delta\omega_i|$), separate components of the magnetization are resolved in a spectrum [60,61]. Corresponding peaks show up on the NOESY diagonal and the exchange process builds up cross peaks that are nearly indistinguishable from those induced by cross-relaxation. This type of dynamics cannot be described with the spectral density function. Instead, the process during the NOESY mixing time τ_{mix} is given by the longitudinal component of the McConnell equations [59]. A N_{ex} -site first-order exchange process in chemical equilibrium is assumed for spin i :



The consequence is that each $I_{i,z}$ magnetization is split into N_{ex} components $I_{ir,z}$ in equation 24 and a modified relaxation matrix $R' = K + R$ is used, where K includes elements describing the exchange rates. The resulting subequation is

$$\frac{d}{dt} \begin{pmatrix} \langle I_{i1,z} \rangle - I_{i1,0} \\ \vdots \\ \langle I_{ir,z} \rangle - I_{ir,0} \\ \vdots \\ \langle I_{iN_{\text{ex}},z} \rangle - I_{iN_{\text{ex}},0} \end{pmatrix} = - \begin{pmatrix} \rho_{i,1} + \sum_{s=2}^{N_{\text{ex}}} k_{i,1s} & \cdot & -k_{i,r1} & \cdot & -k_{i,N_{\text{ex}}1} \\ \cdot & \cdot & \cdot & \cdot & \cdot \\ -k_{i,1r} & \cdot & \rho_{i,r} + \sum_{\substack{s=1 \\ s \neq r}}^{N_{\text{ex}}} k_{i,rs} & \cdot & -k_{i,N_{\text{ex}}r} \\ \cdot & \cdot & \cdot & \cdot & \cdot \\ -k_{i,1N_{\text{ex}}} & \cdot & -k_{i,rN_{\text{ex}}} & \cdot & \rho_{i,N_{\text{ex}}} + \sum_{s=1}^{N_{\text{ex}}-1} k_{i,N_{\text{ex}}s} \end{pmatrix} \begin{pmatrix} \langle I_{i1,z} \rangle - I_{i1,0} \\ \vdots \\ \langle I_{ir,z} \rangle - I_{ir,0} \\ \vdots \\ \langle I_{iN_{\text{ex}},z} \rangle - I_{iN_{\text{ex}},0} \end{pmatrix} \quad (26)$$

If the initial magnetic perturbation is nonselective, the components $I_{ir,z}$ are proportional to the populations of the exchanging sites. In the most extreme case, each $I_{ir,z}$ magnetization has a different autorelaxation rate and different cross-relaxation rates to other spins. It is common, however, to assume that the autorelaxation rate is the same for all r . If the exchange is very slow

($k_{\text{ex}} \ll 1/\tau_{\text{mix}}$), no cross-peak buildup is observable during NOESY mixing and the diagonal peaks have population-weighted volumes.

2.5. The spectral density function

For ensemble-based structure calculations employing exact NOEs, it is important to understand the implications of the impact of the motional behavior of the molecule on the NOE. If a spin gives rise to a single peak, it is associated with a single spectral frequency. The complete information on motion which is accessible by the NOESY experiment is imprinted on the spectral density function. The spectral density function is obtained from equation 8:

$$J_m^{aa'}(\omega) = \int_0^{t_{\text{mix}}} C^{aa'm}(\tau) \cos(\omega\tau) d\tau \quad (27)$$

with the correlation function

$$C^{aa'm}(\tau) = \langle F_m^{a'*}(t+\tau) F_m^a(t) \rangle \quad (28)$$

As F is a *stationary* random function, its dependence on t can be replaced by an evaluation at 0 without loss of generality. As shown in the Appendix (equations A15-A18), the correlation function is independent of m and equation 28 can be further simplified:

$$C^{aa'm}(\tau) = \langle F_0^{a'}(\tau) F_0^a(0) \rangle \equiv C^{aa'}(\tau) \quad (29)$$

Since F_0 is proportional to the spherical harmonic Y_{20} , F_0 can be expressed in a molecule-fixed coordinate system (F_0^{int}) in combination with a time-dependent rotation relating the molecule-fixed to the laboratory frame. Use of the Wigner rotation element $D_{l_0}^2(\Theta^{a,\text{mol}})$ gives [41]:

$$C^{aa'}(\tau) = \sum_{l,l'=-2}^2 \langle D_{0l'}^2(\Theta^{a',\text{mol}}(\tau)) D_{0l}^{2*}(\Theta^{a,\text{mol}}(0)) F_{l'}^{a',\text{int}*}(\tau) F_l^{a,\text{int}}(0) \rangle \quad (30)$$

If the overall molecular tumbling is independent from the internal motions, equation 30 can be written as

$$C^{aa'}(\tau) = \sum_{l,l'=-2}^2 \langle D_{0l'}^2(\Theta^{a',\text{mol}}(\tau)) D_{0l}^{2*}(\Theta^{a,\text{mol}}(0)) \rangle \langle F_{l'}^{a',\text{int}*}(\tau) F_l^{a,\text{int}}(0) \rangle \quad (31)$$

It must be stressed that macromolecular dynamics are generally very complex. In particular, in partially folded or unfolded molecules, mode coupling and/or local diffusion must be accounted for. According models have been developed, but are beyond the scope of this review [62,63]. The formalism presented in the following is sufficient for quantitative NOE investigation in globular proteins. $\langle D_{0l'}^2(\Theta^{a',\text{mol}}(\tau)) D_{0l}^{2*}(\Theta^{a,\text{mol}}(0)) \rangle$ may be expressed in terms of the eigenvalues $1/\tau_p$ of the anisotropic molecular diffusion operator \mathbf{D} :

$$\begin{aligned} 1/\tau_{-2} &= D_x + D_y + 4D_z \\ 1/\tau_{-1} &= D_x + 4D_y + D_z \\ 1/\tau_0 &= 6(D - \sqrt{D^2 - D'^2}) \\ 1/\tau_1 &= 4D_x + D_y + D_z \\ 1/\tau_2 &= 6(D + \sqrt{D^2 - D'^2}) \end{aligned} \quad (32.1-5)$$

$$D' = \sqrt{\frac{D_x D_y + D_x D_z + D_y D_z}{3}}; \quad D = \frac{D_x + D_y + D_z}{3};$$

The derivation using the Green function for rigid body diffusion is lengthy and may be looked up in the literature [64]. The summation over l and l' can be rearranged into a summation over p [65,66]. The correlation function becomes an expression in which each τ_p is the active molecular correlation time for a fractional correlation function of internal motion, $C_{\text{int},p}^{aa'}(\tau)$:

$$C^{aa'}(\tau) = \sum_{p=-2}^2 e^{-\tau/\tau_p} C_{\text{int},p}^{aa'}(\tau) \quad (33)$$

with

$$\begin{aligned} C_{\text{int},-2}^{aa'} &= (r_a^{\text{rigid}})^3 (r_{a'}^{\text{rigid}})^3 \left\langle \frac{1}{r_a^3 r_{a'}^3} \left(\frac{3}{4} \sin^2 \theta_a \sin^2 \theta_{a'} \sin 2\varphi_a \sin 2\varphi_{a'} \right) \right\rangle \\ C_{\text{int},-1}^{aa'} &= (r_a^{\text{rigid}})^3 (r_{a'}^{\text{rigid}})^3 \left\langle \frac{1}{r_a^3 r_{a'}^3} \left(\frac{3}{4} \sin 2\theta_a \sin 2\theta_{a'} \cos \varphi_a \cos \varphi_{a'} \right) \right\rangle \\ C_{\text{int},0}^{aa'} &= (r_a^{\text{rigid}})^3 (r_{a'}^{\text{rigid}})^3 \left\langle \frac{1}{r_a^3 r_{a'}^3} \left(\begin{aligned} &\frac{3\mu^2}{4N^2} \sin^2 \theta_a \sin^2 \theta_{a'} \cos 2\varphi_a \cos 2\varphi_{a'} \\ &-\frac{\sqrt{3}\mu w}{4N^2} [\sin^2 \theta_a \cos 2\varphi_a (3\cos^2 \theta_{a'} - 1) + \sin^2 \theta_{a'} \cos 2\varphi_{a'} (3\cos^2 \theta_a - 1)] \\ &+\frac{w^2}{4N^2} (3\cos^2 \theta_a - 1)(3\cos^2 \theta_{a'} - 1) \end{aligned} \right) \right\rangle \\ C_{\text{int},1}^{aa'} &= (r_a^{\text{rigid}})^3 (r_{a'}^{\text{rigid}})^3 \left\langle \frac{1}{r_a^3 r_{a'}^3} \left(\frac{3}{4} \sin 2\theta_a \sin 2\theta_{a'} \sin \varphi_a \sin \varphi_{a'} \right) \right\rangle \\ C_{\text{int},2}^{aa'} &= (r_a^{\text{rigid}})^3 (r_{a'}^{\text{rigid}})^3 \left\langle \frac{1}{r_a^3 r_{a'}^3} \left(\begin{aligned} &\frac{3w^2}{4N^2} \sin^2 \theta_a \sin^2 \theta_{a'} \cos 2\varphi_a \cos 2\varphi_{a'} \\ &+\frac{\sqrt{3}\mu w}{4N^2} [\sin^2 \theta_a \cos 2\varphi_a (3\cos^2 \theta_{a'} - 1) + \sin^2 \theta_{a'} \cos 2\varphi_{a'} (3\cos^2 \theta_a - 1)] \\ &+\frac{\mu^2}{4N^2} (3\cos^2 \theta_a - 1)(3\cos^2 \theta_{a'} - 1) \end{aligned} \right) \right\rangle \end{aligned} \quad (34.1-5)$$

On the right-hand sides, the indices a and a' designate the interaction vectors of the corresponding interactions in polar angles in the molecule-fixed frame at time points 0 (a) and τ (a'), respectively. If a or a' is a CSA interaction, the distance is replaced by 1. The following abbreviations are used:

$$\mu = \sqrt{3}(D_x - D_y); \quad w = 2D_z - D_x - D_y + 2\Delta$$

$$\Delta = 3\sqrt{D^2 - D'^2}; \quad N = 2\sqrt{\Delta w}$$

$C_{\text{int},p}^{aa',\text{rigid}}$ is the $C_{\text{int},p}^{aa'}$ coefficient in absence of internal motion. For cross-correlated relaxation ($a \neq a'$), the brackets in equations 34 can then be omitted, the distances are canceled out and τ is set to 0. In the case of auto-correlated relaxation ($a = a'$), $C_{\text{int},p}^{a,\text{rigid}} \equiv C_{\text{int},p}^{aa,\text{rigid}}$ is considerably simpler:

$$C_{\text{int},-2}^{a,\text{rigid}} = \frac{3}{4} \sin^4 \theta \sin^2 2\varphi$$

$$C_{\text{int},-1}^{a,\text{rigid}} = \frac{3}{4} \sin^2 2\theta \cos^2 \varphi$$

$$C_{\text{int},0}^{a,\text{rigid}} = \frac{3\mu^2}{4N^2} \sin^4 \theta \cos^2 2\varphi - \frac{\sqrt{3}\mu w}{2N^2} \sin^2 \theta \cos 2\varphi (3\cos^2 \theta - 1) + \frac{w^2}{4N^2} (3\cos^2 \theta - 1)^2 \quad (35.1-5)$$

$$C_{\text{int},1}^{a,\text{rigid}} = \frac{3}{4} \sin^2 2\theta \sin^2 \varphi$$

$$C_{\text{int},2}^{a,\text{rigid}} = \frac{3w^2}{4N^2} \sin^4 \theta \cos^2 2\varphi + \frac{\sqrt{3}\mu w}{2N^2} \sin^2 \theta \cos 2\varphi (3\cos^2 \theta - 1) + \frac{\mu^2}{4N^2} (3\cos^2 \theta - 1)^2$$

2.5.1. Simplifications

For practical purposes these expressions are of prohibitive complexity. In this paragraph, two widely used assumptions are made to reduce equations 32 to 35.

For the majority of the macromolecules, the assumption of axially symmetric molecular tumbling is sufficient to describe relaxation measurements within experimental uncertainty. The relationship $\tau_{-p} = \tau_p$ leads to

$$\begin{aligned}
C_{\text{int},-2}^{aa'} + C_{\text{int},2}^{aa'} &= (r_a^{\text{rigid}})^3 (r_{a'}^{\text{rigid}})^3 \left\langle \frac{1}{r_a^3 r_{a'}^3} \left(\frac{3}{4} \sin^2 \theta_a \sin^2 \theta_{a'} \cos(2\varphi_a - 2\varphi_{a'}) \right) \right\rangle \\
C_{\text{int},-1}^{aa'} + C_{\text{int},1}^{aa'} &= (r_a^{\text{rigid}})^3 (r_{a'}^{\text{rigid}})^3 \left\langle \frac{1}{r_a^3 r_{a'}^3} \left(\frac{3}{4} \sin 2\theta_a \sin 2\theta_{a'} \cos(\varphi_a - \varphi_{a'}) \right) \right\rangle \\
C_{\text{int},0}^{aa'} &= (r_a^{\text{rigid}})^3 (r_{a'}^{\text{rigid}})^3 \left\langle \frac{1}{r_a^3 r_{a'}^3} \left(\frac{1}{4} (3\cos^2 \theta_a - 1)(3\cos^2 \theta_{a'} - 1) \right) \right\rangle
\end{aligned} \tag{36.1-3}$$

and

$$\begin{aligned}
1/\tau_{\pm 2} &= 4D_z + 2D_{x=y} \\
1/\tau_{\pm 1} &= D_z + 5D_{x=y} \\
1/\tau_0 &= 6D_{x=y}
\end{aligned} \tag{37.1-3}$$

Most often, isotropic molecular tumbling is assumed and the diffusion tensor reduces to a scalar with a single correlation time $\tau_p = \tau_c$. Equation 33 becomes

$$C^{aa'}(\tau) = e^{-\tau/\tau_c} \sum_{p=-2}^2 C_{\text{int},p}^{aa'}(\tau) = 1/5 e^{-\tau/\tau_c} (r_a^{\text{rigid}})^3 (r_{a'}^{\text{rigid}})^3 \sum_{l,l'=-2}^2 4\pi \left\langle \frac{1}{r_a^3 r_{a'}^3} Y_{2l'}(\theta_{a'}) Y_{2l}^*(\theta_a) \right\rangle \tag{38}$$

It has been shown that independence between the fluctuations of the vector length and orientation is a good approximation for many proton-proton NOEs [67]. In general, however, caution has to be taken. $C_{\text{int},p}^{aa'}$ can then be factorized as

$$C_{\text{int},p}^{aa'} = (r_a^{\text{rigid}})^3 (r_{a'}^{\text{rigid}})^3 \left\langle \frac{1}{(r_a^3 r_{a'}^3)} \right\rangle C_{\text{int},p}^{aa',Y} \tag{39}$$

For the isotropic molecular tumbling model a further simplification of equation 38 is obtained:

$$C^{aa'}(\tau) = (r_a^{\text{rigid}})^3 (r_{a'}^{\text{rigid}})^3 \left\langle \frac{1}{r_a^3 r_{a'}^3} \right\rangle \left\langle \left(\frac{1}{2} (3\cos^2 \theta_{a,a'} - 1) \right) \right\rangle e^{-\tau/\tau_c} \tag{40}$$

$\theta_{a,a'}$ is the projection angle between the vectors a and a' .

2.5.2. Simplifications for methyl groups

The general expressions for methyl groups are complex, but they simplify under certain assumptions. First, it is noted that autorelaxation rate constants are only of secondary importance. Some approaches for distance extraction do not require any model because experimental rate constants are fitted and reused for the determination of cross-relaxation rate constants. Other approaches use predictions but the outcome of the cross-relaxation rate constants is relatively insensitive to the exact nature of the model. Therefore, a very simple model is employed to express autorelaxation in methyl groups. A detailed derivation is presented in the Appendix. It is assumed that the methyl rotation around the symmetry axis $c3$ happens instantaneously. $J_{ij}^{D,\text{methyl}}(\omega)$ can be evaluated by separation of the rotation around the $c3$ axis from the fluctuation of the $c3$ axis

$$J_{\vec{i}}^{D,\text{methyl}}(\omega_{\vec{i}}) = \int_0^{t_{\text{mix}}} C^{D(\vec{i}),\text{methyl}}(\tau) \cos(\omega\tau) d\tau \quad (41)$$

with the correlation function

$$C^{D(\vec{i}),\text{methyl}}(\tau) = \left(S^{\text{methyl,prot}} \right)^2 \sum_{p=-2}^2 e^{-\tau/\tau_p} C_{\text{int},p}^{D(\vec{i}),\text{methyl},c3}(\tau) \quad (42)$$

where

$$\left(S^{\text{methyl,prot}} \right)^2 = \sum_{\kappa < \iota}^3 \frac{1}{3} \left\langle P_2(\theta_{i_{\kappa}i_{\iota}}^{\text{prot}}) P_2(\theta_{i_{\kappa}i_{\iota}}^{\text{prot}}) \right\rangle = \frac{1}{4} \quad (43)$$

is the order parameter for the fast rotation around $c3$. The correlation function now has the same form as the one for a single proton with an additional factor. An additional simplification in

equation 16 is that the distance is constant, $r_{i_k j_l}(t) = r_{\text{methyl}} = 1.813 \text{ \AA}$ [68]. If the methyl autorelaxation rate constant for a ^{13}C -labeled sample is calculated, the dipolar H-C interaction is calculated in an analog manner. Then, $r_{i_k j=C}(t) = r_{ij=C}^{\text{methyl}} = 1.117 \text{ \AA}$ and since the angle between the c3 and the H-C axes is 110.9° , the squared order parameter is $1/9$ [69].

For auto-correlated relaxation between two distinct groups of equivalent spins the spectral density function is (see equation 19)

$$J_{ij}^{\text{D}}(\omega) = \int_0^{t_{\text{mix}}} C^{\text{D}(\bar{ij})}(\tau) \cos(\omega\tau) d\tau \quad (44)$$

A similar simplification as used in equation 40 is not possible. If the molecular tumbling is isotropic, the correlation function is

$$C^{\text{D}(\bar{ij})}(\tau) = e^{-\tau/\tau_c} \sum_{p=-2}^2 C_{\text{int},p}^{\text{D}(\bar{ij})}(\tau) = e^{-\tau/\tau_c} (r_{ij}^{\text{rigid}})^6 \sum_{l,l'=-2}^2 \frac{1}{N_i N_j} \sum_{\kappa=1}^{N_i} \sum_{\iota=1}^{N_j} \left\langle \frac{Y_{2l'}(\theta_{i_k j_l}(\tau)) Y_{2l}^*(\theta_{i_k j_l}(0))}{r_{i_k j_l}(\tau)^3 r_{i_k j_l}(0)^3} \right\rangle \quad (45)$$

If one group consists of a single spin

$$C^{\text{D}(\bar{ij})}(\tau) = e^{-\tau/\tau_c} \sum_{p=-2}^2 C_{\text{int},p}^{\text{D}(\bar{ij})}(\tau) = e^{-\tau/\tau_c} (r_{ij}^{\text{rigid}})^6 \sum_{l,l'=-2}^2 \frac{1}{N_i} \sum_{\kappa=1}^{N_i} \left\langle \frac{Y_{2l'}(\theta_{i_k j}(\tau)) Y_{2l}^*(\theta_{i_k j}(0))}{r_{i_k j}(\tau)^3 r_{i_k j}(0)^3} \right\rangle \quad (46)$$

In more sophisticated models one internal correlation time is assigned to the rotation around c3 and a second one to the fluctuation of c3 [69], which are then used in the extended Lipari-Szabo formalism [70], or a three-site jump-model with defined jump rates is employed [44]. The jump model (*vide supra*) can be implemented with a $N \times N$ submatrix for an N -site exchange [45]. The magnetization vector is enlarged by two dimensions per methyl group. As mentioned previously, a simplified approach for fast multiple-site exchange uses only one magnetization

intensity (the sum), where the relaxation rate is obtained from the population-weighted average of the individual relaxation rates [50].

2.6. Lipari-Szabo approximation

Lipari and Szabo proposed to approximate the correlation function of the internal motion with a monoexponential decay with a single internal correlation time τ_{int} [71,72]. At infinite time, the correlation function reaches the Lipari-Szabo order parameter. Practically, this order parameter is only sensitive to fast motion ($\tau_{\text{int}} \ll \tau_p$). By analog construction, generalized order parameters can be obtained from $C_{\text{int},p}^{aa'}(\tau)$. Since in experiment the spectral density function integrates $C_{\text{int},p}^{aa'}(\tau)$ over the NOESY mixing time t_{mix} rather than the commonly assumed infinity, these order parameters for fast motion actually are $C_{\text{int},p}^{aa'}(t_{\text{mix}})$. This distinction bears an important implication for the dependence on slow motion (*vide infra*). For practical purposes, the order parameters of fast motion are here defined as fractions of the according coefficient of a rigid molecule:

$$\left(S_p^{aa',\text{fast}}\right)^2 \equiv \frac{\langle C_{\text{int},p}^{aa'}(t_{\text{mix}}) \rangle}{C_{\text{int},p}^{aa',\text{rigid}}} \quad (47)$$

The correlation function becomes

$$C^{aa'}(\tau) = \sum_{p=-2}^2 e^{-\tau/\tau_p} C_{\text{int},p}^{aa',\text{rigid}} \left[\left(S_p^{aa',\text{fast}}\right)^2 + \left(\frac{\langle C_{\text{int},p}^{aa'} \rangle}{C_{\text{int},p}^{aa',\text{rigid}}} - \left(S_p^{aa',\text{fast}}\right)^2 \right) e^{-\tau/\tau_{\text{int}}} \right] \quad (48)$$

$C^{aa'}(\tau)$ still contains an ensemble average which extends over all molecules. If there is additional slow motion present ($\tau_{\text{int}} \gg \tau_p$), not all conformations are sampled by a single molecule during

τ_p . If $t_{\text{mix}} > \tau_{\text{int}}$, this requires that the averaging of $C_{\text{int},p}^{aa'}(\tau)$ over all molecules has to be maintained. If the motion is even slower, that is $t_{\text{mix}} < \tau_{\text{int}}$, the ergodic hypothesis breaks down. The averaging happens at the level of spectral intensities instead of the relaxation rates. In practice, it is usually reasonable to assume that the fast order parameter of a specific molecule is equal to the average over all molecules and the brackets can be omitted in equation 47.

Insertion of expression 48 into equation 27 yields for the spectral density function

$$J^{aa'}(\omega) = \sum_{p=-2}^2 C_{\text{int},p}^{aa',\text{rigid}} \left[(S_p^{aa',\text{fast}})^2 \frac{\tau_p}{1+(\tau_p\omega)^2} + \left(\frac{\langle C_{\text{int},p}^{aa'}(0) \rangle}{C_{\text{int},p}^{aa',\text{rigid}}} - (S_p^{aa',\text{fast}})^2 \right) \frac{\tau_{\text{eff},p}}{1+(\tau_{\text{eff},p}\omega)^2} \right] \quad (49)$$

with the effective correlation times

$$\frac{1}{\tau_{\text{eff},p}} = \frac{1}{\tau_p} + \frac{1}{\tau_{\text{int}}} \quad (50)$$

A specific effective correlation time and order parameter of fast motion are associated with each $C_{\text{int},p}^{aa'}$ coefficient. Implications of equation 49 for cross-correlated relaxation are discussed in detail in reference [66]. Since dipolar auto-correlated relaxation is the dominant mechanism in NOESY spectroscopy, only the case of $a = a' = D(i,j)$ is discussed further. The spectral density function is

$$J^{D(ij)}(\omega) = \sum_{p=-2}^2 C_{\text{int},p}^{D(ij),\text{rigid}} \left\{ (S_p^{D(ij),\text{fast}})^2 \frac{\tau_p}{1+(\tau_p\omega)^2} + \left((r_{ij}^{\text{rigid}})^6 \left\langle \frac{1}{r_{ij}^6} \right\rangle - (S_p^{D(ij),\text{fast}})^2 \right) \frac{\tau_{\text{eff},p}}{1+(\tau_{\text{eff},p}\omega)^2} \right\} \quad (51)$$

Isotropic molecular tumbling leads to

$$J^{D(ij)}(\omega) = (S^{D(ij),\text{fast}})^2 \frac{\tau_c}{1+(\tau_c\omega)^2} + \left((r_{ij}^{\text{rigid}})^6 \left\langle \frac{1}{r_{ij}^6} \right\rangle - (S^{D(ij),\text{fast}})^2 \right) \frac{\tau_{\text{eff}}}{1+(\tau_{\text{eff}}\omega)^2} \quad (52)$$

with

$$\frac{1}{\tau_{\text{eff}}} = \frac{1}{\tau_c} + \frac{1}{\tau_{\text{int}}} \quad (53)$$

$(S^{D(ij),\text{fast}})^2$ is the order parameter for fast internal motion of an isotropically tumbling molecule:

$$\begin{aligned} (S^{D(ij),\text{fast}})^2 &\equiv (r_{ij}^{\text{rigid}})^6 \frac{4\pi}{5} \sum_{q=-2}^2 \left\langle \frac{Y_{2q}(\theta_{ij}(t_{\text{mix}}), \varphi_{ij}(t_{\text{mix}})) Y_{2q}^*(\theta_{ij}(0), \varphi_{ij}(0))}{(r_{ij}(t_{\text{mix}}))^3 (r_{ij}(0))^3} \right\rangle \\ &\approx (r_{ij}^{\text{rigid}})^6 \frac{4\pi}{5} \sum_{q=-2}^2 \left| \left\langle \frac{Y_{2q}(\theta_{ij}, \varphi_{ij})}{(r_{ij})^3} \right\rangle \right|^2 \end{aligned} \quad (54)$$

2.7. Experimental order parameters

It is crucial to investigate what kind of order parameter can actually be extracted from an NOESY experiment. An experimentally accessible NOE order parameter is sensitive to all time scales. It may be defined by the true cross-relaxation rate constant normalized to the one expected for a rigid molecule,

$$(S^{D(ij),\text{exp}})^2 \equiv \frac{\sigma_{ij}^{\text{exp}}}{\sigma_{ij}^{\text{rigid}}} \quad (55)$$

In general, it is not possible to relate the order parameter to a simple analytical expression. For macromolecules at high magnetic fields, however, $1 \ll (\tau_p \omega)^2$ and all terms where the spectral density function samples frequencies other than 0 or $(\omega_i - \omega_j)$ can be neglected. The experimental order parameter can then be written as

$$\left(S^{D(ij),\text{exp}}\right)^2 = \frac{\sum_{p=-2}^2 C_{\text{int},p}^{D(ij),\text{rigid}} \left\{ \left(S_p^{D(ij),\text{fast}}\right)^2 \tau_p + \left(r_{ij}^{\text{rigid}} \right)^6 \left\langle \frac{1}{r_{ij}^6} \right\rangle - \left(S_p^{D(ij),\text{fast}}\right)^2 \right\} \tau_{\text{eff},p}}{\sum_{p=-2}^2 C_{\text{int},p}^{D(ij),\text{rigid}} \tau_p} \quad (56)$$

If the τ_p are not too different from each other, a useful approximation is

$$\left(S^{D(ij),\text{exp}}\right)^2 \approx \sum_{p=-2}^2 C_{\text{int},p}^{D(ij),\text{rigid}} \left\{ \left(S_p^{D(ij),\text{fast}}\right)^2 + \left(r_{ij}^{\text{rigid}} \right)^6 \left\langle \frac{1}{r_{ij}^6} \right\rangle - \left(S_p^{D(ij),\text{fast}}\right)^2 \right\} \frac{1}{1 + \tau_p / \tau_{\text{int}}} \quad (57.1)$$

If the molecule tumbles isotropically, the exact expression is

$$\left(S^{D(ij),\text{exp}}\right)^2 = \left(S^{D(ij),\text{fast}}\right)^2 + \left(r_{ij}^{\text{rigid}} \right)^6 \left\langle \frac{1}{r_{ij}^6} \right\rangle - \left(S^{D(ij),\text{fast}}\right)^2 \frac{1}{1 + \tau_c / \tau_{\text{int}}} \quad (57.2)$$

For internal motions that are much faster than nanoseconds ($\tau_{\text{int}} \ll \tau_p$), $\left(S^{D(ij),\text{exp}}\right)^2$ is fully determined by the order parameters of fast motion as defined in equation 47

$$\left(S^{D(ij),\text{exp}}\right)^2 \approx \sum_{p=-2}^2 C_{\text{int},p}^{D(ij),\text{rigid}} \left(S_p^{D(ij),\text{fast}}\right)^2 \quad (58.1)$$

$$\left(S^{D(ij),\text{exp}}\right)^2 = \left(S^{D(ij),\text{fast}}\right)^2 \quad (58.2)$$

$\left(S^{D(ij),\text{exp}}\right)^2$ is then simply the weighted sum of the squared Lipari-Szabo order parameters of fast motion, or the squared Lipari-Szabo order parameter of the isotropically tumbling molecule, respectively.

For motion much slower than the molecular tumbling ($\tau_{\text{int}} \gg \tau_p$), $\left(S^{D(ij),\text{exp}}\right)^2$ is independent of the angular coordinates and of the diffusion tensor:

$$\left(S^{D(ij),\text{exp}}\right)^2 = \left(r_{ij}^{\text{rigid}} \right)^6 \left\langle \frac{1}{r_{ij}^6} \right\rangle \quad (59)$$

2.8. Practical expressions

The simplest and most common way to extract distances from the measured cross-relaxation rate constant is to use equations 13.4 and 19 under the assumption of a rigid molecule and exclusively retention of the spectral density function sampling the frequency $|\omega_i - \omega_j| \approx 0$ (valid for $1 \ll (\tau_p \omega)^2$, *vide supra*). Motional effects are absorbed into the distance which must be replaced by an effective distance r_{ij}^{eff} . In the following, NOEs involving single spins and groups of equivalent spins are treated separately.

2.8.1. NOEs and distances between single spins

From equation 13.4 follows

$$\sigma_{ij} = \left(\frac{\mu_0}{4\pi} \right)^2 \frac{\gamma^4 \hbar^2}{10} \frac{1}{(r_{ij}^{\text{eff}})^6} J^{\text{D}(ij), \text{rigid}}(0) = \left(\frac{\mu_0}{4\pi} \right)^2 \frac{\gamma^4 \hbar^2}{10} \frac{1}{(r_{ij}^{\text{eff}})^6} \sum_{p=-2}^2 C_{\text{int}, p}^{\text{aa}', \text{rigid}} \tau_p \quad (60)$$

This formula is used for the prediction of the cross-relaxation rate constant if the diffusion tensor is known. If the molecule tumbles isotropically

$$\sigma_{ij} = \left(\frac{\mu_0}{4\pi} \right)^2 \frac{\gamma^4 \hbar^2}{10} \frac{\tau_c}{(r_{ij}^{\text{eff}})^6} \quad (61)$$

More commonly, the distance is extracted from the cross-relaxation rate constant. This is not straight-forward from equation 60 and all studies to date used equation 61 instead (most studies did not make an effort in proving the validity for the specific system). The effective distance is then

$$r_{ij}^{\text{eff}} = \left(\left(\frac{\mu_0}{4\pi} \right)^2 \frac{\gamma^4 \hbar^2}{10} \frac{\tau_c}{\sigma_{ij}} \right)^{1/6} = \left(56.94 \frac{\tau_c / \text{ns}}{\sigma_{ij} / \text{s}^{-1}} \right)^{1/6} \text{ \AA} \quad (62)$$

If the molecular correlation time and the measured cross-relaxation rate constant are inserted in units of nanoseconds and in inverted seconds, respectively, the distance is obtained in units of Ångstrom. The relationship between the distances in a rigid molecule and the effective distances can be expressed with the order parameter:

$$r_{ij}^{\text{eff}} = \frac{r_{ij}^{\text{rigid}}}{\left(S^{\text{D}(ij),\text{exp}} \right)^{1/3}} \quad (63)$$

Note that this holds true for motions on all timescales as well as for cases where $J(2\omega)$ cannot be neglected.

It is noted that an exact extraction of the effective distance requires an accurate measurement of τ_c . In particular, for non-isotope labeled samples this can be a challenging task. Very often the cross-relaxation rate of a spin pair of known distance was chosen as a reference and distances between other spin pairs have been derived as:

$$r_{ij}^{\text{eff}} = r^{\text{ref}} \left(\frac{\sigma^{\text{ref}}}{\sigma_{ij}} \right)^{1/6} \quad (63b)$$

It is clear that this approach entails many traps that are widely discussed in literature [28,73-83] and are not repeated here. Instead, it is recommended to determine an exact values of τ_c with ^{15}N longitudinal and transverse relaxation measurements.

All studies employ one of three approaches to use the effective experimental distance in structure calculations. The first and foremost way is to ignore motional effects completely and

relegate their impact into the experimental error and concomitantly to set large upper (and rarely also lower) limits:

$$\left(S^{D(ij),\text{exp}}\right)^2 = 1 \quad (64.1)$$

and

$$r_{ij}^{\text{eff}} = r_{ij}^{\text{rigid}} \quad (65.1)$$

Despite of its simplicity, it has been shown that for the majority of NOEs this approximation is good [84].

Secondly, the simplest model accounting for motional effects is the so-called $\langle r^{-6} \rangle$ averaging. All motion is treated as if it were slow and equation 57 gives the order parameter.

$$\left(S^{D(ij),\text{exp}}\right)^2 = \left(r_{ij}^{\text{rigid}}\right)^6 \left\langle \frac{1}{r_{ij}^6} \right\rangle \quad (64.2)$$

and

$$r_{ij}^{\text{eff}} = \left\langle \frac{1}{r_{ij}^6} \right\rangle^{-1/6} \quad (65.2)$$

It is clear that the contribution to r^{eff} of temporarily short distances to the NOE is overestimated if part of the motion is in fact fast. In an ensemble structure calculation, true short distances are rejected such that the structure becomes 'deflated'.

In a third approach, $\langle r^{-3} \rangle$ averaging is employed. All motion is treated as if it were fast, but the angular dependence is ignored.

$$\left(S^{D(ij),\text{exp}}\right)^2 = \left(r_{ij}^{\text{rigid}}\right)^6 \left\langle \frac{1}{r_{ij}^3} \right\rangle^2 \quad (64.3)$$

and

$$r_{ij}^{\text{eff}} = \left\langle \frac{1}{r_{ij}^3} \right\rangle^{-1/3} \quad (65.3)$$

On one hand, this model overestimates contributions to the NOE because it neglects the angular dependence of the fast motion. On the other hand, it underestimates contributions from slow motion. It is not easy to quantify the overall effect on the structure calculation. Note that the model is a compromise such that *a priori* structural knowledge is not required.

2.8.2. NOEs and distances between groups of equivalent spins

For NOEs involving groups of equivalent spins, the pseudo-atom model is used. From equation 19 follows

$$\sigma_{ij} = \left(\frac{\mu_0}{4\pi}\right)^2 \frac{\gamma^4 \hbar^2}{10} \frac{N_i}{(r_{ij}^{\text{eff}})^6} J^{D(\bar{i}\bar{j}),\text{rigid}}(0) = \left(\frac{\mu_0}{4\pi}\right)^2 \frac{\gamma^4 \hbar^2}{10} \frac{N_i}{(r_{ij}^{\text{eff}})^6} \sum_{p=-2}^2 \tau_p C_{\text{int},p}^{D(\bar{i}\bar{j}),\text{rigid}} \quad (66)$$

$C_{\text{int},p}^{D(\bar{i}\bar{j}),\text{rigid}}$ contains the double sum over the spins of both groups and can in general not be simplified. Again, this formula can be used for the prediction of the cross-relaxation rate constant if the diffusion tensor is known. If the molecule tumbles isotropically

$$\sigma_{ij} = \left(\frac{\mu_0}{4\pi}\right)^2 \frac{\gamma^4 \hbar^2}{10} \frac{N_i \tau_c}{(r_{ij}^{\text{eff}})^6} \quad (67)$$

and the effective distance between the pseudoatoms becomes

$$r_{ij}^{\text{eff}} = \left(56.94 N_i \frac{\tau_c / \text{ns}}{\sigma_{ij} / \text{s}^{-1}} \right)^{1/6} \text{ \AA} \quad (68)$$

Even if the multiplicity effect of the spins is absorbed into the effective distance between the pseudoatoms, a distinction is made between the dynamics *within* the groups of equivalent spins and *between* them. The effect of intra-group dynamics can be treated with equations 45 and 46. This averaging is employed in all three cases outlined above (rigid model, $\langle r^{-6} \rangle$ averaging and $\langle r^{-3} \rangle$ averaging). Once this averaging is carried out, the cases described by equations 63-65 are applied. The type of the intra-group averaging depends on the spin group and is in principle independent of the type of model given by 63-65. The procedure is obviously somewhat cumbersome. It is therefore convenient to calculate maximum errors induced by the intra-group motion if the pseudoatom is employed in a structure calculation. Then, equations 63-65 are also valid for groups of equivalent spins while the maximum error is absorbed into the allowed upper and lower limits for the structure calculation.

The exact impact of intra group motion is difficult to predict because it depends on exact geometries. For example, a NOE to and from a methyl group depends not only on the distance but also on the orientation of the c3 axis. Thus, an *a priori* known structure is needed. Wüthrich et al. have defined pseudo-atom positions and calculated maximum allowed distances between these and individual group atoms in an amino-acid specific manner for all NOEs involving a backbone H $^{\alpha}$ or H $^{\text{N}}$ proton [46]. In methyl and methylene groups the pseudoatom is placed centrally with respect to the protons. The pseudoatom representing both methyl groups in valine and leucine is located in the center of all six protons. If the H2/H6 and H3/H5 resonances in aromatic rings of phenylalanine and tyrosine are resolved, the pseudoatoms are placed at the C1 and C4 positions, respectively. Otherwise, the pseudoatom representing all four protons is in the

center. For amide groups, it is located at N. A summary of the maximum possible distances between the positions of the pseudoatoms and the individual atoms, \vec{x}_Q and \vec{x}_{ik} , is provided in Table 1. Intraresidual corrections are those for distances with two or three intervening dihedral angles. "Long range" distances are those that depend on more than three intervening dihedral angles. These corrections can also be used for non-stereoassigned diastereotopic resonances and overlapped peaks where only their sum can be evaluated.

These limits can be narrowed if it is assumed that the protons exchange on a fast timescale. The maximum error is then the difference between the true r_{ij} and the apparent r_{ij}^{eff} distance as calculated from the experimental NOE. r_{ij}^{eff} can be simulated with equations 45 and 66 inserted in 68. Corrections based on the Tropp model for fast methyl rotation and on $\langle r^{-6} \rangle$ averaging for other processes such as slow aromatic flips have been calculated by several authors [44,45,85,86]. Corrections for distances to and from methyl groups have also been assessed from molecular dynamics simulation [84]. The various results for NOEs between a single atom and a pseudo-atom are presented in Table 1. The narrowest corrections are presented in bold numbers and recommended for use. In some cases, the corrections for the lower and upper limits are not equivalent and both values are indicated.

Corrections for distances between two pseudoatoms have been obtained from the sum of each correction [85]. For methyl-methyl distances this implies lower and upper limits of -0.40 and +0.40 Å, respectively [85]. Another study proposed a similar lower limit, but obtained an upper limit of +1.15 Å for the most extreme configuration [87]. In the same study corrections for NOEs between an aromatic and a methylene group were simulated [87]. While the upper limit correction is again the sum of the individual corrections (+2.70 Å), the lower limit has a much larger correction of -1.40 Å [87].

Table 1. Pseudoatom corrections for experimentally determined distances between a single atom and a group of equivalent atoms.

correction ^{ab} c [Å]	CH ₃	CH ₂	CH ₃ -CH ₃	aromatic center	aromatic C1, C4	CONH ₂	NH ₃ ⁺
rigid, 1 dihed, intra H ^N [46]		0.17 (G ^α)					
rigid, 1 dihed, intra H ^α [46]	0.21 (A ^β)	0.21 (all ^β)					
rigid, 2 dihed, intra H ^N [46]	0.69 (A ^β)	0.62 (all ^β)					
rigid, 3 dihed, intra H ^N [46]	0.98 (VIT ^γ)	0.87 (all ^γ)	1.73 (V ^γ)				
rigid, 2 dihed, intra H ^α [46]	0.69 (VIT ^γ)	0.65 (all ^γ)	0.76 (V ^γ)				
rigid, 3 dihed, intra H ^α [46]	0.98 (IL ^δ)	0.85 (KR ^δ)	1.68 (L ^δ)	1.96	0.98 (YF ^{C1})		
rigid, 2 dihed, seq H ^N [46]		0.52 (G ^α)					
rigid, 3 dihed, seq H ^N [46]	0.97 (A ^β)	0.86 (all ^β)					
rigid, long range [46]	1.03	0.88 (all)	2.31 (V ^γ L ^δ)	2.48 / 2.43 (intra H ^N - Q)	2.13/ 1.89 (intra H ^N - C1)/ 1.11 (intra H ^N - C4) / 0.62 (H ^α -C4) / 1.32 (seq H ^N -C4)		
motion [45]	-0.15; 0.35 (fast)				2.1 (slow)		
motion [87]	-0.55; 0.63 (fast)	-0.19; 0.77 (slow)			-0.76; 1.93 (slow)		
motion [85]	-0.20 ; 0.20 (fast)	-0.20 ; 0.90 (slow)			-0.70 ; 2.10 (slow)		
motion [86]	0.40 (fast)	0.70 (slow)	1.50 (fast, slow)		2.00 (slow)	0.70 (slow)	0.40 (fast)

^a Recommended corrections are indicated in bold numbers. If no more than three amino acid types contain the pseudo atom they are indicated in one-letter code. For distances between two pseudo-atoms it is recommended to sum the individual corrections.

^b If two values are listed separated by a semicolon, the first and the second values are the corrections to the lower and upper limit, respectively.

^c The models are identified by the type of motion assumed (rigid, fast, slow) and by the partner proton to which the distance is calculated (if any specific atom is used). References are indicated.

It is noteworthy that it has been shown that direct structural refinement over the distances between all individual atoms in a group puts narrower restraints on these groups [86]. However, this approach is only feasible with $\langle r^{-6} \rangle$ averaging and fast motion may be treated incorrectly.

2.8.3. Autorelaxation rate constants

As previously pointed out, the accuracy of the autorelaxation rate constant is less critical, as the analysis either does not require a model or approximate values are sufficient. Given the difficulty of choosing the appropriate molecular geometry required in equation 13.1, motional effects are of secondary nature. It is recommended to estimate the rate constants with the rigid model and isotropic tumbling. Since the CSA contribution is dominated by dipolar relaxation, R_i^{CSA} (equations 14.2) and R_i^{leak} may be set to zero. Alternatively, R_i^{leak} is sometimes set to a value between 0.5 and 2 s⁻¹. The relevant term in the autorelaxation rate constant is

$$R_{ij}^{\text{D}} = \left(\frac{\mu_0}{4\pi} \right)^2 \frac{\gamma^4 \hbar^2}{10} \frac{1}{(r_{ij}^{\text{rigid}})^6} \left[J_{ij}^{\text{D,rigid}}(0) \right] = \left(\frac{\mu_0}{4\pi} \right)^2 \frac{\gamma^4 \hbar^2}{10} \frac{\tau_c}{(r_{ij}^{\text{rigid}})^6} = 56.94 \frac{\tau_c / \text{ns}}{(r_{ij}^{\text{rigid}} / \text{\AA})^6} \text{ s}^{-1} \quad (69)$$

One exception to this approach is the dipolar autorelaxation within groups of equivalent spins. If the motion within the group is fast, the according order parameter may be included. In practice, the only relevant case for macromolecules is the methyl group. The fluctuation of the c3 axis is assumed to be rigid but the proton rotation around it is treated as implied in equations 42 and 43:

$$\begin{aligned}
R_i^{\text{D,methyl}} &= \left(\frac{\mu_0}{4\pi} \right)^2 \frac{\gamma^4 \hbar^2}{5} \frac{1}{(r_{\text{methyl}})^6} \sum_{p=-2}^2 \left(\frac{3\tau_p}{1+(\omega_i \tau_p)^2} + \frac{12\tau_p}{1+(2\omega_i \tau_p)^2} \right) \frac{C_{\text{int},p}^{\text{D}(\vec{i}),\text{methyl},\text{c3},\text{rigid}}}{4} \\
&\approx \frac{1.22 \cdot 10^5}{(\omega_i / 2\pi \text{MHz})^2} \sum_{p=-2}^2 \frac{C_{\text{int},p}^{\text{D}(\vec{i}),\text{methyl},\text{c3},\text{rigid}}}{(\tau_p / \text{ns})} \text{s}^{-1}
\end{aligned} \tag{70}$$

It has been used that $1+(\omega_i \tau_p)^2 \approx (\omega_i \tau_p)^2$ for macromolecules at fields typical in practice.

Isotropic tumbling simplifies the expression to

$$\begin{aligned}
R_i^{\text{D,methyl}} &= \left(\frac{\mu_0}{4\pi} \right)^2 \frac{\gamma^4 \hbar^2}{5} \frac{1}{(r_{\text{methyl}})^6} \left(\frac{3\tau_c}{1+(\omega_i \tau_c)^2} + \frac{12\tau_c}{1+(2\omega_i \tau_c)^2} \right) \frac{1}{4} \\
&\approx \frac{1.22 \cdot 10^5}{(\omega_i / 2\pi \text{MHz})^2 (\tau_c / \text{ns})} \text{s}^{-1}
\end{aligned} \tag{71}$$

Again, the rate constant is easily obtained in units of s^{-1} if the correlation times are inserted in units of nanoseconds and the Larmor frequency in units of 2π MHz (e.g., for a polarizing field of 700 MHz, $\omega = 2\pi \cdot 10^6 \cdot 700 \text{ s}^{-1}$, and $(\omega / 2\pi \text{MHz}) = 700$).

The autorelaxation rate induced by dipolar interaction within the spin group is much weaker than those induced by interaction with remote spin because the spectral density functions do not sample the zero frequencies. It is therefore reasonable to neglect the contributions from equations 67 and 68 in reasonably large molecules.

2.8.4. Continuous distance distributions

The order parameters as defined above are all model-free in the sense that they do not rely on a physical model [71,72]. Although rare for NOE data, some models have been introduced to relate NOEs to realistic dynamical events. The Markley group proposed a method to derive a

continuous probability distribution of rotamers from a combination of scalar couplings and NOEs (CUPID) [88,89]. The distribution is expressed by means of truncated Fourier series (periodic functions of cosine and sine functions).

Another way of interpretation of a continuous distance distribution is the determination of the distribution radius of a disordered group [90]. In this model, one spin is assumed to be in a rigid part of a molecule and a second spin is located in a disordered part with a uniform spherical distribution centered r_{ij}^{rigid} away from the first spin with radius R_p . The order parameter for fast motion is related to the somewhat different order parameter used by Iwahara and Clore ($S^{\text{D}(ij),\text{IC}}$)² as

$$\left(S^{\text{D}(ij),\text{exp}}\right)^2 = \left\langle \frac{1}{r_{ij}^6} \right\rangle \left(r_{ij}^{\text{rigid}}\right)^6 \left(S^{\text{D}(ij),\text{IC}}\right)^2 \quad (72)$$

It can be shown that the r^{-6} averaged distance is

$$\left\langle \frac{1}{r_{ij}^6} \right\rangle = \frac{1}{\left(r_{ij}^{\text{rigid}}\right)^6 \left(1 - \left(R_p / r_{ij}^{\text{rigid}}\right)^2\right)^3} \quad (73)$$

By expressing $\left\langle \frac{1}{r_{ij}^6} \right\rangle$ and $\left(S^{\text{D}(ij),\text{IC}}\right)^2$ as functions of r_{ij}^{rigid} and R_p , it follows that expression 72 is

1. The spectral density function then becomes

$$\begin{aligned} J^{\text{D}(ij)}(\omega) &= \left(S^{\text{D}(ij),\text{fast}}\right)^2 \frac{\tau_c}{1 + (\tau_c \omega)^2} + \left(\left(r_{ij}^{\text{rigid}}\right)^6 \left\langle \frac{1}{r_{ij}^6} \right\rangle - \left(S^{\text{D}(ij),\text{fast}}\right)^2 \right) \frac{\tau_{\text{eff}}}{1 + (\tau_{\text{eff}} \omega)^2} \\ &= \left[\frac{\tau_c}{1 + (\tau_c \omega)^2} + \left(\frac{1}{\left(1 - \left(R_p / r_{ij}^{\text{rigid}}\right)^2\right)^3} - 1 \right) \frac{\tau_{\text{eff}}}{1 + (\tau_{\text{eff}} \omega)^2} \right] \end{aligned} \quad (74)$$

Note that the spectral density function contains $(r_{ij}^{\text{rigid}})^{-6}$ as a prefactor in reference [90]. If r_{ij}^{rigid} and R_p become comparable the $J(2\omega)$ term is not negligible. In practice, the methodology was developed for the NOE between an unpaired electron of a paramagnetic center and a proton.

2.8.5. Expressions for molecular dynamics simulations

It is common to compare experimental results with molecular dynamics simulations. Sometimes, NOEs are also used to generate restraints r_{ij}^{exp} for MD simulations by including a NOE term in the force field, V_{ij}^{NOE} , as (in its simplest form)

$$\begin{aligned} V_{ij}^{\text{NOE}}(r_{ij}^{\text{MD}}) &= \frac{1}{2} K^{\text{NOE}} (r_{ij}^{\text{MD}} - r_{ij}^{\text{exp}})^2 && \text{if } r_{ij}^{\text{MD}} > r_{ij}^{\text{exp}} \\ V_{ij}^{\text{NOE}}(r_{ij}^{\text{MD}}) &= 0 && \text{if } r_{ij}^{\text{MD}} \leq r_{ij}^{\text{exp}} \end{aligned} \quad (75)$$

with the force constant K^{NOE} . More sophisticated forms may have linear dependencies for large violations or avoid forth-power terms [91,92], or the back-calculated values are forced not to be in worse agreement than the best previous ones such that they eventually approach the experimental values [93,94]. Since the trajectories contain time-ordered snapshots of the structure the correct prediction of NOEs from MD must be made with correct averaging. The simplest averaging procedure is the discrete $\langle r^{-6} \rangle$ averaging:

$$r_{ij}^{\text{MD}} = \left(\sum_{a=1}^N \frac{1}{r_{ij,a}^6} \right)^{-1/6} \quad (76)$$

We have previously also employed the $\langle r^{-3} \rangle$ averaging including the angular dependence [33]

$$r_{ij}^{\text{MD}} = \left(\sum_{a=1}^N \frac{1}{r_{ij,a}^3} \sum_{b=1}^N \frac{P_2(\cos \vartheta_{\text{int},ab}^M)}{r_{ij,b}^3} \right)^{-1/6} \quad (77)$$

where a and b run over the N structures in the MD set, P_2 is the Legendre polynomial of second order and $\vartheta_{\text{int},ab}^M$ denotes the projection angle between the two internuclear vectors.

It has been proposed to use a memory function with a characteristic decay time τ_{mem} [95].

$$r_{ij}^{\text{MD}}(t) = \left(\frac{1}{\tau_{\text{mem}}} \int_0^t e^{-t'/\tau_{\text{mem}}} [r_{ij}(t-t')]^{-q} dt' \right)^{-1/q} \quad (78)$$

where q is either 3 or 6. Not surprisingly, structure refinements on test data sets have shown that time-averaged methods lead to truer pictures of conformational sampling [96]. As typical MD trajectories are no longer than a few nanoseconds a single copy of the molecule is likely not to sample the complete conformational space. In that case, the averaging can be carried out over multiple copies of the molecule [97-99]. The van Gunsteren group combined equations 76-78 with ensemble averaging [91]:

$$r_{ij}^{\text{MD}(\text{time,space})}(t) = \left(\frac{1}{\tau_{\text{mem}}} \int_0^t e^{-t'/\tau_{\text{mem}}} [\langle r_{ij}(t-t') \rangle]^{-q} dt' \right)^{-1/q} \quad (79)$$

The ensemble averaging is Boltzmann-weighted ideally with the free energy. Practically, it is easier to use the potential energy also averaged with a short memory function.

It is often more convenient to write the correlation function as an expression of cartesian coordinates [100]:

$$C(t) = \frac{1}{6} \left\langle \frac{1}{r^5(0)r^5(t)} \left(\begin{aligned} & \left((3x^2(0) - r^2(0))(3x^2(t) - r^2(t)) + (3y^2(0) - r^2(0))(3y^2(t) - r^2(t)) \right) \\ & + (3z^2(0) - r^2(0))(3z^2(t) - r^2(t)) \\ & + 9xy(0)xy(t) + 9xz(0)xz(t) + 9yz(0)yz(t) \end{aligned} \right) \right\rangle \quad (80)$$

3. Extraction of exact NOE rates

In this chapter, the various procedures to extract exact NOE rates constants are discussed. In practice, it turned out that the most successful approaches depend on iterative protocols where preliminary values of the NOE rate constants are used to calculate preliminary structures. These, in turn, are used to back-predict theoretical NOEs which are used to improve the experimentally obtained values. Obviously, the extraction of the NOE rate constants is intertwined with the structure calculation and in the following subchapters it is attempted to present the methods as clearly as the complexity allows. In addition, it is difficult to separate biological applications from the methodical aspects as no standard protocol has emerged and each application required rethinking of the method.

3.1. Spin diffusion

All approaches to extract exact cross-relaxation rate constants make use of the simplifications inherent to the Solomon equations presented in equation 24 (which may be extended by equation 26 if exchange causes appearance of additional peaks). For a N -spin 1/2 system, a 2D NOESY pulse sequence element produces in principle $N \times N$ peaks of which N are diagonal peaks and $N \times (N-1)$ are cross peaks. The evolution of the matrix $I(t)$ containing the volumes or intensities of these peaks (not to be confused with magnetization operators) is obtained from equation 24 [19].

$$\frac{d}{dt}I(t) = -RI(t) \quad (81)$$

where the intensity matrix is

$$I(t) \equiv \begin{pmatrix} I_{11}(t) & I_{12}(t) & \cdot & I_{1i}(t) & \cdot & I_{1N}(t) \\ I_{21}(t) & I_{22}(t) & & & & \cdot \\ \cdot & & & & & \cdot \\ I_{i1}(t) & & & I_{ii}(t) & & I_{iN}(t) \\ \cdot & & & & & \cdot \\ I_{N2}(t) & \cdot & \cdot & I_{Ni}(t) & \cdot & I_{NN}(t) \end{pmatrix} \quad (82)$$

At $t = 0$, all off-diagonal elements are zero and the diagonal elements are the intensities at the outset of the NOESY mixing period.

$$R \equiv \begin{pmatrix} \rho_1 & \sigma_{12} & \cdot & \cdot & \cdot & \sigma_{1N} \\ \sigma_{12} & \rho_2 & \cdot & \cdot & \cdot & \sigma_{2N} \\ \cdot & \cdot & & & & \cdot \\ \cdot & \cdot & & & & \cdot \\ \cdot & \cdot & & & & \cdot \\ \sigma_{1N} & \sigma_{2N} & \cdot & \cdot & \cdot & \rho_N \end{pmatrix} \quad (83)$$

In what follows R designates the relaxation matrix of the differential equation in the reduced space spanned by longitudinal single-order operators. The formal solution is obviously

$$I(t) = I(0)e^{-Rt} \quad (84)$$

and R is obtained from

$$R = \frac{\ln \left[I(t)(I(0))^{-1} \right]}{-t} \quad (85)$$

Many approaches have been proposed to obtain the exact cross-relaxation rate constants. It has been recognized early on that peak intensities are not only modified by direct magnetization transfer but also by transfer via a third or more spins [27,74,101]. These transfer pathways are

obtained from the second and higher orders of a Taylor expansion of the exponent in equation 84 [79].

$$I(t) = \left[1 - Rt + \frac{1}{2} R^2 t^2 + \dots \right] I(0) \quad (86)$$

The first two terms describe the linear-regime buildup. The third is the second-order term of the series:

$$\left[\frac{1}{2} R^2 t^2 \right]_{ij} = \frac{t^2}{2} \sum_{k=1}^N R_{ik} R_{kj} \quad (87)$$

The diagonal contribution is

$$\left[\frac{1}{2} R^2 t^2 \right]_{ii} = \frac{t^2}{2} \sum_{k=1}^N R_{ik} R_{ki} = \frac{t^2}{2} \sum_{k=1}^N R_{ik}^2 = \frac{t^2}{2} \left(\rho_i^2 + \sum_{\substack{k=1 \\ i \neq k}}^N \sigma_{ik}^2 \right) \quad (88)$$

The second term denotes magnetization that is transferred to neighboring spins and immediately brought back to the original spin. The contribution to cross peaks is obtained from $i \neq j$:

$$\left[\frac{1}{2} R^2 t^2 \right]_{ij} = \frac{t^2}{2} \sum_{k=1}^N R_{ik} R_{kj} = \frac{t^2}{2} \left(\sigma_{ij} (\rho_i + \rho_j) + \sum_{\substack{k=1 \\ k \neq i, j}}^N \sigma_{ik} \sigma_{kj} \right) \quad (89)$$

The first two terms denote magnetization that is transferred directly with a damping due to autorelaxation of both spins. The third term is spin diffusion via one additional spin. This contribution to the cross peaks is very effective in NOESYs recorded on macromolecules. In particular, the need for a sufficient number of cross peaks often requests that the mixing times are chosen such that the buildup deviates far from the initial linear trend. To obtain exact cross-relaxation rate constants, spin diffusion must be accounted for. In principle, 3D NOE-NOE spectroscopy allows one to dissect spin diffusion to some extent [102,103] and may even be used

for an assignment strategy without isotope labeling [104]. However, spin diffusion should be accounted for at all times during mixing to obtain reliable results.

Most commonly, a full-matrix approach is used that converts spectral peak volumes or intensities recorded with a single NOESY mixing period into cross-relaxation rate constants by finding the solution of equation 84. At first glance, this appears the most elegant approach since it accounts correctly for spin diffusion. Indeed, it has been demonstrated in numerous publications that the cross-relaxation rate constants (and the distances) obtained from this approach are more accurate than those obtained from an isolated two-spin approximation (ISPA) [4,77,105,106]. There are, however, practical complications. For a macromolecule, the intensities of a majority of the cross peaks are weaker than the spectral noise level. In addition, many peaks are overlapped. In either case, I cannot be fully determined. The only way to correct for this is to supplement I with elements estimated from a preliminary structure obtained from conventional structure calculation methods. Also, it is difficult, if possible at all, to follow the propagation of errors (experimental errors, or those due to lack of data) because the complete system must be treated in one step of calculation. The calculation also requires a symmetric I matrix which usually requires extensive modification of the original experimental cross peak intensities. In our experience, it turned out that a non-linear ISPA with subsequent corrections for spin diffusion estimated with a full-matrix approach is superior in practice. On one hand, the data evaluation is straight-forward and all NOEs can be analyzed in an individual manner. On the other hand, iterative application converges to the solution of the complete full-matrix calculation. A study comparing a simpler non-linear ISPA to the full-matrix approach applied to simulated NOEs for the 21-residue endothelin arrived at similar conclusions [107]. An additional advantage is that the approach can easily take partial deuteration of the sample into account. In the following, the original full-matrix approach, an alternative full-matrix approach based on direct refinement against

intensities and the non-linear ISPA with correction for spin diffusion are discussed. Since the later is novel and used by our laboratory it is discussed in more detail.

3.2. Full relaxation-matrix approach

Because the relaxation matrix R is symmetric (asymmetry due to pseudo atoms is neglected), the evolution of the peak intensities can be calculated by means of matrix diagonalization [27,108]:

$$I(t) = U_R e^{-D_R t} U_R^{-1} I(0) \quad (90)$$

where the diagonal matrix containing the eigenvalues of the relaxation matrix R is

$$D_R = U_R^{-1} R U_R \quad (91)$$

and U_R contains the eigenvectors. For example, the program CORMA (COmplete Relaxation Matrix Analysis) is based on this calculation [4]. Rather than extracting the rate constants, structural models may then be used to predict intensities (*vide infra*) [108].

An alternative approach for prediction of the intensity matrix is to split the mixing time into sufficiently short intervals δt and to apply the following operation iteratively [109,110]:

$$I(t + \delta t) = (1 - R\delta t) I(t) \quad (92)$$

This method was slightly faster than the diagonalization approach in the specific application of reference [109] and yields intensities at intermediate times which may be useful in their own right.

Various algorithms for numerical integration have been compared [111]. It has been demonstrated that the Taylor series algorithm is superior to the Euler, the midpoint, and the fourth-order Runge-Kutta algorithms because NOE buildups are smooth curves. On the other hand, the Padé approximation with scaling and squaring, which is frequently used in computation algorithms due to its superiority over the Taylor approximation in the calculation of exponentials, has also been used [112]. It has also been pointed out that cross-relaxation rate constants between spins which are separated by more than a cutoff distance may be set to zero [113]. The complexity of the problem then reduces from N^3 to Nn_{cutoff}^2 , where n_{cutoff} is the average number of the spins within the cutoff.

A slightly different diagonalization has been proposed to directly read out the relaxation matrix R from a NOESY spectrum [74].

$$R = \frac{U_I \ln[D_I] U_I^{-1}}{-t} \quad (93)$$

where the diagonal matrix contains the eigenvalues of $I(t)(I(0))^{-1}$:

$$D_I = U_I^{-1} \left[I(t)(I(0))^{-1} \right] U_I \quad (94)$$

and U_I contains the eigenvectors. In practice, most cross peaks are so weak that they disappear in the noise and their intensities must be set to zero.

3.2.1. Iterative hybrid relaxation matrix approach with restrained MD/DG

A substantial leap forward constitutes the procedure underlying the IRMA (*Iterative Relaxation Matrix Approach*) program [76,114]. At the start, the intensity matrix I is constructed from R which is estimated from a preliminary structure by using equation 84. Then, the off-diagonal elements for which the according intensity can be extracted from a NOESY experiment are replaced by those. This hybrid matrix is diagonalized to obtain an updated R matrix using equation 93. R is converted into distance constraints and used for a structure refinement by restrained molecular (rMD) simulation (it is pointed out that distance geometry (DG) approaches may be used instead). An iteration of these steps is carried out until convergence is achieved. The results of different mixing times are averaged. The strong diagonal peaks are treated purely theoretically (the leakage contribution is also considered in later versions). More recent versions of the program also consider local mobility such as methyl rotation and ring flips and order parameters of fast motion obtained from MD simulations. A stereospecific assignment of methylene protons is also included [115]. A slightly improved procedure predicts R from a bundle of structures rather than from a single structure (so-called "Ensemble" IRMA) [115]. This procedure, however, should not be confused with the calculation of a structural ensemble satisfying experimental rates on average and thus reflecting the true spatial sampling (*vide infra*). At least at the initial development stage, the upper and lower distance constraints were obtained from comparison to a NOE with a calibration distance [76]. Another problem is that back-calculation of R from I may generate negative eigenvalues [81,116]. Then, the logarithm in equation 93 is inhibited and the eigenvalues may be set to zero or slightly positive values. Difficulties arising from the matrix diagonalization or from the propagation of experimental errors have been discussed [81].

A similar procedure has been proposed by Summers et al. [117]. The differences are that distance geometry (DG) instead of rMD is used in each cycle (DSPACE program) and the intensity matrix is calculated by numerical integration (BKCALC and GNOE programs). There is also a stronger focus on the inclusion of leakage terms.

3.2.2. *Direct iterative hybrid relaxation matrix approach*

MARDIGRAS (*Matrix Analysis of Relaxation for DIscerning GeometRY of an Aqueous Structure*) is an approach which is very similar to IRMA [116]. I is calculated with the CORMA (*COmplete Relaxation Matrix Analysis*) program. The difference is that instead of running a computationally expensive rMD in every cycle, it directly enforces internal consistency for the diagonal and off-diagonal elements of R . Another program that employs the same approach is MORASS (*Multispin or, alternately, Multiple Overhauser Relaxation Analysis and Simulation*) [81,118,119].

3.2.3. *Other programs*

CROSREL (*CROsSs RELaxation*) calculates intensities or fits experimental data with full relaxation analysis by optimizing the correlation time or the diffusion tensor and the leakage term [120]. It is the first program to also analyze ROESY spectra with a full-relaxation matrix approach by including corrections for offset effects and J-coupling transfers ("HOHAHA"). It offers two alternatives to scaling of the cross-peak intensity by diagonal peak intensities extrapolated to zero mixing time. Either, it scales the cross-peak intensity by the diagonal-peak

intensity in the same spectrum if only one mixing time is recorded, or by minimizing the difference between calculated and experimental intensities. The latter surely yields poorer values for the cross-relaxation rate constants but does not require diagonal peaks which are typically severely overlapped.

The program FIRM (*Full Iterative Relaxation Matrix*) calculates NOE intensities and refines structures based on the hybrid matrix method [85]. Test structures were calculated with DIANA and molecular mechanics (MM)/MD with AMBER from simulated NOE sets.

A program similar to MARDIGRAS, MIDGE (*Model-Independent Distance GEneration*) has been shown to converge independently of any starting structure [121]. Initial off-diagonal and diagonal values of a normalized intensity matrix I which are not determined experimentally may be set to 0 and any value between 0 and 1, respectively. During the iteration, diagonal elements are recalculated from off-diagonal elements.

In a simpler approach which is implemented in the program DISCON, linear fits to the buildup curve are corrected for the second-order spin diffusion in an iterative manner [107,122].

3.2.4. Inclusion of intermolecular exchange

The most extreme and complex exchange effects on NOEs occur in complexes between proteins, nucleic acids and ligands [16,17]. Thus, the NOE is an attractive tool to observe such intermolecular interactions [7,10]. Given the complexity of the underlying equations (see paragraph 2.4), full-matrix approaches including relaxation and conformational exchange are commonly used to get qualitative or semi-quantitative results. Although not of primary interest in this review, it is pointed out that these techniques rely on the same framework as presented here

and a large body of literature is dedicated to them [6,11,25,26,51,123-129]. The analysis is carried out on the atoms forming the binding pocket/surface and the ligand atoms by use of 2D transferred NOE experiments and saturation transfer difference (STD) experiments. The programs CORCEMA (*COmplete Relaxation and Conformational Exchange MAtrix*), CORCEMA-ST and SICO (*STD-NMR Intensity-restrained CORCEMA Optimization*) can predict according intensities and refine torsion angles of the bound ligand [130-132]. A similar program is CORONA (*Calculated OR Observed NOESY Analysis*) [133]. These programs offer more options for detailed treatment of exchange phenomena than the previously discussed programs written for the use of single structure calculation.

3.3. Structure refinement against NOESY intensities

Rather than extracting the rate constants and generating distance constraints, structural models may be directly refined against NOESY intensities. Initial attempts were based on trial-and-error procedures [108].

The first software which is based on direct optimization of NOESY intensities is COMATOSE (*COmplete Matrix Analysis Torsion Optimized Structure*) which is only designed for the application to nucleic acids [134]. COMATOSE actually predates MARDIGRAS written by the same group. It is based on an iterative least-square refinement of structures yielding CORMA intensities. The following residuals are minimized

$$\Delta^2 = \sum [I_{\text{exp}} - kI_{\text{calc}}]^2 \quad (95)$$

where k is a constant scaling factor applied to all the calculated intensities. This form does not focus on the impact of the shortest distances. To reduce the problem complexity and the number

of adjustable parameters, the conformation is defined by a limited set of torsion angles, sugar pucker parameters and residue coordinates and orientations. A problem with the approach is that as a least-squares minimizing routine, it is susceptible to getting trapped in local minima. It also uses a large amount of computer memory (which may be less of a problem nowadays).

More sophisticated structural refinement is carried out by restrained MD (rMD) calculations or distance geometry (DG), where one term of the penalty function is the intensity violation expressed in equation 95 [80,135,136]. The gradient of the penalty function provides the force constant. The derivative of the intensity I_{calc} of the cross peak between spins i and j with respect to the coordinates of atom μ can then be expressed as [135]

$$\frac{\partial_{\mu} (I_{\text{calc}})_{ij}}{\partial_{\mu} (R)_{kl}} = \sum_{r,u} U_{R,ir} U_{R,rk}^{-1} U_{R,lu} U_{R,uj}^{-1} \left[\frac{e^{-D_{R,rr}\tau_{\text{mix}}} - e^{-D_{R,uu}\tau_{\text{mix}}}}{D_{R,rr} - D_{R,uu}} \right] \quad (96)$$

A computationally more efficient method of finding the left-hand side of equation 96 is [137]:

$$\frac{\partial_{\mu} (I_{\text{calc}})_{ij}}{\partial_{\mu} (R)_{kl}} = - \int_0^{\tau_{\text{mix}}} e^{-R(\tau_{\text{mix}}-s)} e^{-R s} ds \quad (97)$$

A variant of equation 96 allows the derivatives of I_{calc} with respect to any variable [138]. Such variables could be related to the dynamics of the molecules, for example, $(S^{D(ij),\text{fast}})^2$ and τ_{int} .

An expression for the derivative in the dihedral angle space has also been derived and implemented in CIANA [139].

Another software for direct structure refinement against intensities is DINOSAUR (*D*irect *N*Oe *S*imulation *A*pproach for *U*nbelievable structure *R*efinement) which is based on IRMA and is also able to run time- and ensemble-averaged restrained MD simulations [99].

3.4. Non-linear ISPA with correction for spin diffusion

In the first step, all spin pairs giving rise to a cross peak are assumed to form a two-spin system i - j . The exact analytical solution of equation 84 is then [33]:

$$\frac{I_{ii}(t)}{I_{ii}(0)} = \frac{1}{2} \left[\left(1 - \frac{\rho_i - \rho_j}{\lambda_+^{\text{NOE}} - \lambda_-^{\text{NOE}}} \right) e^{-\lambda_-^{\text{NOE}} t} + \left(1 + \frac{\rho_i - \rho_j}{\lambda_+^{\text{NOE}} - \lambda_-^{\text{NOE}}} \right) e^{-\lambda_+^{\text{NOE}} t} \right] \quad (98.1)$$

$$\frac{I_{jj}(t)}{I_{jj}(0)} = \frac{1}{2} \left[\left(1 + \frac{\rho_i - \rho_j}{\lambda_+^{\text{NOE}} - \lambda_-^{\text{NOE}}} \right) e^{-\lambda_-^{\text{NOE}} t} + \left(1 - \frac{\rho_i - \rho_j}{\lambda_+^{\text{NOE}} - \lambda_-^{\text{NOE}}} \right) e^{-\lambda_+^{\text{NOE}} t} \right] \quad (98.2)$$

$$\frac{I_{ij}(t)}{I_{ii}(0)} = \frac{I_{ji}(t)}{I_{jj}(0)} = \frac{-\sigma_{ij}}{\lambda_+^{\text{NOE}} - \lambda_-^{\text{NOE}}} \left[e^{-\lambda_-^{\text{NOE}} t} - e^{-\lambda_+^{\text{NOE}} t} \right] \quad (99)$$

with

$$\lambda_{\pm}^{\text{NOE}} = \frac{(\rho_i + \rho_j)}{2} \pm \sqrt{\left(\frac{\rho_i - \rho_j}{2} \right)^2 + \sigma_{ij}^2} \quad (100)$$

For practical purposes, equations 98.1 and 98.2 are approximated by a single-exponential decay [33]:

$$\frac{I_{ii}(t)}{I_{ii}(0)} = e^{-\rho_i t} \quad (101.1)$$

$$\frac{I_{jj}(t)}{I_{jj}(0)} = e^{-\rho_j t} \quad (101.2)$$

The expression is now independent of the autorelaxation rate of the other spin and of the cross-relaxation rate.

The extraction of the cross relaxation rates is now carried out in three distinct steps (see Figure 3) [33,112]. In the following, the solutions given in equations 99 and 101 are written as transfer functions T^{NOE} and are generalized to (possibly) groups of magnetically equivalent spins.

First, the autorelaxation rate of spin \vec{i} , $\rho_{\vec{i}}$, and the intensity at zero mixing time, $I_{\vec{ii}}(0)$, is obtained from a two-parameter fit to the diagonal-peak decay. Similarly, $\rho_{\vec{j}}$ and $I_{\vec{jj}}(0)$ are obtained.

$$I_{\vec{ii}}(t) = T_{\vec{ii}}^{\text{NOE}}(t)I_{\vec{ii}}(0) \quad (102.1)$$

$$I_{\vec{jj}}(t) = T_{\vec{jj}}^{\text{NOE}}(t)I_{\vec{jj}}(0) \quad (102.2)$$

Then, the cross-relaxation rate between spins \vec{i} and \vec{j} , $\sigma_{\vec{ij}}$, is obtained by inserting $I_{\vec{ii}}(0)$, $\rho_{\vec{i}}$ and $\rho_{\vec{j}}$ into the equation describing the cross-peak buildup with initial magnetization on spin \vec{i} , and $I_{\vec{jj}}(0)$, $\rho_{\vec{j}}$ and $\rho_{\vec{i}}$ into the one describing the cross-peak buildup with the initial magnetization on spin \vec{j} , respectively:

$$I_{\vec{ij}}(t) = N_{\vec{j}}T_{\vec{ij}}^{\text{NOE}}(t)I_{\vec{ii}}(0) \quad (103.1)$$

$$I_{\vec{ji}}(t) = N_{\vec{i}}T_{\vec{ji}}^{\text{NOE}}(t)I_{\vec{jj}}(0) \quad (103.2)$$

The multiplicities of magnetically equivalent spins $N_{\vec{j}}$ and $N_{\vec{i}}$ must be included if the initial magnetization is transferred to a group of equivalent spins. On the other hand, if the magnetization starts on a group of equivalent spins, the extracted cross-relaxation rate is not affected because the intensities on either side of 103.1 and 103.2 are accordingly scaled.

Although not further discussed here, it has been proposed to replace $I_{\vec{ii}}(0)$ and $I_{\vec{jj}}(0)$ by the average of $I_{\vec{ii}}(t)$ and $I_{\vec{jj}}(t)$ in equations 103.1 and 103.2 [140]. The advantage is that one does not have to record spectra with multiple mixing times and extrapolate the diagonal intensities to the zero time point. Also, the transfer functions are modified such that the autorelaxation modulation is relegated to the diagonal peak intensities. The major drawback is that, as soon as the two initial diagonal peak intensities are not equal, the approach produces large errors.

We have shown that the impact of relayed magnetization via neighbour spins on the two-spin solution for the cross relaxation can be kept relatively small in practice [33]. It is, however, in general not completely negligible. Thus, in a third step, we calculate the relative contribution from the neighbor spins on the apparent cross-relaxation rate and expressed it as a correction factor p to the apparent rates. A previously known approximate structure is used and the final cross-relaxation rate is obtained as:

$$\sigma_{ij} = p_{ij} \sigma_{ij}^{\text{app}} \quad (104)$$

A similar correction factor obtained from a sparse matrix approach was applied to experimental distances in the ARIA program [113].

Alternatively, a correction factor for each spectral intensity at each mixing time can be calculated and an improved cross-relaxation rate is obtained from a new fit:

$$I_{ij}(t) = p_{ij}(t) I_{ij}^{\text{app}}(t) \quad (105)$$

In this case, steps 2 and 3 are reversed since the cross-relaxation rate is fitted after the calculation of the correction factors.

We have developed two different approaches to determine p . In the eNORA (*Exact NOE by Relaxation matrix Analysis*) approach, σ_{ij}^{app} (or I_{ij}^{app}) is calculated with the full relaxation matrix approach described in equation 84 [112]. In the DOMINO (*Diffusion Of Magnetization In NOESY*) approach, individual correction contributions from each neighbor spin k are obtained from the exact solutions of three-spin systems ijk and are then summed up [33,34]. Importantly, this method can also be applied to partially deuterated proteins. Understanding the impact of spin diffusion and the correction is very crucial and is discussed in detail in the following section. While the full matrix approach is perfect in principle and many publications compared the

extracted rates to those obtained from ISPA, the DOMINO approach is new and only an approximation. Thus, this review focuses mainly on DOMINO.

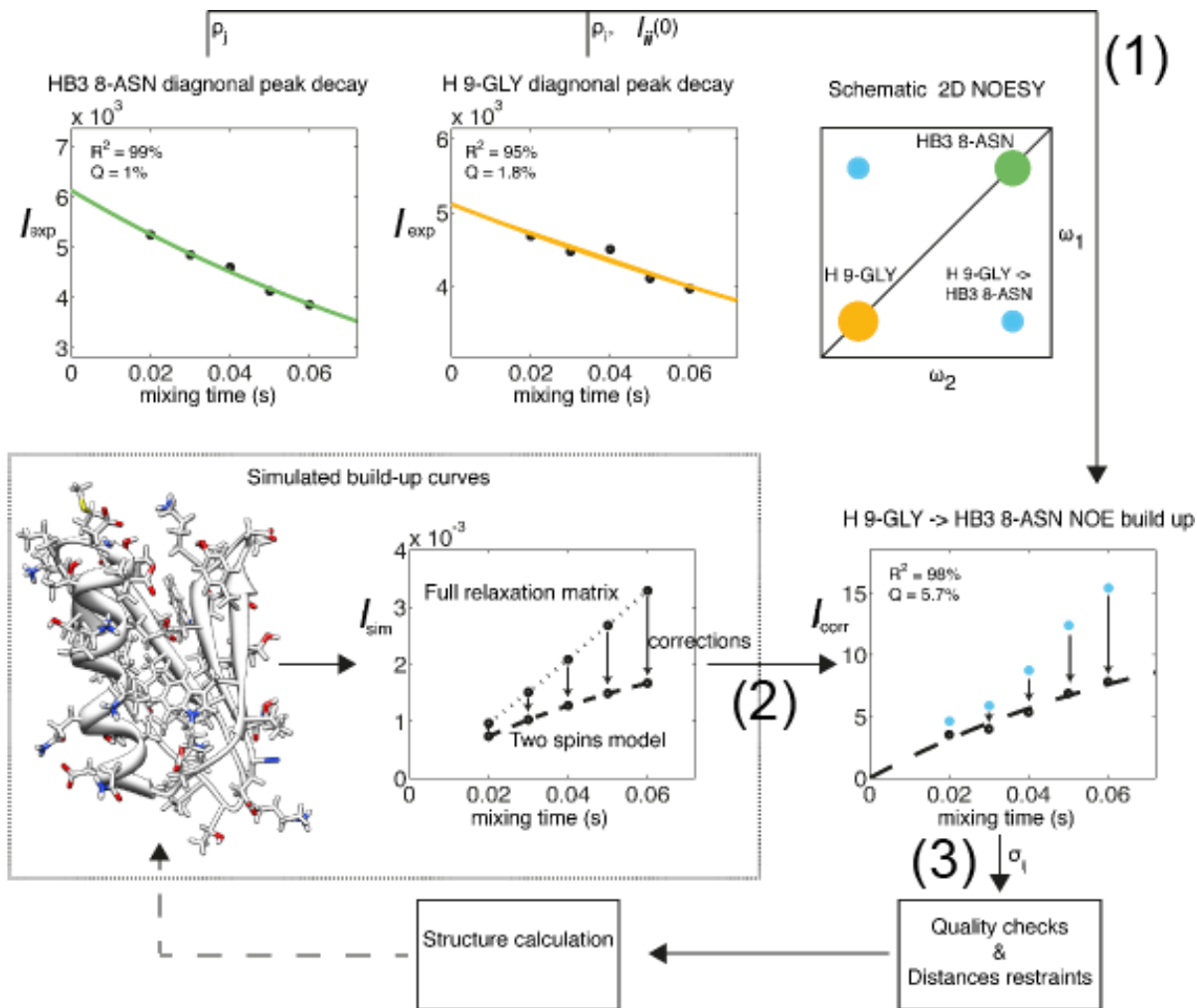


Figure 3. Flow chart outlining the procedure for the determination of eNOE cross-relaxation rates based on the corrections applied to the spectral intensities. As an example, the eNOE originating from the amide H of Gly9 (spin i , orange) and enhancing $H^{\beta 3}$ of Asn8 (spin j , green) of GB3 is shown. (1) The diagonal peak intensities derived from the NOESY spectra are fitted to mono-exponential decay functions to extract the autorelaxation rates, ρ_i , ρ_j , and the initial intensities on spin i , $I_{ii}(0)$. (2) A buildup curve taking into account all magnetization pathways is simulated with the eNORA or DOMINO approach and apparent relaxation rates are determined. The simulation requires previously known 3D structure coordinates as input. Theoretical corrections are applied to the experimental spectral intensities at each mixing time. (3) The NOE buildup is fitted, the quality of the fit is evaluated and distance

restraints are generated. A structure calculation may be performed with the new distance restraints. This structure may be used as an input for (2) in a new cycle as indicated by the broken arrow. Note that steps 2 and 3 are reversed if the correction factors are applied to the apparent cross relaxation rate rather than the intensities. Adapted with permission from Orts, Vögeli and Riek, *J. Chem. Theory Comput.* 8 (2012) 3483-3492. Copyright 2012 American Chemical Society.

Two simpler approaches have also been proposed to account for spin diffusion. In one approach, the linear term of a second-order polynomial fit to the transfer function is used to estimate the cross-relaxation rate constants [80,141]. In the second approach, distances are calculated from comparisons of the cross-relaxation rates corresponding to the distances under investigation and known reference distances at different mixing times. Extrapolation to the zero mixing time should provide distances that are approximately corrected for spin diffusion [80]. These approaches are not considered further here as they are inferior to methods based on *a priori* knowledge of structures.

3.4.1. Correction for spin diffusion

eNORA. In the eNORA routine [112], the diagonal peak intensities derived from the NOESY spectra are fitted to mono-exponential decay functions to extract the auto-relaxation rate constants, ρ_i , ρ_j , and the initial intensities, $I_{ii}(0)$ and $I_{jj}(0)$. Then, cross peak buildup curves are simulated with the full relaxation matrix approach given in equation 84. PDB coordinates of a previously known structure (such as a conventionally determined NMR structure or an X-ray structure) are required. Corrections for the intensities at each mixing time are derived from the simulation and applied to the experimental intensities. The corrected cross-peak buildup curves

are fitted by using ρ_i , ρ_j and $I_{ii}(0)$ and $I_{jj}(0)$ as fixed input parameters and the cross relaxation rate constants σ_{ij} and σ_{ji} as free variables (if the correction is applied to the apparent experimental cross-relaxation rate instead of the intensities σ_{ij} and σ_{ji} are modified accordingly). The quality of the fit is evaluated and σ_{ij} and σ_{ji} are converted into distance restraints r using equation 62. A structure calculation is then performed with the new distance restraints. This new structure may be used again as an input for the next correction calculation and refinement of the structure.

DOMINO. Instead of calculating the simulated intensities via the full relaxation matrix approach, individual correction contributions from each neighboring spin k obtained from the exact (numerical) solution of three-spin systems ijk are summed up [33,34].

$$P_{ij} = \frac{\sigma_{ij}}{\sigma_{ij} + \sum_k (\sigma_{ij}^{\text{app}(k)} - \sigma_{ij})} \quad (106)$$

We have shown that this approach is in agreement with the eNORA approach for a large range of molecular overall tumbling times and NOESY mixing times where the spin diffusion is well traceable. A comparison of the cross-relaxation rates and the effective distances obtained from the eNORA and the DOMINO approach exemplified for spin pairs that were determined experimentally for GB3 [31] is shown in Figure 4. For a molecular tumbling time of ca. 4 ns mixing times as long as 100 ms produce virtually no difference between the methods. The largest systematic disagreement is obtained for NOEs which involve methylene protons. These differences are at least in part caused by different use of the pseudoatoms at the current stage of the programs.

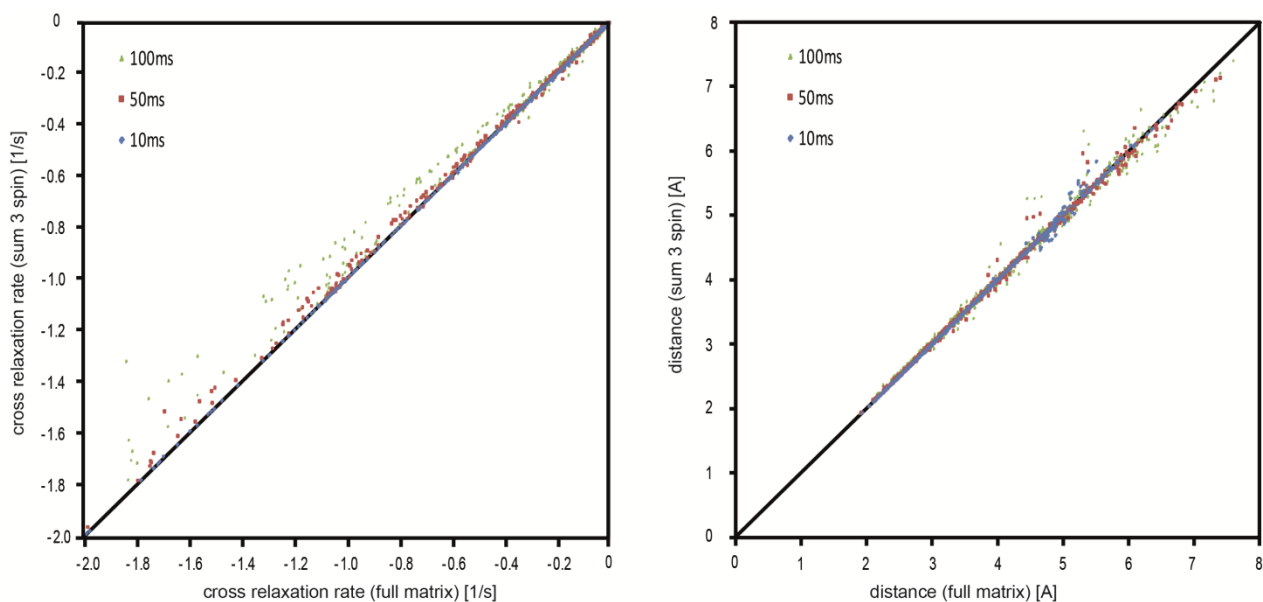


Figure 4. Comparison of the full matrix relaxation approach (eNORA) and the sum of three-spin system approach (DOMINO) in calculating the corrections for spin diffusion for the determination of eNOE-derived distances for the protonated protein GB3. The calculations are based on a proton position-optimized X-ray structure of GB3 [142-144]. Data are shown for spin pairs for which a good NOE buildup fit could be obtained experimentally [31]. In the left panel, the comparison between the correspondingly corrected eNOE rate constants are shown, while in the right panel the derived distances are shown, respectively. All the comparisons are shown for three series of four NOESY spectra with equidistant mixing-time steps simulated with maximal mixing times $t_{\text{mix,max}}$ of 10, 50 and 100 ms. The black lines indicate a slope of 1. The eNORA approach is indicated in the x-axis description as “full matrix”, while the DOMINO approach is indicated as a “sum 3 spins” on the y-axis. Reprinted with permission from Orts, Vögeli and Riek, *J. Chem. Theory Comput.* 8 (2012) 3483-3492. Copyright 2012 American Chemical Society.

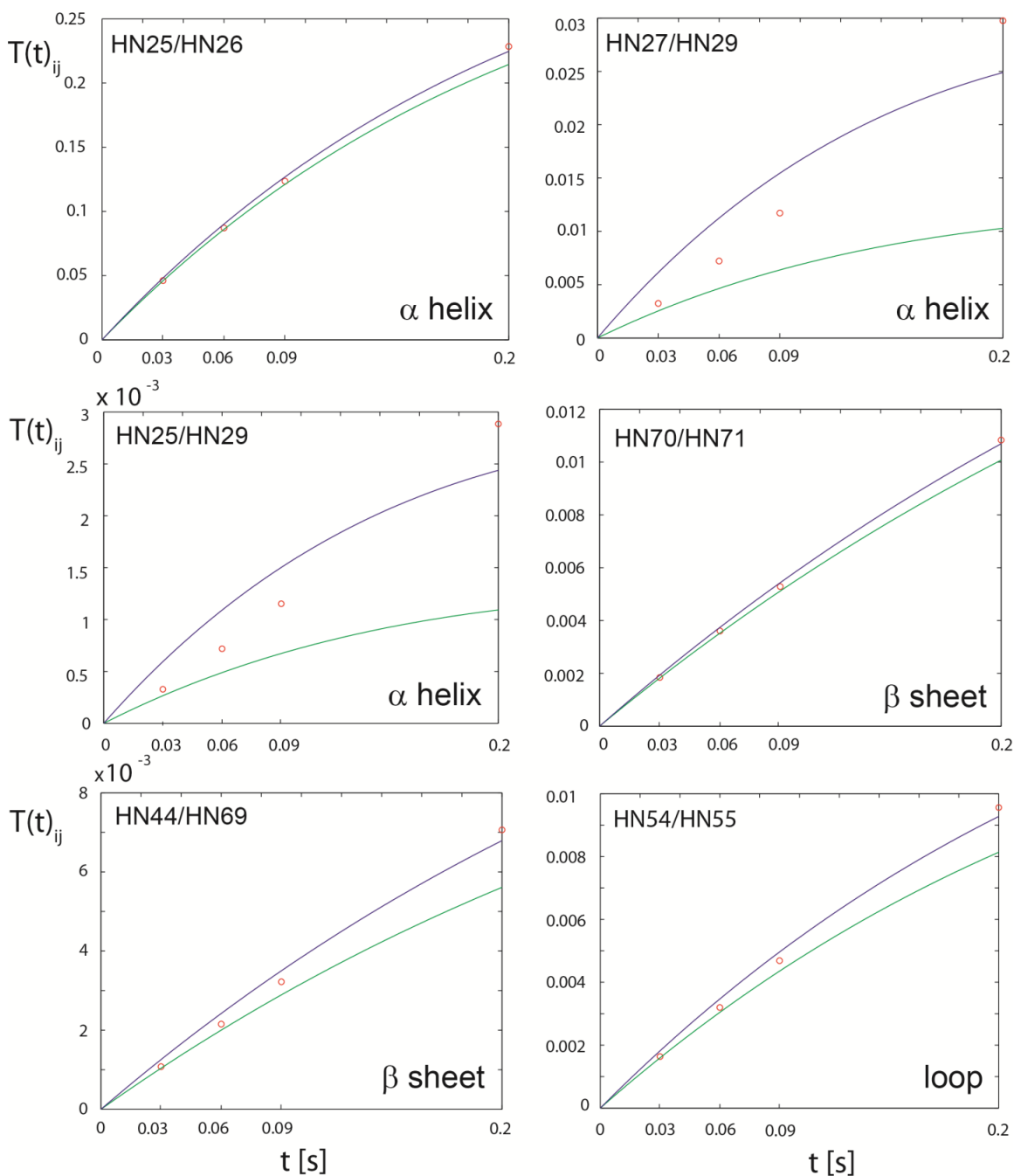


Figure 5. A representative set of simulated NOE buildup curves of perdeuterated ubiquitin is shown during 0.2 s mixing time. The set includes spin pairs from all types of secondary structural elements. The green NOE buildup curves expressed as transfer functions T_{ij}^{NOE} are calculated under the assumption of a two-spin system. Intensities simulated at the mixing times used in the analysis are calculated in presence of spin diffusion pathways via spins that are within 5 Å of both spins in the pair (red circles). Fits through these points assuming a two-spin system are shown as blue curves.

Spin diffusion in (partially) deuterated molecules. Almost all quantitative measurements of NOE buildups were conducted on protonated samples. In practice, this approach is limited to molecules no larger than ca. 35 kDa. To bypass this limitation, samples with partial deuteration are used to reduce spectral overlap and relaxation. We have recently shown that quantitative observation of NOE buildups is also possible in deuterated and perdeuterated samples [33,34]. The Kainosho group estimated across-disulfide bond distances from NOEs between β_2 and β_3 protons in an otherwise deuterated sample without correction for spin diffusion [145]. Even in samples as highly deuterated as 99 % for H^α and 95 % for other carbon-bound protons, spin diffusion pathways through residual protons cannot be neglected. For example, in ubiquitin with an overall correlation time of 7.7 ns (measured at high concentration at 284 K), ρ_i is typically 2 s^{-1} and the largest σ_{ij} are ca. 1.5 s^{-1} . We have fitted equations 101 and 99 up to mixing times of 90 and 200 ms [33]. As shown in Figure 5, the approximations were good for most NOEs in the amide proton network without corrections for spin diffusion. An averaged overestimation of only 9 % in the rate translates into an error of 1 % in the averaged distance. However, the approximation breaks down for protons in non-consecutive residues in the α helix and loops, where corrections of 10 to 50 % are required. A comparison of corrections for a perdeuterated and a protonated sample is shown in Figure 6.

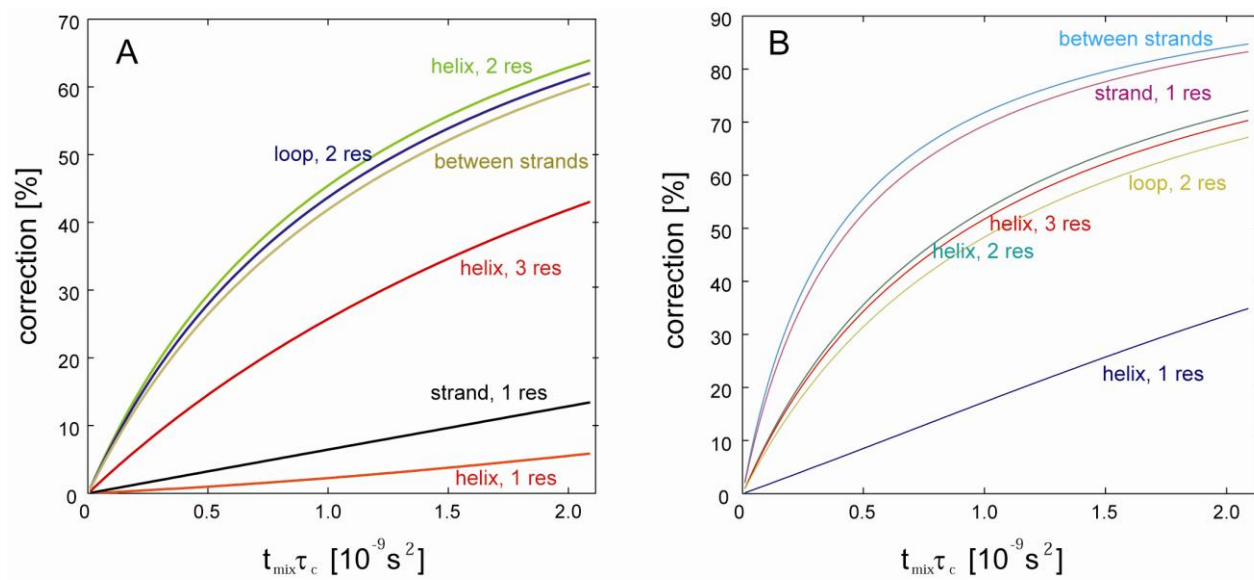


Figure 6. Influence of spin diffusion on the determination of NOE rate constants between amide spin pairs in dependence of the NOE mixing time t_{mix} and the overall correlation time τ_c . The corrections which must be applied to apparent experimental cross-relaxation rate constants are shown for a perdeuterated (A) and a protonated protein (B). Representative spin pairs from ubiquitin are selected. Spins in a α helix separated by one, two and three residues are exemplified by spin pairs 27/28, 27/29 and 27/30, spins separated by one residue in a β strand by 15/16 and from different β strands by 2/15, and spins separated by two residues in a loop by 58/60. The ratio of τ_c and t_{mix} is fixed at 10^{-7} . For the perdeuterated protein, the deuteration level is assumed to be 99 % for H^α and 95 % for all other non-exchangeable protons. Reprinted from Vögeli, Friedmann, Leitz, Sobol and Riek, *J. Magn. Reson.* 204 (2010) 290-302. Copyright 2010 Elsevier Inc.

For a higher residual proton level the effect is increased. For example, whereas the effect of spin diffusion via residual aliphatic protons in the helix is negligible, it is approximately linearly dependent on the protonation level for consecutive spin pairs in the β sheet and non-uniform for spin pairs between the β strands (Figure 7).

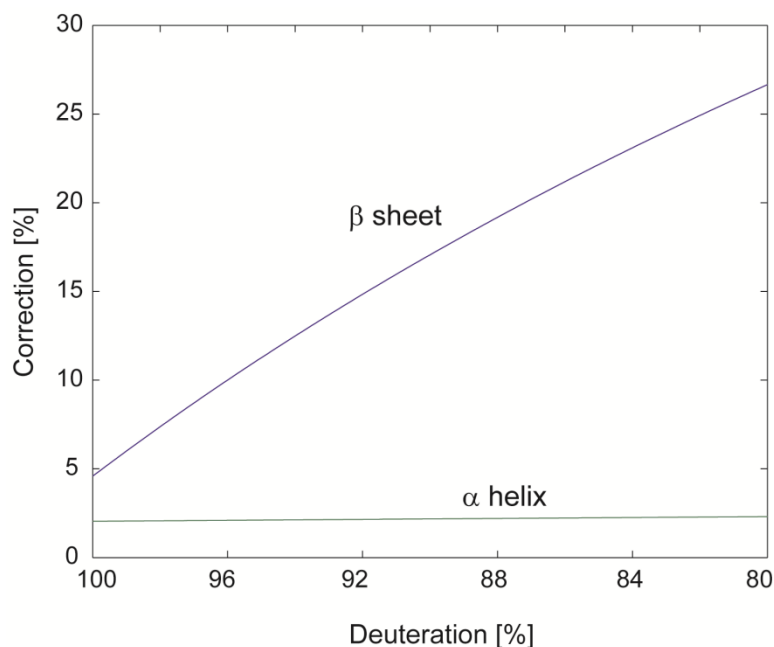


Figure 7. Influence of residual aliphatic protonation on the determination of NOE rate constants between sequential amide protons in an α helix (grey line) and a β sheet (blue line). Corrections to apparent experimental cross-relaxation rates are calculated for spin pairs of amide protons of residues 15/16 and 27/28 of ubiquitin, assuming a mixing time $t_{\text{mix}} = 100$ ms and $\tau_c = 9.3$ ns and fixing the deuteration level of all protons except for amide and H^α to 95 %. Reprinted from Vögeli, Friedmann, Leitz, Sobol and Riek, *J. Magn. Reson.* 204 (2010) 290-302. Copyright 2010 Elsevier Inc.

In general, the pattern of the distribution of the residual protonation level is highly complex in a macromolecule. Popular deuteration schemes are deuteration between 70 and 90 % or methyl-reprotonation in otherwise deuterated samples. In principle, an individual calculation of each possible isotopomer is required. To account for non-uniform deuterium levels at individual atom positions by a simple modification of the relaxation matrix has not been demonstrated yet. However, the problem can be significantly simplified if the calculation of the overall contribution is divided into individual contributions from 3-spin systems (DOMINO approach). The impact of the deuteration levels can be accounted for by scaling the according contribution by the residual

protonation level without restriction from non-uniformity in the deuteration level. As a rule-of-thumb, it is recommended to maintain a constant product of the NOE mixing time and the overall tumbling time of ca. $5 \times 10^{-10} \text{ s}^2$ for deuterated samples, while for protonated samples the value is approximately $2.5 \times 10^{-10} \text{ s}^2$.

3.4.2. Transfer function in the presence of conformational exchange

The theory of conformational or chemical multi-site exchange is discussed in section 2.4. The two-site exchange process can easily be adapted in the non-linear ISPA framework. The exact solution of equation 26 for exchange between conformations 1 and 2 of spin i is given by references [57,61]. For conformational exchange (and possibly also for chemical exchange), there is no cross relaxation present. The transfer functions of the cross peaks connecting the two resonances associated with the states 1 and 2 are then

$$T_{i,11}^{\text{ex}}(t) = \frac{1}{2} \left[\left(1 - \frac{\rho_{i,1} - \rho_{i,2} + k_{12} - k_{21}}{(\lambda_+^{\text{ex}} - \lambda_-^{\text{ex}})} \right) e^{-\lambda_-^{\text{ex}} t} + \left(1 + \frac{\rho_{i,1} - \rho_{i,2} + k_{12} - k_{21}}{(\lambda_+^{\text{ex}} - \lambda_-^{\text{ex}})} \right) e^{-\lambda_+^{\text{ex}} t} \right] \quad (107.1)$$

$$T_{i,22}^{\text{ex}}(t) = \frac{1}{2} \left[\left(1 + \frac{\rho_{i,1} - \rho_{i,2} + k_{12} - k_{21}}{(\lambda_+^{\text{ex}} - \lambda_-^{\text{ex}})} \right) e^{-\lambda_-^{\text{ex}} t} + \left(1 - \frac{\rho_{i,1} - \rho_{i,2} + k_{12} - k_{21}}{(\lambda_+^{\text{ex}} - \lambda_-^{\text{ex}})} \right) e^{-\lambda_+^{\text{ex}} t} \right] \quad (107.2)$$

and the transfer functions of the diagonal peaks are

$$T_{i,12}^{\text{ex}}(t) = \frac{k_{21}}{(\lambda_+^{\text{ex}} - \lambda_-^{\text{ex}})} \left[e^{-\lambda_-^{\text{ex}} t} - e^{-\lambda_+^{\text{ex}} t} \right] \quad (108.1)$$

$$T_{i,21}^{\text{ex}}(t) = \frac{k_{12}}{(\lambda_+^{\text{ex}} - \lambda_-^{\text{ex}})} \left[e^{-\lambda_-^{\text{ex}} t} - e^{-\lambda_+^{\text{ex}} t} \right] \quad (108.2)$$

with

$$\lambda_{\pm}^{\text{ex}} = \frac{(\rho_{i,1} + \rho_{i,2} + k_{12} + k_{21})}{2} \pm \sqrt{\left(\frac{\rho_{i,1} - \rho_{i,2} + k_{12} - k_{21}}{2}\right)^2 + k_{12}k_{21}} \quad (109)$$

Usually, it is a good approximation to assume that $\rho_{i,1} = \rho_{i,2} = \rho_i$:

$$T_{i,11}^{\text{ex}}(t) = \frac{1}{2} \left[\left(1 - \frac{k_{12} - k_{21}}{k_{12} + k_{21}}\right) + \left(1 + \frac{k_{12} - k_{21}}{k_{12} + k_{21}}\right) e^{-(k_{12} + k_{21})t} \right] e^{-\rho_i t} \quad (110.1)$$

$$T_{i,22}^{\text{ex}}(t) = \frac{1}{2} \left[\left(1 + \frac{k_{12} - k_{21}}{k_{12} + k_{21}}\right) + \left(1 - \frac{k_{12} - k_{21}}{k_{12} + k_{21}}\right) e^{-(k_{12} + k_{21})t} \right] e^{-\rho_i t} \quad (110.2)$$

are the transfer functions of the diagonal peaks and

$$T_{i,12}^{\text{ex}}(t) = \frac{k_{21}}{k_{12} + k_{21}} \left[1 - e^{-(k_{12} + k_{21})t}\right] e^{-\rho_i t} \quad (111.1)$$

$$T_{i,21}^{\text{ex}}(t) = \frac{k_{12}}{k_{12} + k_{21}} \left[1 - e^{-(k_{12} + k_{21})t}\right] e^{-\rho_i t} \quad (111.2)$$

are the transfer functions of the cross peaks.

For the case $k_{12} = k_{21} = k$ in addition to $\rho_{i,1} = \rho_{i,2} = \rho_i$:

$$T_{i,11}^{\text{ex}}(t) = T_{i,22}^{\text{ex}}(t) = \frac{1}{2} \left[1 + e^{-2kt}\right] e^{-\rho_i t} \quad (112)$$

$$T_{i,12}^{\text{ex}}(t) = T_{i,21}^{\text{ex}}(t) = \frac{1}{2} \left[1 - e^{-2kt}\right] e^{-\rho_i t} \quad (113)$$

If chemical exchange (rather than conformational exchange) takes place between two spins they may also have non-vanishing cross relaxation. Prominent examples are exchangeable OH, NH, NH₂ and water protons. Then, the transfer functions are [61]:

$$T_{i,11/22}^{\text{ex,d}}(t) = \frac{1}{2} \left[\left(1 \mp \frac{\rho_{i,1} - \rho_{i,2} + k_{12} - k_{21}}{\lambda_+^{\text{ex,d}} - \lambda_-^{\text{ex,d}}}\right) e^{-\lambda_-^{\text{ex,d}} t} + \left(1 \pm \frac{\rho_{i,1} - \rho_{i,2} + k_{12} - k_{21}}{\lambda_+^{\text{ex,d}} - \lambda_-^{\text{ex,d}}}\right) e^{-\lambda_+^{\text{ex,d}} t} \right] \quad (114)$$

$$T_{i,12/21}^{\text{ex,d}}(t) = \frac{k_{i,12/21} - \sigma_{ij}}{\lambda_+^{\text{ex,d}} - \lambda_-^{\text{ex,d}}} \left[e^{-\lambda_-^{\text{ex,d}} t} - e^{-\lambda_+^{\text{ex,d}} t} \right] \quad (115)$$

with

$$\lambda_{\pm}^{\text{ex,d}} = \frac{(\rho_i + \rho_j + k_{i,12} + k_{i,21})}{2} \pm \sqrt{\left(\frac{\rho_i - \rho_j + k_{i,12} - k_{i,21}}{2}\right)^2 + (\sigma_{ij} - k_{i,12})(\sigma_{ij} - k_{i,21})} \quad (116)$$

In general, it is difficult to separate the two mechanisms. Exchange effects in simple spin systems are analyzed in references [146]. For proteins, three-spin systems embracing an exchanging spin pair located in tyrosine residues are of particular interest.

Solutions for an exchanging spin pair where both spins are jointly in either of the two conformations can be looked up in [6].

If k_{12} and k_{21} are much smaller than the inverse NOESY mixing time (that is, less than 10 s^{-1}) the transfer functions given in equations 108 and 111 vanish such that the peak intensities of the two diagonal peaks decay with the according autorelaxation rates in a decoupled manner. In this case, two sets of distance restraints may be used in two separate structure calculations to obtain two conformations.

3.4.3. Validation and selection of experimental buildups

It is crucial to assess the quality of the NOEs. For example, the NOEs that produce unreliable cross-relaxation rates should only be interpreted conservatively or dismissed completely. One obvious benchmark is the correction factor p that should be as small as possible. It is also important to assess the quality of the buildup curve *per se*. This check should be available at different stages of the overall procedure (for example, before or after peak intensity correction for spin diffusion). The quality of the buildup fits is jeopardized by two main contributions: Firstly, the validity of the assumptions made in equations 99 and 101 (this depends, for example, on the

extent of spin diffusion or possible peak overlap); secondly, the signal-to-noise ratio. Different quality factors have been proposed to judge the agreement of the cross-peak buildup and the two-spin approximation. We initially used the following expression [31]:

$$\chi = \frac{1}{\max |I_{\text{exp}}|} \sqrt{\frac{1}{N_{\text{mix}} - 1} \sum_{i=1}^{N_{\text{mix}}} (I_{\text{exp}}(\tau_{\text{mix}}(i)) - I_{\text{fit}}(\tau_{\text{mix}}(i)))^2} \quad (117)$$

where N_{mix} is the number of mixing times and I_{exp} and I_{fit} are the experimental and back-predicted peak intensities, respectively. For the fits for protonated GB3, this quality factor was in close agreement with benchmarking by human inspection [31]. “Good fits” are obtained for $\chi < 0.08$ and “bad fits” for $\chi > 0.15$ for the mixing times of 20, 30, 40, 50 and 60 ms. If these values are also appropriate on a more general level remains to be established.

eNORA calculates two other values for quality assessment of the fits (see Figure 3) [112].

One is Pearson's correlation coefficient R^2 and the other one Q :

$$R^2 = \frac{\left(\sum_{i=1}^{N_{\text{mix}}} (I_{\text{exp}}(\tau_{\text{mix}}(i)) - \bar{I}_{\text{exp}})(I_{\text{fit}}(\tau_{\text{mix}}(i)) - \bar{I}_{\text{fit}}) \right)^2}{\sum_{i=1}^{N_{\text{mix}}} (I_{\text{exp}}(\tau_{\text{mix}}(i)) - \bar{I}_{\text{exp}})^2 \sum_{i=1}^{N_{\text{mix}}} (I_{\text{fit}}(\tau_{\text{mix}}(i)) - \bar{I}_{\text{fit}})^2} \quad (118)$$

$$Q = \sqrt{\frac{\sum_{i=1}^{N_{\text{mix}}} (I_{\text{exp}}(\tau_{\text{mix}}(i)) - I_{\text{fit}}(\tau_{\text{mix}}(i)))^2}{\sum_{i=1}^{N_{\text{mix}}} I_{\text{exp}}(\tau_{\text{mix}}(i))^2}} \quad (119)$$

In our experience, "good peaks" as obtained in the same data set as mentioned above have R^2 values larger than 0.8 which is set as a default value in eNORA. Note, however, that it is only a good criterion if the buildup is approximately linear as R^2 is a measure for the linear dependence between I_{exp} and I_{fit} . Q is a variant of χ where the normalization is modified.

For technical reasons, an exact experimental cross-relaxation rate constant can only be obtained if the buildups of both cross peaks caused by a spin pair i - j can be fitted (*vide infra*). In that case the two fitted values are combined to the experimental value as follows:

$$\sigma_{ij}^{\text{exp}} = \sigma_{ji}^{\text{exp}} = \sqrt{\sigma_{ij}^{\text{fit}} \sigma_{ji}^{\text{fit}}} \quad (120)$$

Note that it has also been proposed to use the arithmetic mean of the two fitted cross-relaxation rate constants [77]. The justification of equation 120 will be given in equation 124.

3.4.4. Practical aspects, NMR spectroscopy

NMR spectroscopy. All examples of structure calculations previous to ours presented in the following chapter are based on the determination of exact cross-relaxation rate constants from two-dimensional [$^1\text{H}, ^1\text{H}$]-NOESY experiments. The introduction of isotope-labeling of heavy atoms enabled heteronuclear three-dimensional NOESY experiments that simplify the analysis of proton-proton NOEs significantly [147]. The possibilities offered by the large array of available 3D and 4D NOESY experiments promise improvement in extraction of a large number of eNOEs. As of now we have used series of 3D [^{15}N]-resolved or 3D [$^{15}\text{N}, ^{13}\text{C}$]-resolved [$^1\text{H}, ^1\text{H}$]-NOESY spectra (see Figure 8). Two main types of these experiments, the NOESY-HXQC and HXQC-NOESY schemes, are distinguished, where X stands for S (single) or M (multiple). In the NOESY-HXQC, [$^{15}\text{N}, ^1\text{H}$]-HXQC and [$^{13}\text{C}, ^1\text{H}$]-HXQC elements [148,149] are employed simultaneously after indirect proton chemical shift evolution and [$^1\text{H}, ^1\text{H}$]-NOE mixing (Figure 8a). In the HXQC-NOESY, parallel [$^{15}\text{N}, ^1\text{H}$]-HXQC and [$^{13}\text{C}, ^1\text{H}$]-HXQC elements including the heteronuclear and the indirect proton chemical shift evolutions [148,149] are employed before [$^1\text{H}, ^1\text{H}$]-NOE mixing (Figure 8b). The choice of the order of the elements gains an additional

significance for the measurement of eNOEs. The intensity of detected $^1\text{H}_j$ magnetization I_{ij} originating from the initial $^1\text{H}_i$ magnetization with intensity I_i^{init} can be expressed as follows for HXQC-NOESY and for NOESY -HXQC [33]:

$$I_{ij}(\tau_{\text{mix}}) = \alpha_i^{\text{rec}} I_i^{\text{init}} T_{ii}^{\text{HXQC}} T_{ij}^{\text{NOE}}(\tau_{\text{mix}}) T_{jj}^{\text{WS,acq}} \quad (121)$$

$$I_{ij}(\tau_{\text{mix}}) = \alpha_i^{\text{rec}} I_i^{\text{init}} T_{ij}^{\text{NOE}}(\tau_{\text{mix}}) T_{jj}^{\text{HXQC}} \quad (122)$$

α_i^{rec} is the fractional part of the magnetization that has recovered during the interscan delay [37], T_{ii}^{HXQC} the loss of magnetization during the HXQC element, $T_{jj}^{\text{WS,acq}}$ the loss of magnetization during the water suppression element and effects during acquisition (such as decoupling artefacts), and T_{ij}^{NOE} is provided by equation 99 for $i \neq j$ and by equation 101 for $i = j$, respectively. If the NOESY element is placed after the HXQC element relaxation during HXQC is identical for the diagonal and every of its cross peaks since they share the same magnetization pathway (as long as $T_{jj}^{\text{WS,acq}}$ can be assumed identical). T_{ij}^{NOE} can now be extracted by normalization of the cross-peak intensities ($i \neq j$) to the diagonal peak intensity ($i = j$) at $t = 0$:

$$T_{ij}^{\text{NOE}}(\tau_{\text{mix}}) = \frac{I_{ij}(\tau_{\text{mix}})}{I_{ii}(0)} \quad (123)$$

The advantage of this approach is that σ_{ij} and σ_{ji} are obtained independently and can be used for error estimation. In addition, if one of the pathways cannot be evaluated (e.g. due to peak overlap) the cross-relaxation rate constant can still be obtained. On the other hand, if quantitative NOEs to aliphatic protons are evaluated, the water suppression sequence (typically WATERGATE or a binomial suppression) suppresses in part the $^1\text{H}^\alpha$ signals which results in a frequency-dependent $T_{jj}^{\text{WS,acq}}$ value and hence the uniformity assumption is not valid anymore.

Similarly, if signal intensities rather than volumes are analyzed the non-uniform linewidth of various proton types also alters $T_{jj}^{\text{WS,acq}}$. If one of the cross peaks is missing no value can be obtained or a larger error has to be tolerated. In our experience, superior water suppression is achieved with NOESY-HSQC experiments where it can be based on gradients and trim pulses. A more exact value for the cross-relaxation rate constants obtained from HXQC-NOESY with non-uniform $T_{jj}^{\text{WS,acq}}$ and all NOESY-HXQC is calculated as

$$T_{ij}^{\text{NOE}}(\tau_{\text{mix}}) = T_{ji}^{\text{NOE}}(\tau_{\text{mix}}) = \sqrt{\frac{I_{ij}(\tau_{\text{mix}})I_{ji}(\tau_{\text{mix}})}{I_{ii}(0)I_{jj}(0)}} \quad (124)$$

This equation is also the rationale behind equation 120.

Another way to deal with the different magnetization pathways in NOESY-HXQC experiments is to determine T_{jj}^{HXQC} from a 2D HXQC experiment or to simulate it based on predicted relaxation rates [152]. For a conventional HSQC element, T_{jj}^{HXQC} is mostly determined by the transverse relaxation rates of $^1\text{H}_j$ and $^{15}\text{N}_j$ or $^{13}\text{C}_j$. In a sensitivity-enhanced HSQC (which is $\sqrt{2}$ more sensitive in principle [153]), however, additional non-uniform loss is caused by the fact that no INEPT delay allows simultaneously full magnetization transfer for CH_1 , CH_2 and CH_3 (or HN_1 and HN_2) groups [152].

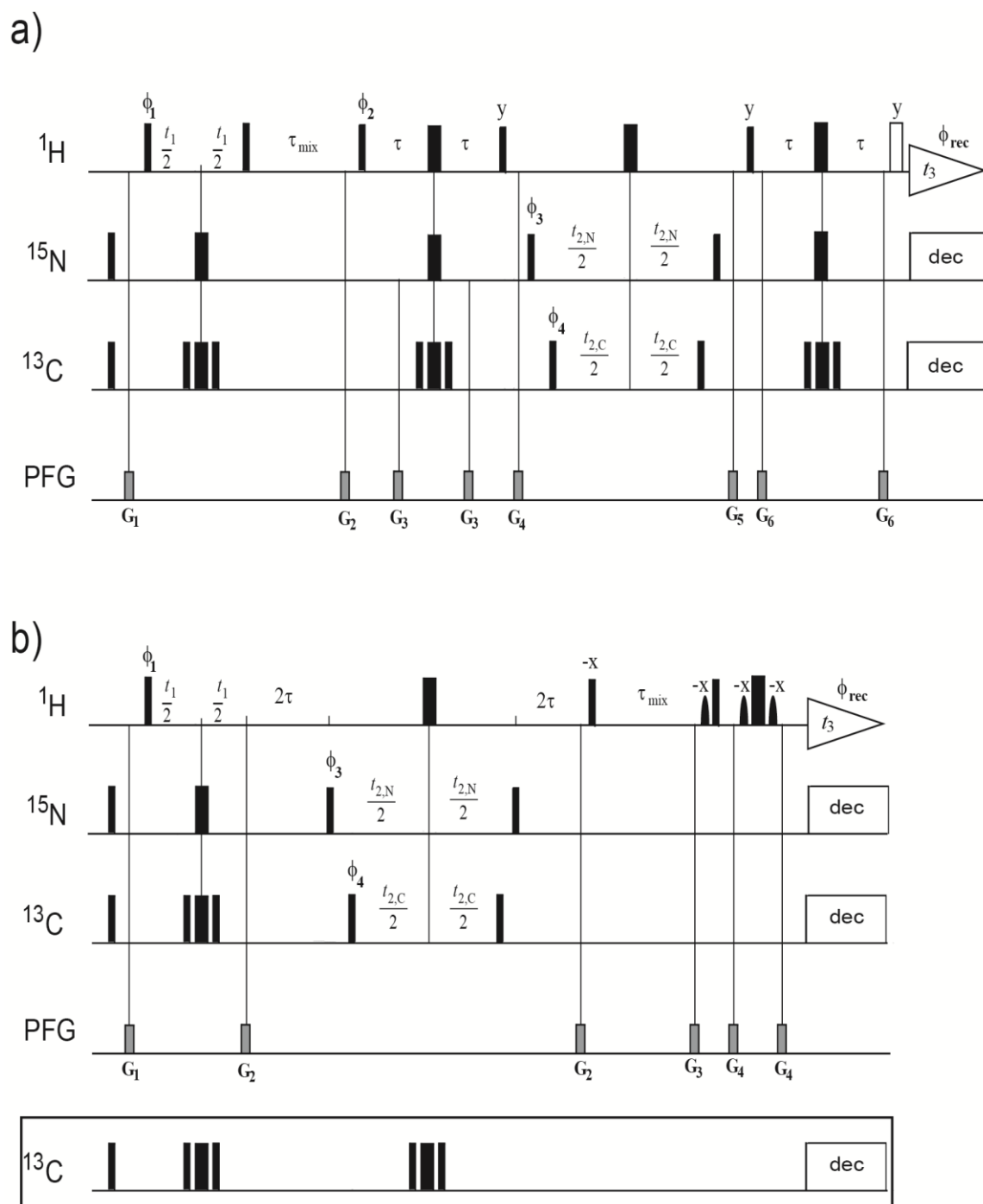


Figure 8. Pulse sequences of the 3D [^{15}N , ^{13}C]-resolved [^1H , ^1H]-NOESY experiments for the measurement of NOE buildups. Narrow and wide black bars indicate non-selective 90° and 180° pulses. The white bar and the curved shape indicate a trim pulse of 1 ms duration [150] and a Gaussian-shaped 90° pulse of 1 ms duration, respectively. The delay $\tau = 1.7$ ms is optimized for ^1H - ^{13}C transfers. Unless indicated otherwise, all radio-frequency pulses are applied with phase x. **a)** 3D [^{15}N , ^{13}C]-resolved NOESY-HSQC experiment. Alternatively, τ can be set to 2.7 ms and the ^{13}C

180° pulses during the transfers are shifted by 1 ms to optimize both the ^1H - ^{15}N and ^1H - ^{13}C transfers. The phase cycle is: $\phi_1 = \{x, x, x, x, -x, -x, -x, -x\}$; $\phi_2 = \{x, x, -x, -x\}$; $\phi_3 = \{x, -x\}$; $\phi_4 = \{x, -x\}$; $\phi_{\text{rec}} = \{-x, x, x, -x, x, -x, -x, x\}$. **b)** 3D [^{15}N , ^{13}C]-resolved HMQC-NOESY experiment. If only [^{15}N]-resolution is desired, the ^{13}C sequence is replaced by the one indicated in the box and $\tau = 2.7$ ms. The phase cycle is: $\phi_1 = \{x, x, -x, -x\}$; $\phi_3 = \{x, -x\}$; $\phi_4 = \{x, -x\}$; $\phi_{\text{rec}} = \{-x, x, x, -x\}$. In all experiments, quadrature detection in the $^1\text{H}(t_1)$ and simultaneous $^{15}\text{N}/^{13}\text{C}(t_2)$ dimensions is achieved by the States-TPPI method [151] applied to the phases ϕ_1 , ϕ_3 , ϕ_4 and ϕ_{rec} .

Once the cross-relaxation rate constant is obtained by fitting, it has to be corrected for deuteration effects if exchangeable atoms (mostly amide protons) are in exchange with solvent deuterons (see Figure 9). The most common case is the $\text{D}_2\text{O}/\text{H}_2\text{O}$ solvent where deuterated water is added for the lock signal. Very importantly, the correction is only applied if the spin that receives the magnetization is exchangeable (if the spin from which the initial magnetization originates is exchangeable, $I(0)$ is also reduced and the effect is already accounted for in equations 123 and 124). The true cross-relaxation rate constant is then obtained as:

$$\sigma_{ij}^{\text{true}} = \frac{\sigma_{ij}^{\text{fit}}}{1 - \text{Deut} / 100\%} \quad (125)$$

Deut is the D_2O level in percent (%). In our experience, 3 % D_2O is sufficient for a strong lock signal and causes minimal signal loss in the NOESY.

To assess experimentally the effects of swapping the HXQC and the NOESY elements both pulse sequences were run and analysed with the triple-labeled GB3 sample (see also the next chapter) [34]. The slope in a correlation plot of the $^1\text{H}^{\text{N}}\text{-}^1\text{H}^{\text{N}}$ cross-relaxation rate constants deviates by 1 % from 1 and Pearson's correlation coefficient is 0.99. This shows that virtually no systematic error is introduced by swapping. If the cross-relaxation rate constants in both transfer directions are determined individually for the NOESY-HSQC experiment, the rmsd between the two symmetry-related cross-relaxation rate constants is *circa* twice as large as in the HMQC-

NOESY experiment (0.82 s^{-1} versus 0.35 s^{-1}). However, if both cross peaks can be evaluated, equation 124 can be used and the obtained NOE rates are equally accurate as those from the HXQC-NOESY experiment.

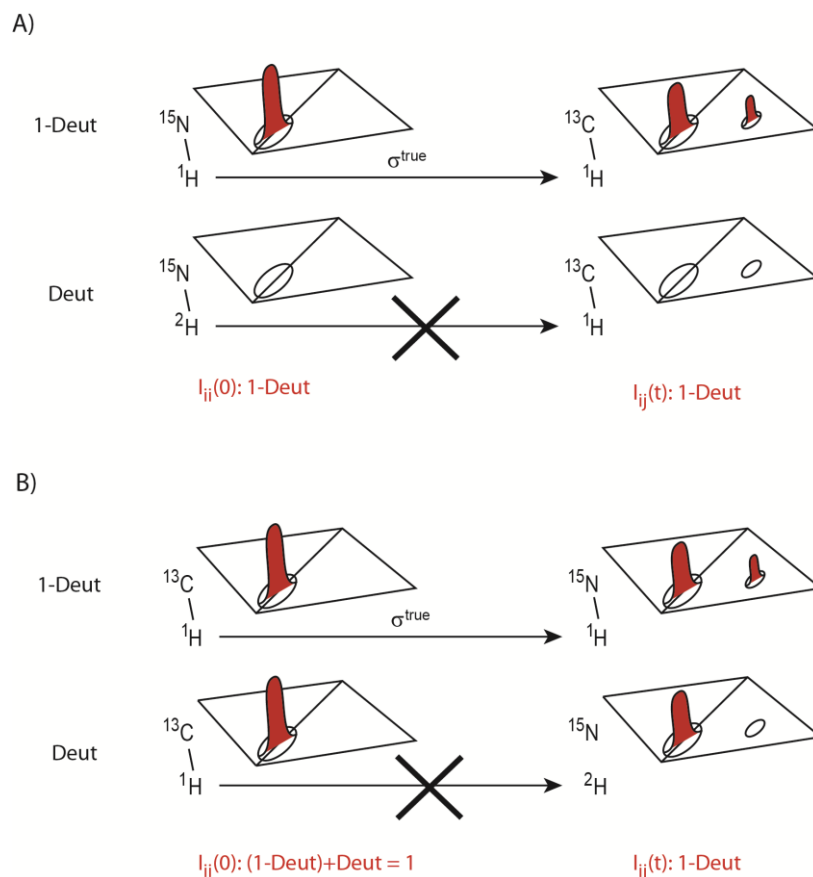


Figure 9. The effect of deuteration of the solution on the apparent cross-relaxation rate. The situation where the initial magnetization is on an exchangeable proton is shown in A) and where the receiving proton is exchangeable in B). If the solvent is partially deuterated and in proton exchange with the molecule under study the apparent NOE may be described by a superposition of two microscopic possibilities. The diagonal and cross peaks expected in a 2D NOESY spectrum after 0 and a finite mixing time are schematically depicted in red on the left- and right-hand side, respectively. It is seen that in case A) both peaks are scaled by (1-Deut), whereas in case B) only the cross peak is rescaled and a correction has to be applied to the apparent cross-relaxation rate.

Typical experimental settings are four to six mixing times τ_{mix} and a maximum value of ca. $5 \cdot 10^{-10} \text{ s}^2/\tau_c$ for deuterated samples and $2.5 \cdot 10^{-10} \text{ s}^2/\tau_c$ for protonated samples. The spectra were recorded with $200(^1\text{H}^{\text{indirect}}) \times 40(^{15}\text{N}/^{13}\text{C}) \times 1024(^1\text{H}^{\text{direct}})$ complex points, maximal evolution times $t_{\text{max},1\text{H}} = 22 \text{ ms}$, $t_{\text{max},15\text{N}} = 14 \text{ ms}$, $t_{\text{max},13\text{C}} = 8 \text{ ms}$, and $t_{\text{max},1\text{H}} = 102 \text{ ms}$, an interscan delay of 1 s and 4 scans per increment which results in a measurement time of 1.5 days per spectrum. Of course, several parameters must be adjusted to the specific case, such as a longer interscan delay for larger proteins, etc. ^{15}N -decoupling may be achieved with GARP [154] and ^{13}C -decoupling with a p5m4 supercycle [155,156], for example consisting of CHIRP pulses [157].

The measurement of eNOEs is very sensitive to even slight distortion of the baseline. It is beyond the scope of this work to discuss the baseline correction procedures. The interested reader finds overviews on baseline corrections in references [11,35,40,77,158-161].

Distance Calculation. In our application, effective distances, which absorb all motional effects, are obtained from equations 62 and 68. As mentioned previously, this procedure is superior to the calibration with an NOE with a known distance between the interacting spins. The molecular tumbling can be assumed to be isotropic with a single effective correlation time τ_c for most practical situations. The maximum error imposed on the extracted cross-relaxation rate constant and the distances can be estimated from the plot shown in Figure 10. For example, 3 % error is expected at most for the cross-relaxation rates but much less for most distances in the case of GB3 [34]. However, Withka et al. show that anisotropic tumbling cannot be neglected for a DNA with $D_z / D_{x=y} = 5$ [162]. The error can be as large as 17 % for 4 Å distances. On the other hand, very importantly, they show that internal motions diminish the effect of anisotropic tumbling which may be one of the reasons that the simple r^{-6} relationship works so well in practice [162]. Duben and Hutton arrived at similar and more detailed conclusions [163].

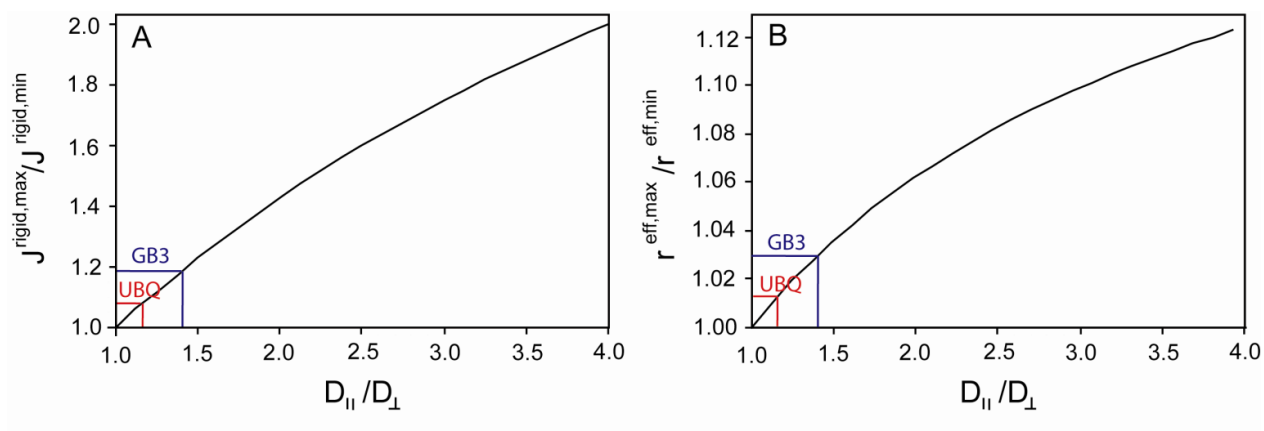


Figure 10. Variability of the spectral density J^{rigid} (A) and effective distance r^{eff} (B) of a rigid molecule versus the diffusion anisotropy $D_{\parallel}/D_{\perp} = D_z/D_{x=y}$. The variability is expressed as the maximal divided by the minimal value. The values for ubiquitin and GB3 are indicated in red and blue, respectively. Reprinted from Vögeli, Friedmann, Leitz, Sobol and Riek, *J. Magn. Reson.* 204 (2010) 290-302. Copyright 2010 Elsevier Inc.

For the structure calculation (*vide infra*), we translated r_{ij}^{eff} into an upper and lower limit for a distance restraint. If both magnetization pathways had been analyzed following equation 124, the upper and lower distance bounds were both set to r_{ij}^{eff} . If the NOE rate could be determined from one pathway only, the lower and upper distance bounds were set to $0.85 r_{ij}^{\text{eff}}$ and $1.15 r_{ij}^{\text{eff}}$, respectively. This choice was based on a comparison with a high accuracy structure where the violations appear approximately symmetrical. The corresponding cross-relaxation rate constants are twice (lower distance limit) and half as large (upper distance limit) as the exact value as shown in Figure 11. It may be argued that in practice the error is expected to be symmetric in the cross-relaxation rate constant rather than in the effective distance. Such a choice would result in a non-symmetric tolerance for the upper and lower distance limit. The advantages of such limits and the generality of the bounds used for the GB3 data sets are subject of ongoing research in our lab.

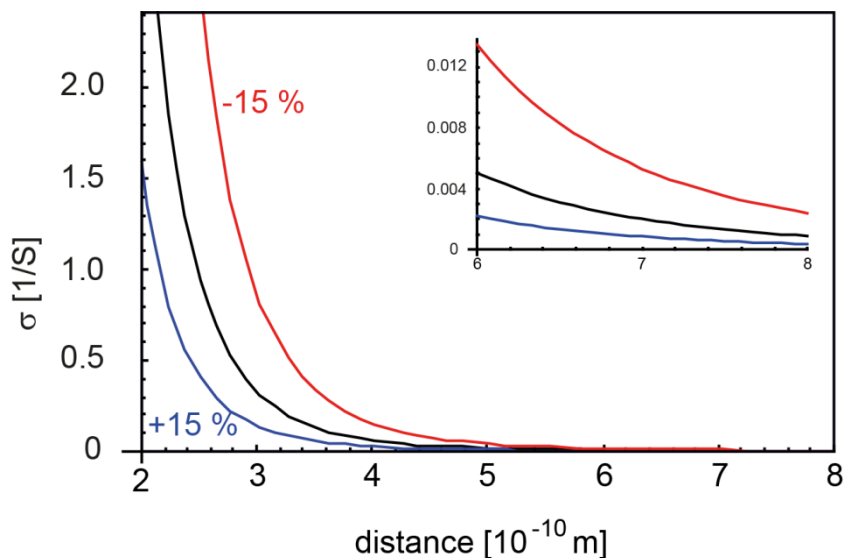


Figure 11. Relationship between the cross-relaxation rate constant and the corresponding distance. The black curve indicates the rate constant corresponding to the true distance. The blue and red curves are the resulting rate constants upon addition of 15 % to and subtraction of 15 % from the true distance, respectively. The inset shows a blow-up of the relationship for the long distances.

In general, it appears very challenging to estimate the experimental error and thus a reasonable choice of upper and lower limits. The accuracy of the full matrix approach as such has been analyzed, in particular the impact of the diagonalization in combination with experimental errors [81,164]. Limitations of the method are demonstrated but it is not straight-forward to translate these results into rules for the choice of bounds. The influence of spin diffusion and internal motion in secondary structures has also been studied [75].

3.4.5. *Impact of motion*

If motion is not explicitly accounted for in the analysis of r_{ij}^{eff} as obtained from equations 62 and 68, the question arises as to what influence dynamics has on the experimental values. It may be desirable to neglect its impact or estimate the induced error in a "rigid structure" analysis. One special case, the one concerning motion within a group of equivalent spins, has been discussed previously. Here, the fluctuation of the vector connecting atoms or pseudo atoms (if a group of equivalent spins is present) is considered.

The amide proton-amide proton NOE order parameters due to fast motion have been estimated for ubiquitin [165]. The calculation is based on the experimentally determined H^N-N order parameters obtained from relaxation measurements [166]. The nitrogen atoms were assumed to be located on a rigid backbone and the amide protons to sample a cone with Gaussian distributed weights (depending on the excursion from the average orientation) consistent with the H^N-N order parameters. The results are plotted in Figure 12a and are rationalized by theoretical calculation shown in Figure 12b. As the large majority of the H^N-N order parameters are larger than 0.8, all NOE order parameters fall between 0.95 and 1.1 with the majority clustered within 3 % deviation around 1. The reasons for this effect are twofold. Firstly, the distances between two protons are larger than the H^N-N distances. Secondly, the angular and distal effects counteract to a large extent [67]. Note also that the estimation constitutes an upper limit to the expected impact from fast motion because it is likely that the motions are in part correlated and thus reduce the effect. Very similar conclusions were drawn from the calculation of fast motion order parameters from the RDC-derived EROS ensemble 2k39 [167]. Conclusively, the impact of fast motion can be approximately neglected for H-H spin pairs as long as the local H-X order parameters are

larger than 0.5 [165], which is usually fulfilled in globular proteins except for highly flexible tails and loops.

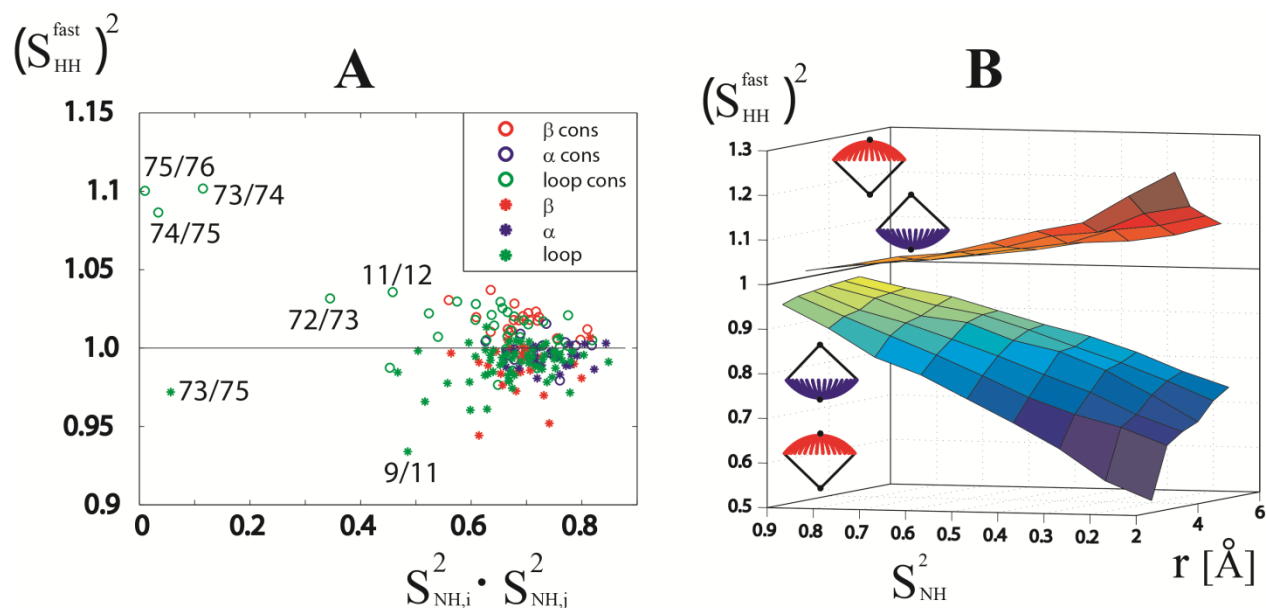


Figure 12. Relationship between order parameter of the NOE between backbone amide proton spins i and j , $(S_{HH}^{\text{fast}})^2$, and the local order parameters of the H^N -N vectors of residues i and j , $(S_{NH}^{\text{fast}})^2$. **A)** Fast-motion NOE order parameters versus the product of the corresponding local order parameters of ubiquitin determined experimentally at 288 K [166]. Consecutive residues in α helices, β sheets and loops are represented by open circles, and non-consecutive residues by filled circles, respectively. For large and small values of $(S_{HH}^{\text{fast}})^2$ the involved residues are indicated. **B)** Theoretical surface plot showing $(S_{HH}^{\text{fast}})^2$ versus the product of two corresponding $(S_{NH}^{\text{fast}})^2$ (having identical values) and the distance between the two cones in the interval from 2 to 5 Å. The two conformational scenarios yielding the most extreme values, cones opposing (top surface) or facing each other (bottom surface), are illustrated. Facing yields an order parameter smaller than 1 while opposing larger than 1. Reprinted with permission from Leitz, Vögeli, Greenwald and Riek, J. Phys. Chem. B 115 (2011) 7648-7660. Copyright 2011 American Chemical Society.

The situation is not as trivial if side-chain atoms are involved in the NOEs. Obviously, assumptions of Gaussian fluctuation around a single energy minimum conformation is an extreme simplification. A 800 ps molecular dynamics (MD) simulation of the cyclic decapeptide

antamanide in chloroform has been run to examine the order parameters of fast motion. It was concluded that independence between the fluctuations of the vector length and orientation is indeed a good approximation for many proton-proton NOEs. If the order parameter is larger than 0.5 the approximation is always very rigorous. The largest violations are obtained mostly for NOE involving side-chain atoms of phenylalanine. The majority of all NOEs (including all backbone NOEs) have order parameters larger than 0.8. To assess the situation in a larger protein, Post estimated order parameters from a 102 picosecond trajectory of an MD simulation of lysozyme [84]. Overall, the order parameter is 0.91 with 0.94 ± 0.36 and 0.87 ± 0.29 for interior and surface NOEs. The radial contribution is 1.05 ± 0.44 and 1.05 ± 0.32 in both cases, and the angular contribution is 0.90 ± 0.09 and 0.83 ± 0.13 . More than 10 % of the NOEs would give more than 10 % error for the extracted distance. In these calculations, the rigid structure was an energy-minimized average simulation structure. Without energy minimization, all the standard deviations are smaller by a factor of two. Most extreme averaging involves dihedral transitions. In the protein interior, half of the extreme intraresidue order parameter values involve side-chain arginine and lysine protons. An earlier MD trajectory of lysozyme has also been used to explore the impact of fast internal motions on NOEs [168]. Changes of apparent rates by as much as a factor 2 were reported for side chains.

Similarly, MD simulations of a DNA octamer have been used to improve the IRMA protocol (*vide infra*) [169]. Order parameters were obtained by averaging the plateau values of the correlation functions of 20 ps free MD trajectories. A similar convergence was observed for all values taken from averages over each type of proton pair. The observed range of mobility was $S^2 = 0.92$ for intrabase H6-H5 vectors to $S^2 = 0.60$ for the interresidue vectors from H6/H8 to sugar H2'/H2". The inclusion of these order parameters gave rise to small differences in the distance constraints of 10 % at most.

The use of order parameters derived from MD simulations of holo-forms of Protein Kinase A (PKA) increased the discrimination power of INPHARMA [129], a methodology to select docked ligand orientations by employing transferred NOEs [127,128]. The generic (not squared) order parameters S_i and S_j are tabulated for different atom types involved in NOEs in Table 2. The NOE-specific squared order parameter is obtained by their product:

$$\left(S_{ij}^{\text{gen}}\right)^2 = S_i^{\text{gen}} S_j^{\text{gen}} \quad (126)$$

Table 2. Generic atom-type specific order parameters.^a

	interresidual		intraresidual	
	S^{gen}	$SD(S^{\text{gen}})^{\text{b}}$	S^{gen}	$SD(S^{\text{gen}})^{\text{b}}$
H ^α	0.95	0.03	0.90	0.05
H ^{methyl}	0.62	0.04	0.52	0.04
H ^{β,methylene}	0.82	0.05	0.77	0.06
H ^{γ,methylene}	0.70	0.06	0.65	0.07
H ^{δ,methylene}	0.64	0.08	0.55	0.09
H ^{ε,methylene}	0.47	0.07	0.37	0.05
H ^{methylene,proline}	0.80	0.01	0.76	0.01
H ^{methine}	0.86	0.04	0.79	0.05
H ^{aromatic}	0.73	0.09	0.83	0.09

^a Taken from reference 129.

^b Standard deviation.

A similar table can be generated by the comparison of experimental cross-relaxation rate constants with those predicted from a highly accurate structure following equation 55. The averaged values for backbone amide proton-amide proton NOEs shown in Table 3 are obtained from a linear regression in a plot of experimental versus predicted rate constants of GB3 [33]. Only very slight differences are obtained between the isotropic and anisotropic model. A larger impact has the type of secondary element in which the spins are located. Overall, the average of the order parameters is *circa* 0.87. This is somewhat smaller than what is expected from the

considerations discussed above. The reason for this discrepancy remains elusive. The relative values of NOEs between consecutive residues in β sheet and across β sheets, however, is as expected (Figure 12).

Table 3. Averaged order parameters $(S_{ij}^{\text{exp}})^2$ obtained from a comparison of experimental and calculated $\text{H}^{\text{N}}\text{-H}^{\text{N}}$ cross-relaxation rate constants of GB3^a assuming either isotropic or fully anisotropic tumbling^b.

model	all	all consec	all non-consec	consec β strand	between β strands	consec α helix	non-consec α helix	loops
isotropic	0.86	0.84	0.95	1.03	0.96	0.88	0.89	0.83
anisotropic	0.87	0.86	0.98	1.00	0.96	0.91	0.88	0.84

^a Coordinates are taken from the RDC-refined 1.1 Å X-ray structure (PDB code 2OED) [142] with optimized proton positions [143,144].

^b Diffusion tensor taken from reference [170].

Table 4. NOE order parameters $(S_{ij}^{\text{exp}})^2$ and Pearson's correlation coefficients r of experimental versus predicted cross-relaxation rate constants σ_{ij} , and slopes of linear regressions s and r of internuclear distances r_{ij} grouped into backbone and side-chain spins^a.

location of atom i	location of atom j	$(S_{ij}^{\text{exp}})^2$	$r(\sigma_{ij})$	$s(r_{ij})$	$r(r_{ij})$	# spin pairs
all	all	0.75	0.93	0.97	0.92	295
bb	bb	0.84	0.97	0.99	0.98	112
bb	$\text{H}^{\beta}, \text{H}^{\beta 2}, \text{H}^{\beta 3}, \text{Q}^{\beta}$	0.63	0.84	0.98	0.92	107
bb	sc, rest	0.50	0.71	0.96	0.77	57
sc	sc	0.24	0.05	0.91	0.82	19

^a Coordinates are taken from the RDC-refined 1.1 Å X-ray structure (PDB code 2OED) [142] with optimized proton positions [143,144].

Table 4 presents NOE order parameters involving spins located throughout the GB3 [31]. In addition, Pearson's correlation coefficients of the plot are indicated as well as the slopes of linear regressions and correlation coefficients of corresponding plots showing the distances. Overall, the averaged order parameter is 0.75 and lower than the figure for amide proton-amide proton NOEs only. The further away from the backbone a spin is located the lower the values. This effect is due to increased motion in side chains. When one spin is located in the backbone and the other one at a β position the value is still 0.63. The order parameter between two side-chain spins drops to 0.24 (note, however, that the statistics is poor with only 19 evaluated NOEs and absence of any correlation with the predicted rate constants). Interestingly, the correlation between experimental and predicted distances is still high (slope almost 1, correlation coefficient almost 0.8).

3.4.6. Validation of experimental distances

We measured amide proton-amide proton NOE buildups with a series of 3D [^{15}N]-resolved HMQC-NOESY experiments on a perdeuterated ubiquitin sample [33]. Then, we derived effective distance with equation 62 without applying any correction for spin diffusion. An excellent correlation is obtained with distances calculated from a high-resolution X-ray structure (Figure 13). The estimated experimental random error is ≈ 0.07 Å or on average *circa* 2 % for distances up to 5 Å. This error is smaller than the pairwise rms deviation from corresponding distances extracted from high-resolution NMR or X-ray structures (pdb codes: 1D3Z and 1UBQ, both 0.24 Å). Remarkably, it is also smaller than the pairwise rmsd between the corresponding distances in the X-ray and NMR structures (0.15 Å). eNOE-derived motions appear to have smaller amplitudes and are possibly of a different character than present in a 20 ns molecular

dynamic simulation of ubiquitin in water using the GROMOS force field [33]. Furthermore, a recently published ensemble of structures representing the conformational distribution over time scales up to milliseconds (pdb: 2K39) satisfies the NOEs obtained at 307 and 326 K better than the single X-ray structure [165]. However, NOEs at 284 K show a better correlation with the X-ray structure which may be caused by the fact that the NMR restraints for the bundle were measured at 298 K [165,167].

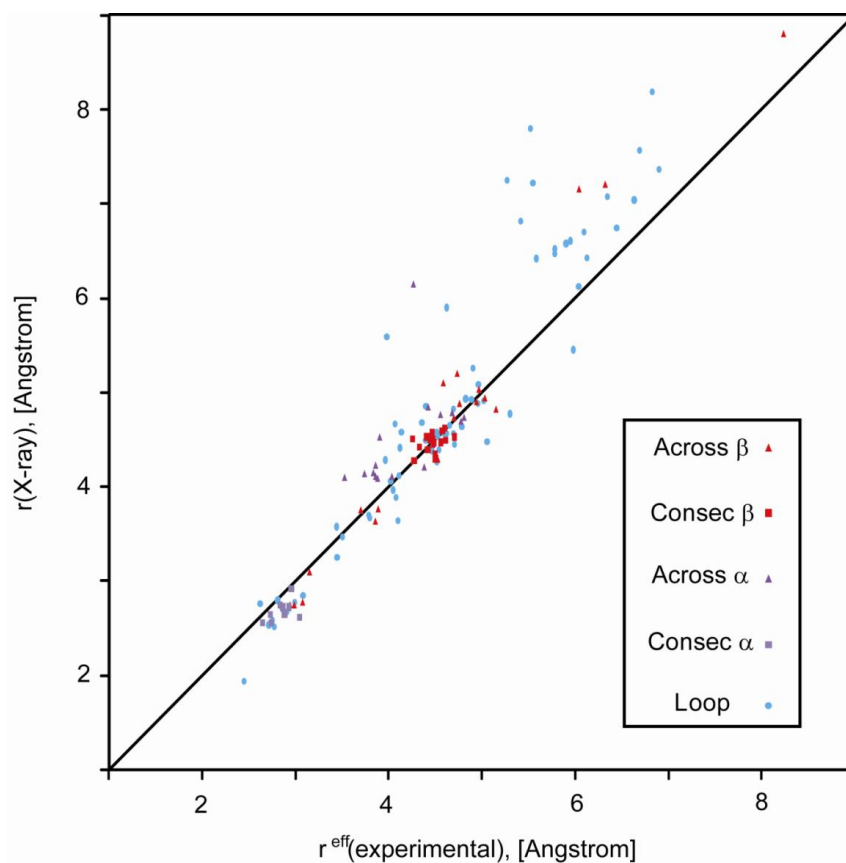


Figure 13. Correlation plot showing H^N-H^N distances obtained from the X-ray structure 1UBQ [171] with protons placed at ideal positions versus effective distances extracted from experimental cross-relaxation rates without correction for spin diffusion. Distances between two spins in the β sheet are red, α helix purple, and involving one or two spins in a loop blue. Distances between two spins of consecutive (nonconsecutive) residues in a secondary structural element are triangular (square). The slope of the black line is 1. Reprinted with permission from Vögeli, Segawa, Leitz, Sobol, Choutko, Trzesniak, van Gunsteren and Riek, *J. Am. Chem. Soc.* 131 (2009) 17215-17225. Copyright 2009 American Chemical Society.

Subsequently, Butts et al. showed the method yields very accurate distances (within a few percent of the true values) for rigid organic molecules as exemplified on the model compound strychnine [172]. 1D and 2D NOESY experiments were conducted with 500 ms mixing times. Instead of determining the overall correlation time and correcting for spin diffusion, proportionality of cross-relaxation rate constants and r^{-6} was assumed.

The approach was also used to demonstrate the calculation of exact distances from quantitative NOEs between the β -proton pairs across individual disulfide bonds [145]. To this end, BPTI was fully deuterated except for the β -proton pairs in cystein residues as previously mentioned. Even without correction for spin diffusion a high correlation between the experimental distances and distances in an X-ray structure was obtained.

The next question is whether distances obtained from eNOEs measured on protonated macromolecular samples with a much denser spin network are of similar quality. We measured amide proton-amide proton NOE buildups with two series of 3D [^{15}N]-resolved HMQC-NOESY and 3D [^{15}N]-resolved NOESY-HSQC experiments on a deuterated GB3 sample (data sets DNC-A and DNC-B), and a series of 3D [^{15}N]-resolved NOESY-HSQC experiments on a protonated GB3 sample (data set NC) [34]. Table 5 compares the derived effective distances after correction for spin diffusion. All slopes of linear regressions through correlation plots of any two sets deviate from 1 by less than 2 %. All correlation coefficients are larger than 0.95 and larger than 0.97 for distances derived from both cross peaks. Plots of the DNC-A and -B sets versus the NC set are shown in Figure 14.

Table 5. Slopes of linear regressions s and Pearson's correlation coefficients r between effective H^N-H^N distances r_{HN-HN}^{eff} in GB3 originating from different experiments after correction for spin diffusion.

dataset x axis	dataset y axis	s	r
DNC-A	DNC-B	0.989 (0.993) ^a	0.991 (0.957) ^a
DNC-A	NC	1.009	0.971
DNC-B	NC	1.017 (1.015) ^a	0.986 (0.958) ^a

^a Spin pairs for which one or both cross peaks could be evaluated for DNC-B.

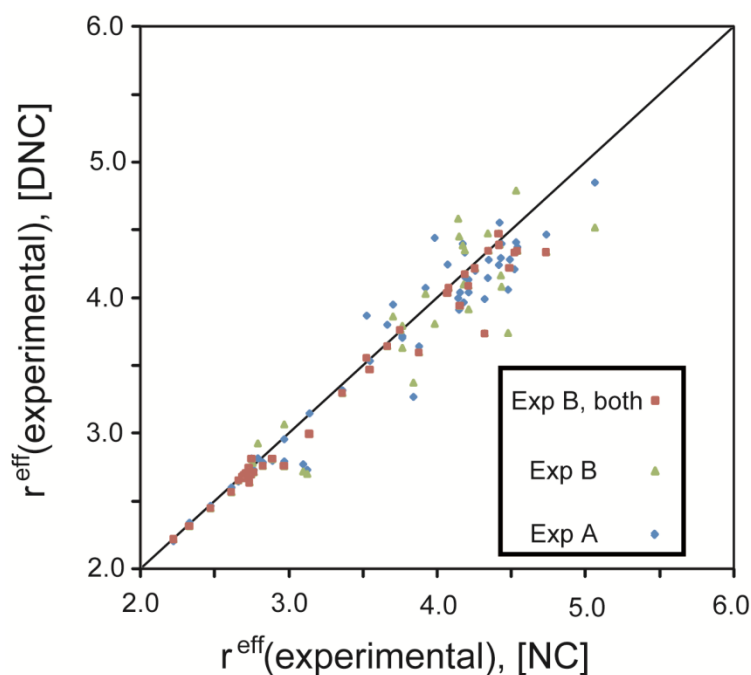


Figure 14. Correlation plots of experimental effective distances r of GB3 obtained from a triple (DNC) versus those from a double labeled sample (NC). Corrections for spin diffusion have been applied. Distances are obtained from the triple labeled sample using experiment DNC-A (HMQC-NOESY, blue diamonds) or DNC-B (NOESY-HSQC, purple squares and green triangles, respectively, if both and only one cross peak could be fitted). Isotropic tumbling is assumed. The black line has a slope of 1. Reprinted from Vögeli, Friedmann, Leitz, Sobol and Riek, J. Magn. Reson. 204 (2010) 290-302. Copyright 2010 Elsevier Inc.

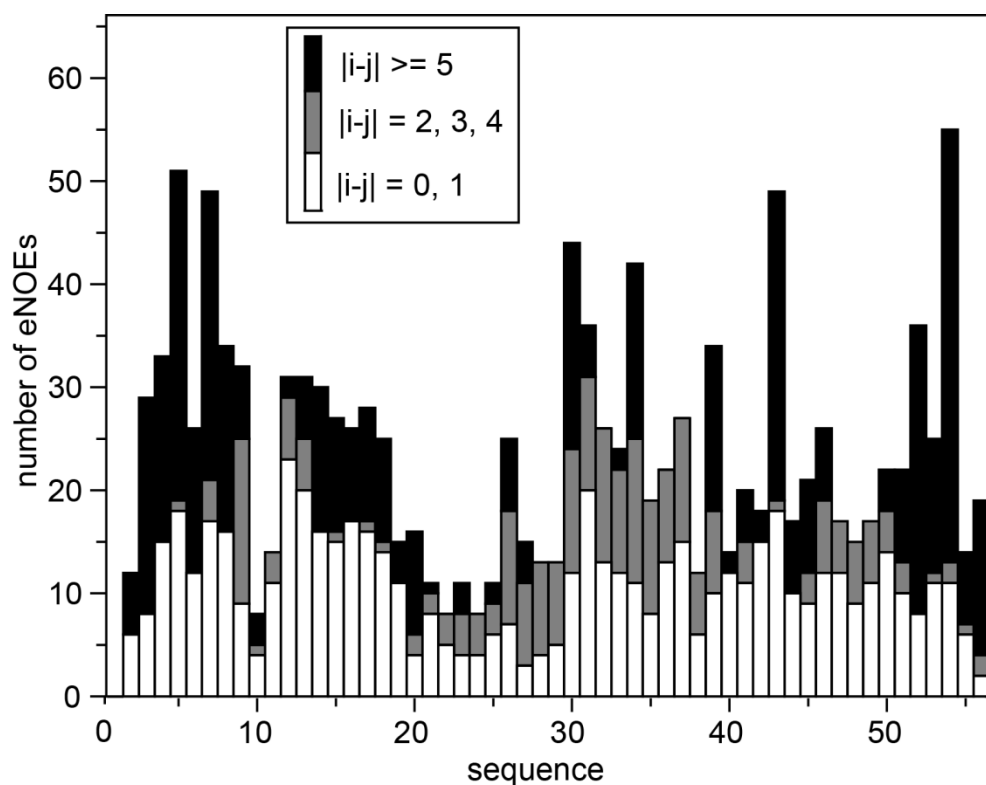


Figure 15. Number of eNOE-derived distance restraints for GB3 versus residue number. The counts are classified as short-range (white), medium-range (gray), and long-range (black), where i and j are the residue numbers of the involved spins. Reprinted by permission of Taylor & Francis Ltd from Vögeli, Güntert and Riek, Mol. Phys. 111 (2013) 437-454.

Subsequently, we used a protonated GB3 sample to derive eNOE-based distance constraints between any proton types from a series of 3D [^{15}N , ^{13}C]-resolved NOE [31]. Overall, 1092 buildup could be fitted (typically satisfying the criterion $\chi < 0.15$ with χ defined in equation 117). 562 of them constitute pairs of both transfer pathways of a specific spin system resulting in $562/2 = 281$ exact cross-relaxation rate constants. The remaining 530 do not have the corresponding counterpart and resulted in 530 less exact cross-relaxation rate constants. For the structure calculation (*vide infra*), $\text{H}^{\text{N}}\text{-H}^{\text{N}}$ distances were calculated from various data sets [31,33,34] and an average overall set was used which has a residue-averaged random error of only 0.06 \AA moving

31 NOEs obtained from a single cross peak to the group with 0 % error tolerance and yielding an additional 12 eNOEs (in total, 324 from both pathways/multiple H^N-H^N data sets, and 499 from one pathway or pairs involving methyl groups). The sequence-specific distribution of the restraints is shown in Figure 15.

The cross-relaxation rates were corrected for spin diffusion and converted into effective distances under the assumption of isotropic molecular tumbling following equations 62 and 68. The determined effective distances absorb all motional effects. Figure 16 shows correlation plots between the experimental effective and predicted distances. Statistics are listed in Table 4. The slope of the linear regression including all distances is 0.97, whereas it is 0.99 for backbone distances only. The slope drops as the protons are located further out in the side chains which is attributed to motion, as stated already above. Pearson's correlation coefficient for all distances for which both pathways could be evaluated is 0.92, while for the backbone only it is 0.98. Inclusion of distances calculated from only one cross peak lowers it to 0.84 for all distances and 0.96 for the backbone. It can be concluded that the correlation between the experimental and true distances is very good. Taking into account that the reference structure was determined under different conditions and necessarily introduces an additional error from the shortcomings of a single conformer representation, the experimental eNOE data are of extraordinarily high precision. Since the quality factors χ for NOEs for which a side-chain proton was involved are comparable to those for backbone NOEs, the precision and accuracy of these distances are expected to be similar to those in the backbone. However, the correlation of the distances between spins in the side chains is not as good as those in the backbone. This apparent discrepancy is mainly attributed to the more pronounced side-chain motion which is evidently insufficiently represented by the single-state X-ray reference structure.

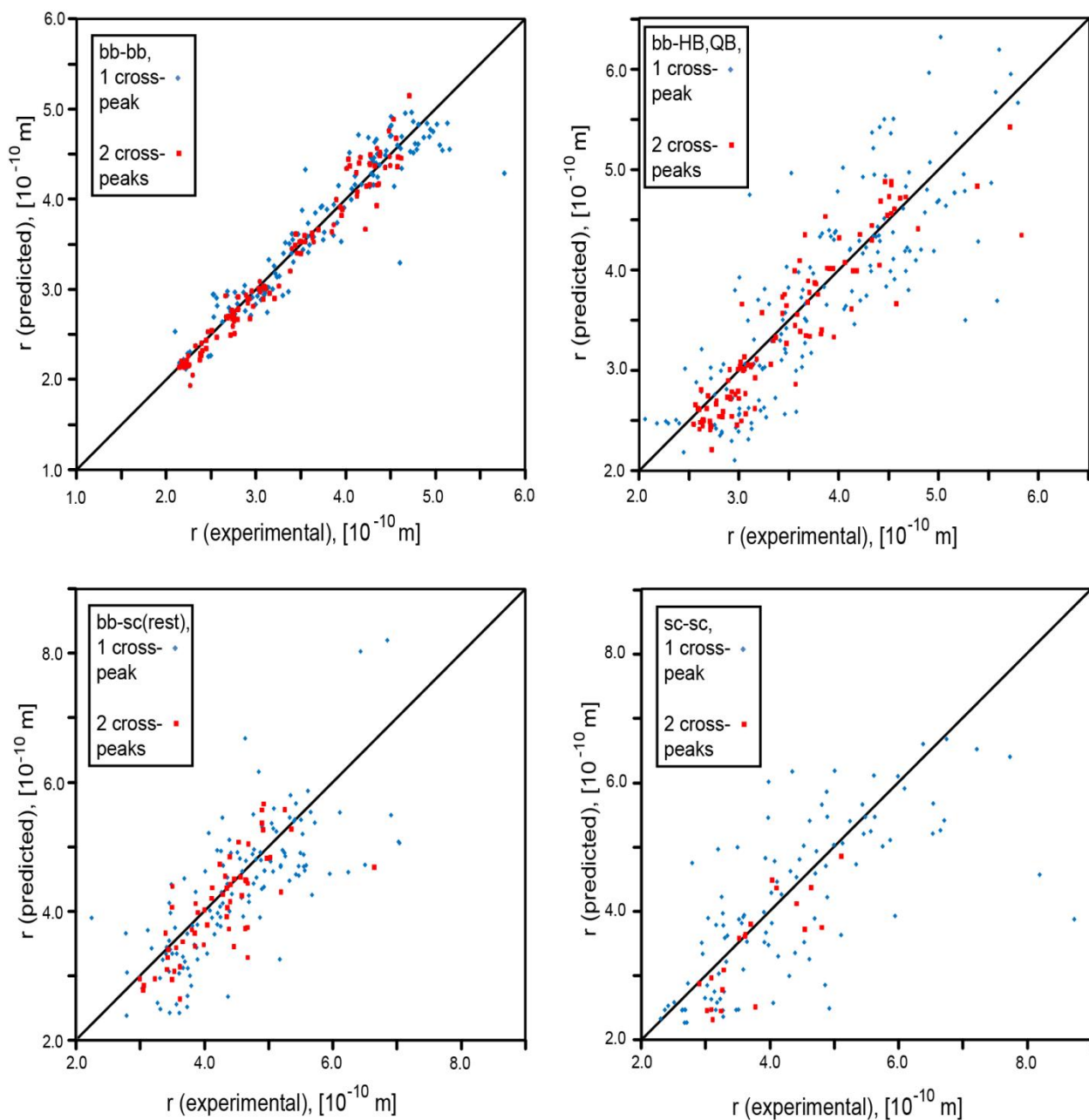


Figure 16. Predicted versus experimental distances in GB3. Experimental distances were calculated under the assumption of isotropic molecular tumbling with a correlation time $\tau_c = 4.15$ ns at 298 K following equations 62 and 68. Predictions are based on the 2OED structure with RDC-optimized backbone proton positions [142-144]. The panels show the distances between (top left) two spins located in the backbone (bb); (top right) one in the backbone and one being a side-chain $H^{\beta(2,3)}/Q^{\beta}$; (bottom left) one in the backbone and one being another side-chain proton (sc, rest); and (bottom right) both in the side chain as indicated in the black boxes. Black lines indicate slope 1. Reprinted by permission of Taylor & Francis Ltd from Vögeli, Güntert and Riek, Mol. Phys. 111 (2013) 437-454.

3.4.7. Temperature dependence of amide proton-amide proton eNOEs

It is evident that even minute changes in effective distances can be detected by eNOEs. These distances are sensitive to the average distances as well as their fluctuations. Thus, the eNOE is a very attractive tool for the detection of (translational) motions between atoms that are far apart in the sequence. We measured NOE buildups between amide protons in ^{15}N , ^{13}C , ^2H -labeled ubiquitin at three temperatures (284, 307 and 326 K, Figure 17) [165]. The temperature changes cause strong alternation of the intensities because the cross-relaxation rates are approximately proportional to the overall tumbling time [3]. Even upon correction for the temperature effect on the tumbling time the rates are different (Figure 18). Comparisons among the three corrected data sets reveal that, whereas the rate constants decrease by 18 % from 284 to 307 K, those at 326 K decrease by 32 % as compared to those at 284 K. Subsequently, we calculated effective distances using equation 62. The average NOE increases translate into effective distance changes of 2.4 % and 4.0 % in the measured temperature ranges. The data demonstrates that the determination of quantitative NOEs is indeed a powerful tool for extracting small structural and dynamical changes in biomolecules.

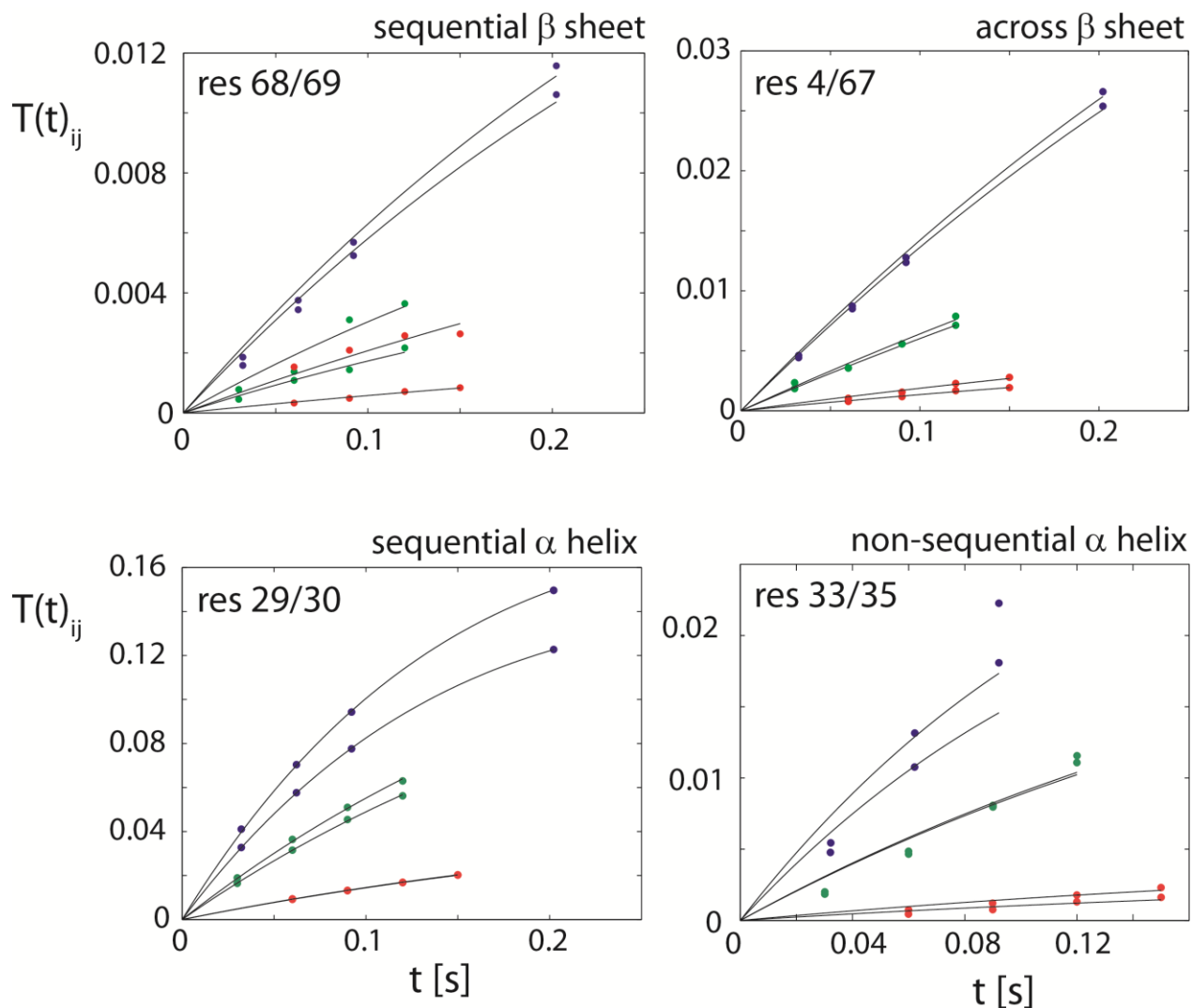


Figure 17. Experimental amide proton-amide proton NOE buildup curves measured on deuterated ubiquitin at three temperatures. The involved spins are located in various secondary structural elements: sequentially along β strands, across β strands and sequentially and non-sequentially within the α helix. The x axis shows the mixing time (30, 60, 90, and 200 ms for 284 K; 30, 60, 90, and 120 ms for 307 K; and 60, 90, 120, and 150 ms for 326 K), whereas both NOE transfer functions T^{NOE}_{ij} and T^{NOE}_{ji} are plotted on the y axis. Measured values are indicated by filled circles (blue, 284 K; green, 307 K; red, 326 K), and the fit of the data using the exact two-spin solution is illustrated by the black lines (without corrections for spin diffusion). Reprinted with permission from Leitz, Vögeli, Greenwald and Riek, *J. Phys. Chem. B* 115 (2011) 7648-7660. Copyright 2011 American Chemical Society.

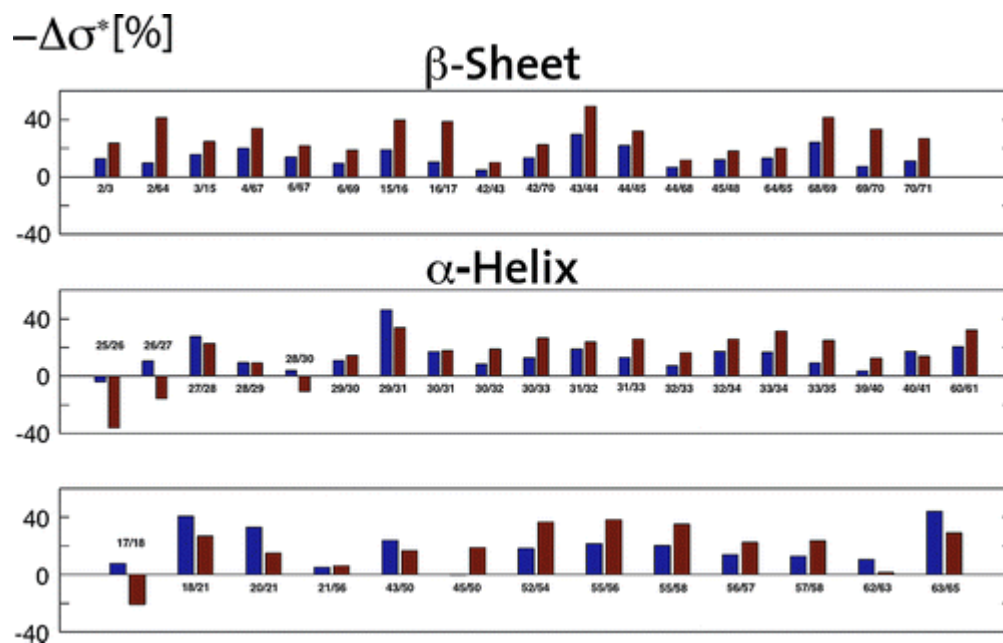


Figure 18. Relative temperature-dependent changes of amide proton-amide proton NOE rate constants. Blue and red bars show the reductions of the τ_c -corrected σ_{ij} (σ_{ij}^*) in percentages between 284 and 307 K, and between 284 and 326 K, respectively. The corresponding residue numbers are indicated. Reprinted with permission from Leitz, Vögeli, Greenwald and Riek, J. Phys. Chem. B 115 (2011) 7648-7660. Copyright 2011 American Chemical Society.

4. Structure calculation

Structure calculation using the full-matrix approach can hardly be separated from the extraction of cross-relaxation rates from NOEs and has been touched on in the previous chapter. Since no consensus procedure has emerged yet, it is also nearly impossible to separate the biological context from the specific method. First, the most innovative examples are reviewed. Soon after the first structure calculations it has been recognized that some NOEs can only be explained by multiple conformations. The development of the calculation of multiple-conformation ensembles (sometimes referred to as sets) of structures rather than single structures is reviewed in the next section. Keeping in mind that scientific progress proceeds as a continuum rather than in large steps and the very large body of literature covering the topic, both sections are necessarily subjected to the authors personal selection of literature and many more references may be found in the listed reviews. In the last section, the approach to calculate an ensemble from eNOEs developed in our laboratory is discussed in more detail.

4.1. Structure calculation using the full-matrix approach

The first application of the full relaxation-matrix approach to 2D NOESY was probably the conversion of six cross-peak and four diagonal-peak intensities into six distances of the small molecule proflavine [173]. The distances were within 10 % of those obtained from an X-ray crystal structure. This important work was followed by an increasing number of applications to increasingly more challenging systems. Most applications have been carried out on nucleic acids rather than proteins. The structural characteristics of RNA and DNA are more subtle and often

small differences determine their function due to the lack of tertiary structure. In addition, the lower proton density (3.4 neighboring protons within a sphere of 3 Å in B-DNA versus 4.7 Å in a globular protein [4]) drove the development with more urgency.

4.1.1. Nucleic acids

The first primitive approach towards macromolecular structure calculation was undertaken on nucleic acid fragments. The very first report dates back to 1985 when James et al. used the full-matrix approach to predict intensities from a standard DNA B-form and a energy-minimized DNA B-form structure obtained from AMBER. Both intensity sets were compared to experimental 2D NOESY spectra of the DNA octamer [d(GGAATTCC)]₂ recorded with four mixing times assuming different correlation times [174]. In another application, they show that the DNA octamer [d(GGTATACC)]₂ in solution is well represented by the regular B-form [175]. Subsequently, the same group analyzed the structure of the DNA fragment [d(A-T)₅]₂ using the same approach and showed that the data best corresponds to a wrinkled D form among many previously proposed forms based on NMR or X-ray diffraction [176].

A 20 base-pair DNA fragment corresponding to the Trp operator of *Escherichia coli* was refined by minimizing the residuals of 153 predicted and back-calculated NOE intensities I in a NOE-difference spectrum (51 different NOEs at three different irradiation times!) [110]:

$$\Delta^2 = \sum [I_{\text{exp}} - I_{\text{calc}}]^2 / \sigma^2 \quad (127)$$

σ is the standard deviation of I .

The first example of a direct structure calculation via exact NOEs is the use of the IRMA program to obtain the DNA octamer d(GCGTTGCG):d(CGCAACGC) with an estimated

correlation time of 1 ns in 1989 [114]. 167 cross-peak volume buildups were obtained from a series of eight 2D [¹H, ¹H]-NOESY spectra with mixing times ranging from 5 to 200 ms. After 100-300 steps of steepest-descent restrained energy minimizations, the restrained MD calculations were performed for 40 ps. The averaged MD structures were used as updated structure input after another energy minimization. After three IRMA cycles convergence was achieved for canonical A- and B-form starting structures. Convergence criteria were either convergence of the experimental distances or of the rms deviation between different starting structures. Importantly, all starting structures converged towards the B-form. Subsequently, the protocol has been improved on the same molecule by using the order parameters (which are usually set to 1) provided by equations 64.2 and, for methyl groups, 64.3 [169]. The values are obtained by averaging the plateau values of the correlation functions of 20 ps free MD trajectories. A similar convergence was observed when the values were taken from averages over each type of proton pair.

Another pioneering application to nucleic acids was a structural refinement of the extrahelical adenosine tridecamer d(CGCAGAATTCGCG)₂ with the MORASS program together with rMD calculations in AMBER [119,177]. Convergence was judged with the following percentage *RMS* figure and *R* factor (not to be confused with the relaxation matrix *R*):

$$\% RMS = \left[\frac{1}{N} \sum \left(\frac{I_{\text{exp}} - I_{\text{calc}}}{I_{\text{calc}}} \right)^2 \right]^{1/2} \times 100 \quad (128)$$

and

$$R_{\text{factor}} = \frac{\sum |I_{\text{exp}} - I_{\text{calc}}|}{\sum I_{\text{exp}}} \quad (129)$$

The sum runs over all intensities (which could possibly also extend over different mixing times). The R factor criterion is analogous to that used in X-ray crystallography. However, the authors recommend the use of % RMS because it is not dominated by short distances. A 2D NOESY with 150 ms mixing time yielded 258 constraints. The correlation time was estimated to be 4.5 ns. A crystal structure shows the extrahelical adenosine looped out way from the duplex. However, the NMR data established that it stacks into the duplex. Importantly, the ISPA approach alone was not able to place the extrahelical adenosine.

Other R factors have also been proposed [82]:

$$\tilde{R}_{factor} = \frac{\sum |I_{exp}^{1/6} - I_{calc}^{1/6}|}{\sum I_{exp}^{1/6}} \quad (130)$$

This figure of merit relates the intensities to the coordinate space of the structure. The weak NOEs have again more weight than in the previous expression. The R factor has also been calculated with a well potential where the flat bottom dimension is determined by experimental errors [136].

4.1.2. From peptide to proteins

As early as in 1986 exact distances derived from the full-relaxation matrix approach have been used in an additional force field in AMBER to analyze a complex of ristocetin pseudo-aglycon and Ac2-Lys-D-Ala-D-Ala [73]. Subsequently, the same lab tested different refinement approaches with 37 highly accurate and 21 less accurate distances extracted with the full relaxation-matrix approach on cyclic peptide designed to inhibit human renin [178].

The MADRIGRAS program has been tested on 2D-NOESY data simulated for bovine pancreatic trypsin inhibitor (BPTI) [83]. The rms deviation of the NOE-derived structure from the correct structure improved by ca. 8-15 % relative to an ISPA-derived structure for a poor initial model, and even more for a better one.

To the best of our knowledge, the first protein structure obtained from the full relaxation-matrix approach with experimental data was that of a 18-residue peptide with an amino-acid sequence comprising the first zinc-finger like domain from the *gag* protein p55 of HIV in 1990 [117]. A series of five 2D [¹H,¹H]-NOESY spectra with mixing times ranging from 5 to 500 ms yielded 226 distance constraints. The DSPACE distance geometry program was used to generate initial structures in the standard manner. The cycle between generation of the *I* and *R* matrices was reiterated with the BKCALC and GNOE programs. Early cycles were repeated until the predicted and experimental spectra were visually identical. Later cycles produced a match between calculated and experimental buildup and decay curves. Additional refinement steps such as simulated annealing were finally applied.

The first refinement of a protein using the direct-intensity approach was carried out on the 29-residue squash trypsin inhibitor CMTI-I [136]. An energy term for NOE intensities was included in X-PLOR [179]. NOE data was collected for a 2D NOESY series with mixing times 50, 100, 150, 200 and 250 ms in H₂O, and one with 150 ms in D₂O. 235 cross peaks were used for all mixing times and additional 190 for 150 ms and longer. Refined NMR structure yielded *R* factors of 0.26 (X-ray averaging, equation 129) and 0.06 ($I^{1/6}$ averaging, equation 130).

In test applications of the FIRM program, the structures of the proteins motilin (22 amino acids) and parvalbumin (108 amino acids) were calculated with DIANA and molecular mechanics (MM)/MD with AMBER from simulated NOE sets [85]. It is shown that the *R* factors of accurate structures range from 0.31 to 0.39. Those of random structures range from 0.9 to 1.3.

Another early example is the structure determination of the 46-residue protein crambin (Pro-22/Leu-25 species) consisting of two α helices and a short β sheet and containing three disulfide bridges (although the structure was previously known from X-ray diffraction) [115]. Data was recorded from a series of 2D NOESYs with mixing times 20, 40, 80, 120, 160 and 250 ms at a 500 MHz magnet. The calculation was based on 411 IRMA distance restraints, 132 qualitative distance restraints, 31 ϕ dihedral angles from backbone scalar couplings and 13 χ_1 dihedral angles from assignments of cross peaks. The IRMA restraints were calibrated using a proportionality constant corresponding to 3.5 Å and upper/lower bounds were obtained by adding/subtracting 10 %. The *R* factor (weights for different mixing times included) is shown to be somewhat lower for "Ensemble" IRMA than regular IRMA (0.35 versus 0.36). It is also shown that the result is independent of the starting model.

More recently, many applications of a partial relaxation-matrix approach appeared in the field of structure calculation of ligand-protein complexes [26].

It must be noted that virtually in all studies distances were extracted by comparing cross-relaxation rate constants to those of NOEs with known distances. This procedure is correct if the reference vector has a similar value for the order parameter and a similar extent of spin diffusion as the vector under investigation. This is a strong simplification and not recommended for future studies. Instead, the overall correlation time should be determined as shown, for example, in references [180] or [181].

4.2. Ensemble calculations using conventional NOE-distance restraints

The rationale behind ensemble calculation is that an NMR observable of the average structure is not equal to the average of the observables taken for each snapshot [182]. Some distances in the previously mentioned ristocetin pseudo-aglycon/Ac2-Lys-D-Ala-D-Ala complex derived from the full relaxation-matrix approach were inconsistent with energy-minimized structures [73]. Another 10 ps MD run revealed two clusters of low-energy structures with different orientations of the F and G rings. It was concluded that the NOEs are averaged over both conformations. The same effect on NOEs and scalar couplings has been demonstrated for the cyclic decapeptide antamanide which was known to undergo conformational exchange on a slow NMR time scale [183].

In the following, approaches to generate ensembles of structures are lined out. Two main categories may be distinguished. The first introduces an additional force field or similar into MD simulations, called restrained MD or rMD. As such, it is a time-averaged approach. The second one collects all other approaches, which calculate ensembles in more direct ways which are essentially conformational averages. Note that most of these approaches also employ rMD to some extent and a strict separation is somewhat arbitrary.

4.2.1. Restrained molecular dynamics simulation

In a first systematic approach to account for NOE averaging, a 20 ps rMD simulation has been run with the memory function as proposed in equation 78 with $q = 3$ [95] on the 74-residue tendamistat with 842 distance restraints [92]. For that purpose, the force field was replaced by a

constructed force in order to avoid occasional large forces due to forth-power terms. The violations were shown to be reduced as compared to a conventional rMD run.

A rMD simulation as proposed by Torda et al. [95] was also demonstrated for a nucleic acid, namely the DNA fragment [d(GTATAATG)].[d(CATATTAC)] [184]. It yielded the lowest R factors the group has ever obtained for a DNA octamer. A similar approach with DINOSAUR also yielded a lower R factor (\tilde{R}_{factor} as defined in equation 130) for the previously mentioned protein crambin with a time-independent averaging or averaging with a memory constant of 5 ps, both calculated from a 50 ps trajectory, than for instantaneous restraints [99]. An ensemble-average over 8 parallel MD trajectories showed similar characteristics. As expected, time-averaged restraints result in larger fluctuations of the interproton vectors.

In a further developed approach, MD trajectories based on simultaneous time- and space Boltzmann-weighted averaging have been shown to yield a more appropriate description of experimental NOE data than single-molecule methods for the small cyclic peptide analogue somatostatin [91].

In attempts to augment the input data set, restraints for scalar coupling constants have been used to generate a rMD trajectory of antamanide [185] and an ensemble as exemplified on the side-chain conformation of a phenylalanine in a Ala-Phe-Ala tripeptide [98]. Subsequently, many ensemble calculations based on NOEs were supplemented with scalar coupling restraints.

4.2.2. Direct structural ensemble calculation

The first protocol to directly extract multiple conformations from NOE data (and other NMR data) was MEDUSA (*Multiconformational Evaluation of Distance information Using a*

Stochastically constrained minimization Algorithm) [186]. The protocol makes use of both distance restraints and anti distance restraints (that is, absence of a cross peak). First, a large set of static structures is generated by fulfilling all anti distance restraints and a subset of the distance restraints. Then, a clustering procedure selects an ensemble of structures that fulfills all distance restraints. MEDUSA was applied to antamanide with 23 distance restraints, 108 anti distance restraints and scalar couplings. From 1176 initial structures, a considerable number of pairs adequately satisfied the experimental data.

Subsequently, more straight-forward procedures were introduced. A 15-residue peptide corresponding to the N-terminal sequence of bovine pancreatic trypsin inhibitor (BPTI) destabilized by replacement of the two cysteines by serines was synthesized to mimick a folding intermediate [97]. As it is disordered and presumably cannot satisfy NOEs with a single conformation well an ensemble-calculation protocol has been implemented. 93 initial buildup rates were converted into identical upper and lower distance restraints by calibration with the NOE between H^δ and H^ε in tyrosine. After calculating initial structures by a standard procedure, 8-member ensembles were generated by performing energy minimization and molecular dynamics with $\langle r^{-3} \rangle$ averaging. The work was carried out with a program suite consisting of Metrize, Optimize and Ensemble. It turned out that some local structure mediated mostly by an interaction between the aromatic ring of Tyr10 and the amide group of Gly12 is retained.

r^{-6} -averaging was tested with X-PLOR 3.1 on an ensemble representations of GB3 (56 residues, 854 distance restraints) and ragweed allergen *Amb t V* (40 residues, 1031 distance restraints) for which synthetic distance restraints were generated [187]. Violations were significantly reduced upon using twin conformers instead of one structure and the correct variability was reproduced. Using more structures appears to cause overfitting. This can be

validated by the violation of NOEs predicted from the calculated structures that were not used as input [188]. It is also recognized that the tightness of the upper and lower bounds critically determines the optimal number of structures to be used. The data set defining the loop 21-27 of *Amb t V* has been tested on the possibility of calculating two conformers with the relative populations as free variable [189]. Synthetic data for 25%/75% and 75%/25% populations have been created. Standard data is not sufficient to obtain the populations but distances with upper and lower bounds within 10% deviation from the true value would serve the purpose. Real NOE/scalar coupling data sets for the proteins interleukin 4 (130 residues, 1735 NOE and 27 hydrogen bond distance restraints) and interleukin 8 (71 residues, 1764 NOE and 116 hydrogen bond distance restraints) are analyzed and their effective *B* factors are compared to previously determined crystallographic *B* factors [187]. While one structure appropriately represents the interleukin 4 ensemble (with a *B* factor considerably lower than the X-ray analog), twin conformers are appropriate for interleukin 8. For the latter, the NMR and X-ray *B* factors are similar. The difference is driven by two conformations in the loop comprising residues 16-22. Unfortunately, details on the generation of the experimental distance restraints are not provided. If the authors chose upper and lower limits by changing the experimental distances by 10% (as done with the synthetic data), the experimental error would be much larger than these adjustments since a regular procedure for NOE extraction has been most likely used.

Upper and lower distance limits derived from initial NOE buildup curves were used for an ensemble calculation of the linear peptide YQNPDGSQA [122]. Only peaks of the major isomer (corresponding to *trans*-Pro-4) were analysed and resulted in 122 NOE restraints, 55 anti-NOE restraints and 41 angular restraints from scalar couplings. The NOE buildup curves were followed by 2D [¹H,¹H]-NOESY experiments with mixing times of 50, 150, 250, 350, and 450 ms. The curves were iteratively corrected for second-order spin diffusion effects using the

program DISCON and normalized to the volumes of the diagonal peaks. The resulting distances were calibrated with a Tyrosine H^{δ} - H^{ϵ} cross-relaxation rate and adjustments of at least +10 and -20 % lead to upper and lower limits, respectively (the constraints were set more loose if an automated DISCON procedure produced a wider range). An initial conventional structure obtained with X-plor with heavy atom backbone rms deviations of 0.26 Å produced a NOE violation average of 0.25 Å which could be reduced to 0.167 Å with modified atom sizes. A conventional structure calculation with the program CONGEN (*CON*formation *GEN*erator) (rmsd 0.22 Å) produced an average violation of 0.125 Å that could be increasingly lowered with two-, three- and four-member ensembles to 0.041 Å, 0.029 Å and 0.021 Å, respectively. In all ensembles, one member is similar to the conventional structure. The other members, however, are much less constrained. To avoid oversampling of the conformational space, ensembles were calculated by only employing the constraints in an averaged manner if they show a large violation in the conventional procedure. Now, the NOE violations are 0.058 Å, 0.046 Å and 0.042 Å. Order parameters predicted from these ensembles agree better with order parameters obtained from relaxation measurements and an MD simulation [190]. The results demonstrate that the conformational space is restricted by hydrogen bonds that produce a high population of β -hairpin conformations.

The MARDIGRAS program was used to back-calculate distances from synthetic NOEs simulated for an A- and a B-form of DNA [191]. In this way, it was shown that it is possible that the distances discern an ensemble of rapidly interchanging conformations from a single conformation.

Clore and Schwieters resurrected the multiple-conformer ensemble calculation on the model proteins GB3 and ubiquitin by torsion angle simulated annealing and Cartesian space

minimization in Xplor-NIH [192,193]. Major progress is achieved by the larger experimental data sets. Typically, the experimental input data comprised NOEs, scalar couplings (J) and residual dipolar couplings (RDCs) [194] measured in multiple alignment media. The minimized energy term is

$$E_{\text{total}} = E_{\text{NOE(only UBQ)}} + E_J + E_{\text{RDC}} + E_{\text{covalent_geometry}} + E_{\text{nonbonded_contacts}} + E_{\text{RAP}} + E_{\text{shape}} \quad (131)$$

The NOE energy term is a flat-bottom (accounting for uncertainties) quadratic harmonic well with back-calculated distances taken as r^{-6} -average. RDCs depend on the orientation of the vector spanned by two protons relative to a molecule-fixed frame and thus contain complementary information to the NOE input. A relative atomic position (RAP) term is introduced that prevents single members to stray too far from ensemble-averaged positions [192]. It was applied to the C^α atoms. It has the same form as the NOE term, with the uncertainties replaced by an allowed distance deviation. A molecular shape term prevents excessive rotation and deformation of single members. Cross-validation on ubiquitin and GB3 shows that no further improvement is achieved if more than two structures are used [192,193]. $S^2(\text{jump})$ for backbone H^N -N vectors is usually larger than 0.8 with values as small as 0.3 for flexible residues. In GB3, extensive anticorrelated crankshaft motion is observed along the backbone [193].

Another improvement in ensemble averaged structure determination comes from an energy term for an order parameter obtained from relaxation measurements [93]. This order parameter is sensitive to sub-nanosecond dynamics [71,72]. In the DER (Dynamic Ensemble Refinement)

protocol the NMR observables were matched to values calculated for typically 16 copies of the molecule with biased molecular dynamics (BMD), a type of restrained MD:

$$E_{\text{total}} = E_{\text{CHARMM}} + E_{\text{NOE}} + E_{S2} \quad (132)$$

E_{CHARMM} is the CHARMM force field energy and E_{S2} is the order parameter potential. NOE restraints are calculated with r^{-3} -averages. Cross-validation of a ubiquitin ensemble was achieved by back-prediction of RDCs and scalar couplings whose comparison with experimental values showed a remarkable agreement. The same experimental data set has been subsequently used in the new algorithm MUMO (*Minimal Under-restraining Minimal Over-restraining*) to further improve the cross validation with independent RDC data and across-hydrogen bond scalar couplings [94]. This MD-based algorithm considers the fact that different NMR observables (here, NOEs and relaxation order parameters) have different optimal copy numbers to reproduce these and other observables. An analysis of synthetic data revealed the following important insights: Different copy numbers are optimal for reproduction of average conformations and spatial sampling. For (conventional) NOE data, the best average structure is produced with a single copy. The optimal number of copies to reproduce the spatial sampling and also for cross-validation with independent RDCs and scalar couplings is two. Not surprisingly, increasing the number of NOEs causes an increase of the number of copies where overfitting occurs. On the other hand, it is predicted that using tight limits on NOE restraints, however, would be much more effective. Combining the conventional NOEs with order parameters yields optimal cross validation with motional observables (scalar couplings) for copy numbers of 8 or 16. However, the average structure is worse upon addition of order parameters and is better produced by a low copy number with NOEs only. Overall, NOEs are more prone to overfitting, while order

parameters are more prone to underfitting. In MUMO, the strengths are combined and NOEs are restrained for pairs of copies, while order parameter restraints are applied to 8 or 16 copies.

Subsequently, Clore and Schwieters recalculated the GB3 ensemble including the E_{S2} term and a new term $E_{Bfactor}$ reflecting the crystallographic B factor in X-plor-NIH [179,195]. $E_{Bfactor}$ rendered E_{RAP} unnecessary and was omitted. Now, the optimal ensemble contains between 4 and 8 members. Still the ensemble embodies low-amplitude, high-probability, anisotropic motion in the backbone on the picosecond to nanosecond time regime. NMR observables predicted from the ensemble were in excellent agreement with independently measured, highly accurate data such as backbone H-H RDCs and scalar couplings [196,197].

An ensemble of ubiquitin was recalculated from NOEs (r^{-6} averaging) and large sets of RDCs with the EROS protocol [167]. The refinement with the GROMACS package was achieved by simultaneous application of NOE and RDC restraints on subensembles of eight structures. The resulting ensemble with a mean backbone rmsd of 1.22 Å covers the complete spatial heterogeneity represented by 46 crystal structures. Each of these structures is within less than 0.8 Å backbone rms deviation from one NMR ensemble member. Since most of these structures are in complex with other molecules it was concluded that conformational selection is sufficient to explain the molecular recognition dynamics. The calculation is dominated by the RDC data which is sensitive to motions faster than tens of milliseconds. The authors conclude from comparison to other NMR observables (such as fast motion order parameters) that part of the dynamics occurs in the 'blind' time window of nanoseconds to tens of microseconds. In a follow-up study, the 640-member ensemble termed ERNST (*Ensemble Refinement for Native proteins using a Single alignment Tensor*) with a backbone rmsd of 0.83 Å was obtained using ensemble MD simulations restrained by 2663 NOEs and 1971 H^N-N RDCs [198]. The structure calculations were carried out with the CHARMM27 force field in explicit solvent. To ensure that the structure of ubiquitin

was well-reproduced, the NOEs were restrained over pairs of structures. The ensemble was validated by comparison of predicted cross-correlated relaxation rates to independently measured rates. Finally, collective motions spanning the β -strands separated by up to 15 Å were identified and characterized. These correlations are in part mediated by the hydrogen-bonding network and link molecular recognition sites.

For the sake of completeness, it is noted that further ensembles (and rMD simulations) were calculated without NOEs. The most prominent NMR observables for this purpose are RDCs and scalar couplings [199-202].

4.2.3. Continuous distances distributions

The determination of the distribution radius of a disordered group as lined out in section 2.8.4. was demonstrated with NOEs between an unpaired electron of a paramagnetic center and a proton [90]. The distribution was determined for an EDTA-Mn²⁺ group covalently attached to a thymine base through a flexible linker in the SRY/DNA complex. R_p was determined together with the internal correlation time τ_{int} from contributions to longitudinal and transverse relaxation observed at 600 and 800 MHz fields. Based on 22 vectors, R_p was determined to 6.9 Å.

4.3. Multiple-state structural ensemble calculation using eNOEs

The information content of upper (and lower) limit restraints derived from NOEs has been subject to theoretical studies [94,187,189,203]. It is clear that tighter constraints than those usually used would lead to better defined structural ensembles. In particular, addition of lower

limit restraints improve the definition further. It has also been shown that the sensitivity of a single NOE to the exact nature of conformation distributions is relatively low [204]. Instead, the power of the eNOEs for defining structures and dynamics lies in the cumulative effect of multiple eNOEs [32]. For example, it has been demonstrated that from many possible structures of the prostanoid analog SQ-28989 that are in agreement with exact NOEs at least two conformations are required to predict scalar couplings correctly [107]. Due to the technical challenges outlined above, all structural ensembles published as of now are obtained from conventional NOEs with one exception (to the best of the author's knowledge). As mentioned in the previous paragraph, upper and lower distance limits derived from initial NOE buildup curves were used for an ensemble calculation of the linear peptide YQNPDGSQA [122]. As summarized in section 3.4., we established a procedure to obtain effective distances of high precision from eNOEs for the protein GB3. In what follows, a protocol for multiple-state structure calculation in CYANA [205-207] is presented and exemplified with GB3 [30,31]. We use the term 'multiple-state' structure which is equivalent to the previously used 'multiple-conformer' structure. In doing so, a conformer may still be used to designate the outcome of one structure calculation (which includes several simultaneously obtained copies). In a conventional structure calculation, one conformer is produced per calculation and is obviously also one member of a bundle representation.

4.3.1. Conventional structure calculation

For the conventional structure calculation, 1953 upper distance limits calculated from the cross-peak intensities of the NOESY with a mixing time of $\tau_{\text{mix}} = 100$ ms resulted in 1041 constituted meaningful restraints. Additional experimental restraints were $^3J_{\text{HN}\alpha}$, $^3J_{\text{HNC}}$, and

$^3J_{\text{HNC}\beta}$ scalar couplings [197], N-H^N and C ^{α} -H ^{α} RDCs, and angular restraints from $^{13}\text{C}^{\alpha}$ chemical shifts. Using these restraints a standard structure calculation was performed with the software package CYANA [205-207] starting with 100 randomized conformers. Simulated annealing with 50'000 torsion-angle dynamics steps was applied and the 20 conformers with the lowest final target function values were selected. The small rms deviations from the mean structure of 0.95 Å for the backbone atoms and 1.38 Å for all heavy atoms, respectively, indicate good convergence of the structure calculation. The 9 structures with the lowest target functions are shown in Figure 20 on the left.

4.3.2. Multiple-state structure calculation protocol

For the multiple-state ensemble calculation, the set of effective distances presented in section 3.4.6. was used. The following error tolerances were chosen: $\pm 0\%$, $\pm 15\%$, and $\pm 20\%$ (-1 Å per methyl group for lower limit) for distances calculated from both cross peaks/multiple H^N-H^N sets, one cross peaks, and those involving two methyl groups, respectively. For NOEs involving at least one aromatic proton H ^{δ} or H ^{ϵ} of Phe or Tyr an upper limit of 8 Å was used. In addition, the scalar couplings, RDCs and chemical shifts mentioned above were used. All of these observables are sensitive to motion on the millisecond timescale (the 'slow' NMR timescale).

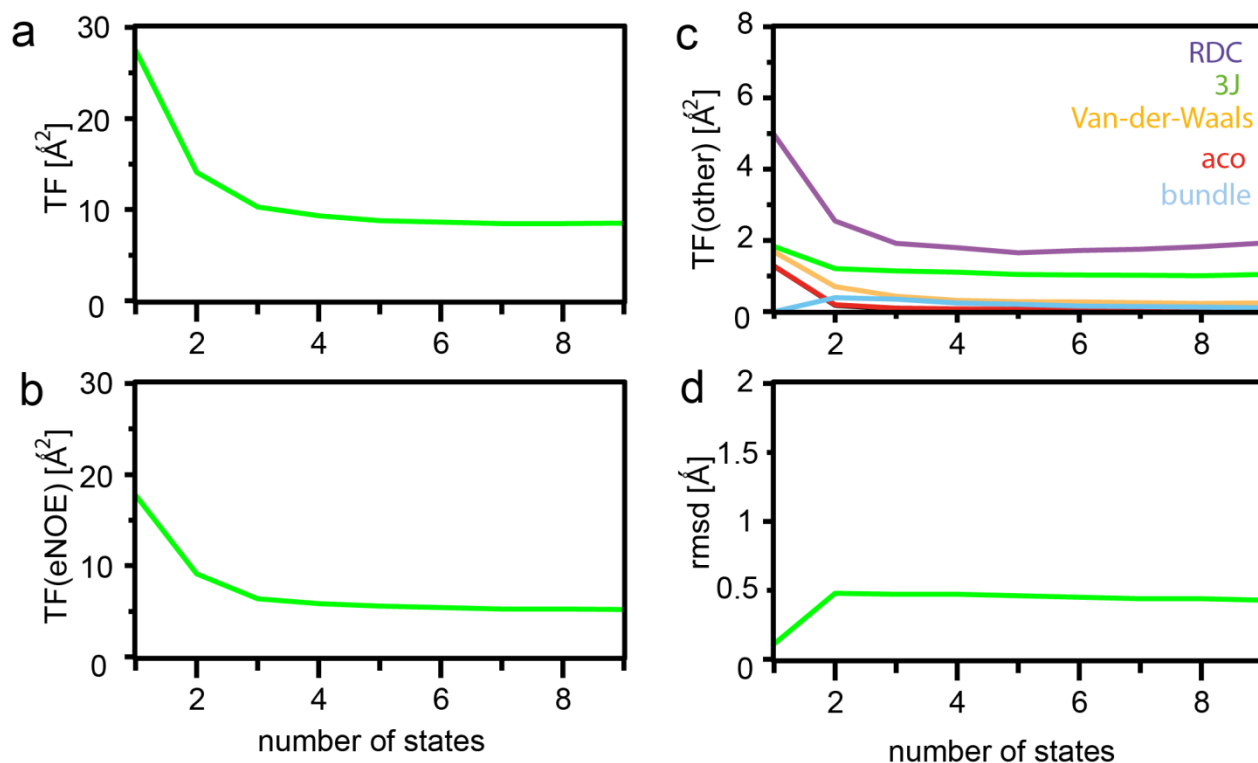


Figure 19. Target functions values (TF) obtained from structure calculations versus the number of simultaneously optimized states (**a-c**) and their rms deviations (**d**). The overall TF is shown in (**a**), the contributions from the eNOEs in (**b**), and those from the RDC, J coupling, van-der-Waals, C^α angular and bundling restraints in (**c**), respectively.

As for the conventional structure calculation protocol, 100 conformers were calculated with the software package CYANA and the 20 conformers (here, 20 ensembles) with the lowest target function were then used to represent the calculated structure. Ensembles encompassing 1 to 9 states of the entire protein were calculated simultaneously, using the same number of initial conformers and the same simulated annealing schedule as for the conventional structure calculation (see Figure 19). The squared differences between each eNOE-derived effective distance and the corresponding distance obtained by r^{-6} -averaging over the states is minimized. Similarly, the 3J coupling restraints and the RDC restraints were applied to the arithmetic mean of the corresponding quantities in the individual states. In addition, the angular restraints derived

from ^{13}C chemical shifts are required to be fulfilled and steric repulsion between atoms of different states was excluded.

Due to the r^{-6} -dependency long distances contribute minimally to the NOE. This may result in an unphysically loose packing of the ensemble. Bundling restraints were applied in order to keep the individual structural states together in space as far as permitted by the experimental restraints [192]. To this end weak upper distance bounds of 1.2 Å were applied to all distances between the same nitrogen and carbon atoms in different states. The weight of these bundling restraints was 100 times lower than for NOE upper distance bounds, except for the backbone atoms N, C $^{\alpha}$, C', and C $^{\beta}$, for which a 10 times lower weight than for NOEs was used. This weight is such that the restraints can easily be overridden by the experimental restraints and it also ensures that the different χ_1 rotamer states of the side chains are within the rms deviation without violating the bundling restraint.

The number of states necessary to describe the experimental data is not known *a priori*. Therefore, an array of structure calculations with the number of states varying from 1 to 9 was performed (see Figure 19). Among these ensembles the one with the minimal number of states that satisfies the experimental data well is selected as the appropriate representative. This ensemble with X states is obtained if the three following criteria are fulfilled: (i) The target function drops significantly from state $X - 1$ to X , (ii) the target function does not drop significantly anymore upon an increase of the number of states to $X + 1$, and (iii) a jackknife error estimation does not produce a lower-than-random target function for omitted eNOEs upon an increase of the number of states to $X + 1$. Following these criteria, it appears that the ensemble with $X = 3$ states is an appropriate representation of the structure. The 20 three-state conformers

with the lowest target function were deposited in the protein data bank (PDB code 2lum, BMRB ID 18531).

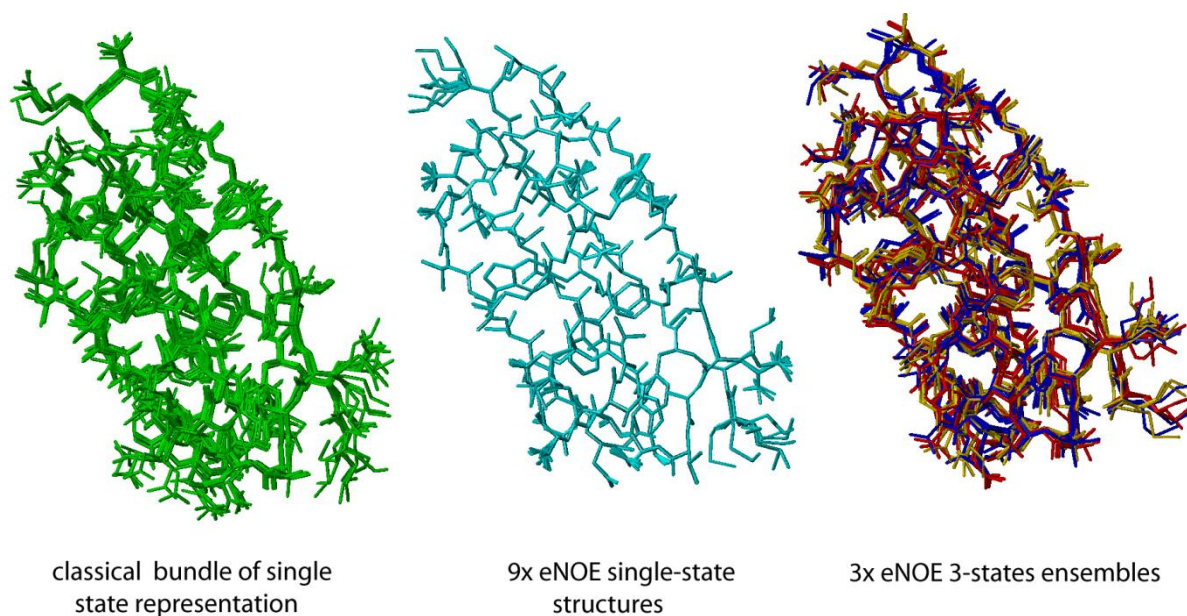


Figure 20. Heavy-atom structural representations of GB3 obtained from either the classical protocol with NOEs as experimental input, the classical protocol with eNOEs, or the ensemble-based protocol with eNOEs. Left: Bundle calculated with a classical protocol based on standard NOE measurements. Nine conformers are shown. Middle: Single-state bundle calculated with eNOEs. Nine conformers are shown. Right: 3 three-state ensembles obtained from eNOEs. The three most similar structures from each three-state conformer are grouped in gold, red and blue. Reprinted by permission from Macmillan Publishers Ltd: Vögeli, Kazemi, Güntert and Riek, *Nat. Struct. Mol. Biol.* 19 (2012) 1053-1057, copyright 2012.

9 members of the single-state bundle are shown in Figure 20 in the middle. The input data results in an extremely tight structure with a small backbone pairwise rms deviation of 0.11 Å and an all-heavy-atom rmsd of 0.60 Å only (compare to conventional bundle, left). Furthermore, the eNOE-based single-state NMR structure coincides closely with the RDC-optimized X-ray structure [142-144] with an rmsd of 0.57 Å for the backbone and 1.17 Å for all heavy atoms. However, the large target function value of 27.5 Å² resulting from many distance restraint

violations indicates that the structure does not agree with the experimental data. The large number of violations of experimental restraints can be attributed to the motion-averaged nature of the measured NOE, while the structure calculation protocol is based on a single static structure. In contrast, the three-state ensemble shown on the right of Figure 20 yields rms deviations to the RDC-refined X-ray structure of 0.72 Å and 1.31 Å for the backbone or all heavy atoms, respectively. The increases are caused by the larger pairwise rmsd values of the ensemble (0.47 Å and an all-heavy-atom rmsd of 0.86 Å only). Interestingly, the entire β sheet and some of the loops undergo conformational exchange between the three states in a concerted fashion [30]. In contrast, the α helix appears to be decoupled from the conformational exchange of the β sheet. Another set of conformers selected to describe structural states of the α helix indicates that the backbone of the α helix shows also distinct structural states, but the correlation is weaker than for the β sheet and is localized to the residues that face the hydrophobic core.

4.3.3. Cross-validation of the ensemble

To validate the three-state ensemble representation of GB3, a comparison with independently obtained data and a check of the self-consistency of the input data was performed. The checks were undertaken in two ways (Figure 21a). First, the eNOE-derived distances obtained from both cross peaks were arbitrarily changed according to normal distributions with standard deviations of 5, 10, and 15 %, and all eNOE-derived distances by 10 %, respectively. The target function values of the corresponding structure calculations are considerably larger in all cases, for example by a factor of two in the case of 10 % changes. In a second check, the eNOE data is

cross-validated by a jackknife error estimation [188]. 10 structure calculations were run from which 10 % of the input distance restraints were randomly omitted (each NOE is omitted in exactly one calculation). Then, an overall target function was calculated by summing over the target functions calculated for the omitted data. This cross-validation target function tends to decrease with increasing number of states. The target function for the three-state ensemble is 40 % lower than the one for the single-state structure. This outcome indicates that the three-state ensemble obtained with the reduced experimental data set is already close in structure to the one calculated with the entire data set. Therefore, the data set is at least in part over-determined.

Independent checks for the three-state ensemble of GB3 may also be obtained by comparison of X-ray and NMR parameters that quantify spatial sampling. For example, the angular spatial sampling of the backbone H^N-N vectors can be quantified by order parameters. Good agreement between those calculated from the ensemble and order parameters derived from RDCs measured under six alignment conditions [142-144] was obtained (Figure 21b). The minimal number of states previously determined to represent the data well is also the minimal number that yields satisfying order parameters. Another example constitutes a comparison between the obtained side-chain rotamer states and those in the 1.1 Å X-ray structure with PDB code 1IGD [208]. For residues 15, 21 and 35, the same two rotamer states as in the crystal structure are observed. Furtheron, the NMR ensemble includes all the rotamer states observed in the crystal structures with the exception of residues 7 and 47. Scalar and residual dipolar couplings as well as cross-correlated relaxation rates measured under liquid-state conditions are also in very good agreement with the rotamer states of the structural ensemble including residues 7 and 47. Some inconsistencies may be due to different sample conditions such as crystalline/liquid state or different buffer conditions. A very detailed comparison of the ensemble rotamer states with X-ray and NMR data is presented in reference [31].

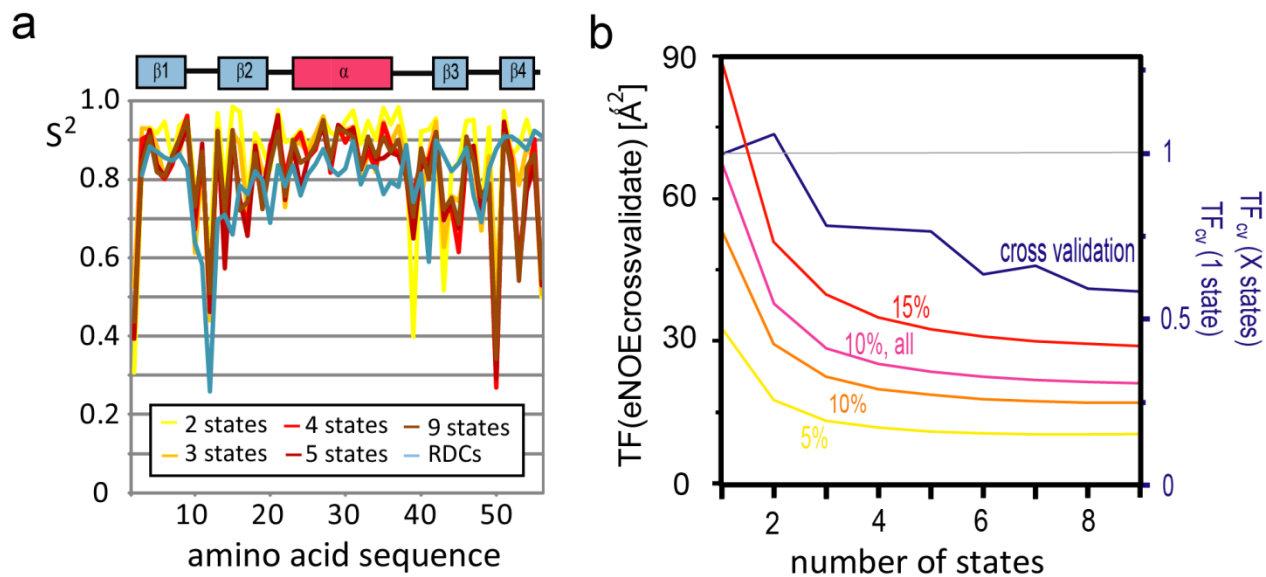


Figure 21. Cross-validation of the optimal number of states. **(a)** Backbone H^{N} -N order parameters obtained for ensembles calculated with 2, 3, 4, 5, and 9 states versus the amino sequence of GB3 are shown. For comparison, order parameters obtained from RDCs are drawn in blue. **(b)** The cross-validation target functions (TF) for three-state ensembles are shown. TFs obtained from a jackknife procedure are shown in blue, and upon random alteration of the distances obtained from both cross peaks by 5, 10, and 15 % in yellow, orange, and red, respectively, and upon random alteration of all distances by 10 % in pink.

5. Outlook

In conclusion, it is shown how highly precise and accurate NOEs can be measured (exact NOEs, eNOEs). It is relatively simple to record and evaluate the data. A simple conversion results in very exact averaged distances which allow to uncover even small effects. In particular, the eNOE is very sensitive to translational motion between (groups of) spins. The quality of the experimental data recorded on the protein GB3 was sufficient to calculate multiple-state ensembles which can be regarded as a discrete three-dimensional representation of protein motion.

At this point, our work is at a developing stage. We are currently exploring the potential of the method in answering biological questions. Nevertheless, there remains a number of open questions and challenges. Answering and overcoming these would pose major advances for the method. In the following, a list of the most important points (in the authors view, that is) are formulated.

5.1. Future challenges: 14 questions

5.1.1. Experimental

1. Can a complete excitation profile be achieved in the heavy-atom dimension of a NOESY experiment? In our experiments used so far, eNOEs were only evaluated for spin pairs that involve at least one proton that is bound to a nitrogen or an aliphatic carbon atom. Pathways that involve chemical shift labeling of aromatic carbons were only analysed in a semi-quantitative manner because the rectangular carbon excitation pulse and its counterpart after the evolution do

not sufficiently excite the frequency range above 100 ppm. To a smaller extent, the same effect is one of the reasons for a looser choice of the upper and lower distance restraints if only one cross peak can be evaluated. One obvious solution is to run a second buildup series with a shifted carrier frequency. However, this is not attractive since it would double the measurement time. It is conceivable that two more dedicated pulses may be used to cover the full carbon frequency range, possibly with different time increments (much like the simultaneous use of ^{15}N and ^{13}C evolution). Such a procedure may even allow to record two different spectral widths and resolutions for the two covered carbon frequency ranges.

2. How short must the mixing time be? eNOEs were obtained from NOESY experiments with mixing times which are shorter than used in conventional experiments. We provided a rule-of-thumb which is based on the overall tumbling time and allows for reliable estimates for the correction for spin diffusion from an approximate (previously known) structure [112]. Many cross peaks are thus lost in the noise. Although longer mixing times cause larger uncertainties, theoretically, iterative structure calculation and spin diffusion correction should converge also for long mixing times.

Previously, a simple approach to run longer NOESY mixing and thus extraction of many more and longer distances was based on a statistical analysis of the distance-intensity relationship [209]. Simulations of spectra of up to 400 ms mixing time for protonated proteins with 2 and 5 ns tumbling times show that possibly hundreds of additional peaks may be evaluated. Peaks corresponding to distances of 9 Å were observable. For example, for crambin with 5 ns tumbling time the peaks that were newly observed at 400 ms but not at 200 ms correspond to an average distance of 6.4 Å. Upper and lower bound limits may be obtained for these NOEs by using twice the standard deviation of the distance distribution, 1.5 Å.

3. How far can we see? For the perdeuterated sample of ubiquitin used in our analysis, the largest extracted distances are 8 Å. On one hand, the question is related to the previous one concerning the optimal mixing time. On the other hand, special isotope labelling should allow to record NOESY spectra with cross peaks between spins that are further apart than the typical 5 Å. Observation of NOEs over distances up to 12 Å in highly deuterated samples with protons incorporated into isoleucine δ 1-methyl sites has been reported [210]. Optimal mixing times were 1.25 and 0.8 s for ubiquitin and γ S crystallin in 2D NOESYs. The authors show that spin diffusion contributes no more than 12 % [210]. Obviously, another type of NOE, the historically previously observed dipolar interaction between a proton and an unpaired electron can be detected over distances of 25 Å [90].

4. How large can the studied systems be? Our detailed studies of eNOEs have been limited to the model proteins GB3 and ubiquitin with 6.5 and 8.5 kDa, respectively. Larger systems pose two fundamental challenges. First, large systems have large overall correlation times, which cause stronger transverse relaxation effects. As a consequence, magnetization is lost along the pathways during the pulse sequence. Longitudinal relaxation is reduced and thus the interscan delays must be increased. However, NOESY experiments belong to the group of experiments that can be used on very large systems because the transfer relies on longitudinal magnetization that is more favorable than transverse magnetization in terms of relaxation and the transfer is increasingly more efficient for increasing overall tumbling times. Theoretical considerations and experiments demonstrate that NOESY can be recorded with large deuterated proteins of several hundred kilodaltons [211].

The second limitation is caused by increased peak overlap for large systems. The problem is particularly pressing with respect to the diagonal peaks. Overcoming this hurdle is an active research field and holds promise for the future. Recording NOESYs with additional dimensions, such as 4D HXQC-NOESY-HXQC type pulse schemes would separate the two proton resonances by two heavy atom resonances [212]. In general, approaches to achieve a higher signal-to-noise ratio also allow a higher resolution. Mixed-time parallel (PARE) evolution in the [$^1\text{H}, ^{15}\text{N}$]-HMQC element of the 3D NOESY achieved a gain of a factor 1.7 for a 125 kDa complex of tetrameric KscA and SDS mixed micelles [213]. Another way to make the experiments more efficient (and allowing higher resolution) is the use of sparse sampling [214,215]. Simple Fourier transform is not the optimal processing of the data. Initially, Maximum Entropy Reconstruction (MaxEnt) was proposed to take full advantage of the approach [216]. Sparse sampling may also be combined with multidimensional decomposition (MDD) [217]. Good spectral quality for a double ^{13}C -resolved experiment was demonstrated with the 82 kDa Malate Synthase G [214]. Co-processing of the 4D spectra and a high-resolution 2D spectrum yielded 50-100 % more peaks as demonstrated with the integral human membrane protein VDAC-1 (overall tumbling time 70 ns due to detergent micelles) [218]. A challenge which is particularly emphasized for NOESY is the large dynamic range of the peak intensities (typically up to three orders of magnitude). Compressed sensing (CS) reconstruction of undersampled 3D NOESY promises to alleviate this problem substantially [215]. The dynamic range in time-shared 4D NOESY experiments was also substantially improved with the SCRUB algorithm which efficiently removes artifacts introduced by sparse sampling [219]. This technique has been shown to achieve a dynamic range of 10000/1 and reproduce correct peak intensities and lineshapes with 1.2 % of the data required for Nyquist sampling with 23 kDa and 29 kDa test samples. An alternative approach to reduce overlap is projection spectroscopy [220]. Simultaneous chemical

shift evolution on different spins can be used to resolve a maximum number of resonances. Detection of NOEs between amide protons has been demonstrated with a 2D spectrum where the [$^1\text{H}, ^{15}\text{N}$]-HMQC element of a HMQC-NOESY is projected on a single mixed dimension for a protein-DNA complex of 121 kDa [221]. Automated projection spectroscopy (APSY) makes use of evolution in several mixed dimensions subjected to different angles within the space spanned by the indirect dimensions to automatically generate peak positions in this higher-dimensional space [222].

5. eNOEs in solid-state NMR? So far, efficient and exact determination of internuclear distances via solid-state NMR in uniformly-labelled samples has proven difficult. Techniques such as rotational resonance (R^2) for homonuclear ^{13}C - ^{13}C spin pairs and rotational echo double resonance (REDOR) for heteronuclear ^{13}C - $^{15}\text{N}/^{19}\text{F}$ spin pairs have been used to quantify distances between isolated spin pairs [223]. The uncertainty is smaller than 1 Å. However, it would be desirable to have an analog to liquid-state NOESY that delivers distances throughout the entire molecule. In such experiments, the longitudinal ^{13}C magnetization may be exchanged while the proton decoupler is switched off (*Proton Driven Spin Diffusion*, PDSD) or operates at a weak field (*Dipolar-Assisted Rotational Resonance*, DARR) [224]. Due to the strong dipolar truncation in first-order recoupling small couplings cannot be detected. Instead, second-order recoupling sequences which exhibit a weaker truncation effect are used. Other experiments such as CHHC and NHHC make use of ^1H - ^1H transfer [225]. For routine structure calculation, the results of several types of experiments are used. Typically, the presence of a cross peak is interpreted as an upper distance limit of 5 Å. The determination of the distance in a more quantitative manner is hampered by the fact that a powder-averaged spectrum cannot be exactly

described by a rate equation. Nevertheless, approximations have been used to extract quantitative distances [226].

5.1.2. Ensemble calculation

6. How many eNOEs are needed? Since the cross-validation procedures indicated that the experimental data set of GB3 is in part over-determined, the question arises as to how much data is needed to obtain at least two distinct states in an ensemble. For example, we reduced the experimental input for the GB3 ensemble calculation by omitting the J coupling and the RDC data [31]. Interestingly, the rmsd is virtually identical for the three-state ensemble. However, extraction of the concerted motion is less straight-forward, although it is still present. Therefore, it is recommended to measure a small set of J couplings and/or RDCs in addition to the eNOEs. On the other hand, we did not use eNOEs involving pseudoatoms of methylene groups, only conventional upper limits for aromatics and very conservative restraints for methyl groups. We are currently working on the quantitative use of all these eNOEs.

7. What is the best choice for upper and lower limits? So far, we have used limits that are symmetric about distance restraints. As already outlined in the text previously, more intuitively, the limits should be symmetric about the cross-relaxation rate constants. This choice, however, seems not substantiated by the comparison between the experimental distances and those extracted from the high-resolution structure. In addition, the generality of our choice of numeric tolerances if only one cross peak for a spin pair could be evaluated remains to be established/refined.

8. Is there a perfect cross-validation? Complete self-consistent over-determination will probably never be achieved. Typically, well-defined regions of a molecule may be partially overdetermined while other parts are strongly underdetermined. Although many cross-validation procedures have been proposed, an ideal self-consistency check is very difficult to establish. To account for the incomplete definition of an NMR structure an inferential structure determination protocol has been proposed [227]. For characterization of the structure, Bayesian inference is used to derive a probability distribution [227]. The protocol was applied to the determination of an ensemble from averaged data [228].

9. How can we represent segmental optimal numbers of states? In our approach, the entire molecule is represented with a uniform number of states. However, it is likely that flexible parts of the molecule require more states and rigid ones less for a proper representation. For example, one may wonder what happens in a segment with two very distinct, equally populated states if a three-state ensemble is calculated.

It has been proposed to select only those restraints for ensemble averaging that cause a large violation in a conventional structure calculation [122].

As mentioned above, inferential structure determination may turn out to be the protocol of choice [227,228].

10. Can we correctly incorporate the time scales? In virtually all ensemble refinement protocols all NMR observables are averaged in a uniform manner, irrespective of the time windows they are sensitive to. To make things even worse, the NOE rate averages differently over short and long time scales, and the practical choice of averaging (r^{-6} versus r^{-3}) seems rather heuristic in most publications.

11. Can/shall we incorporate anisotropic tumbling? All studies rely on the assumption of isotropic overall tumbling of the molecule. The reason is that the anisotropic model requires *a priori* knowledge of the structure and is mathematically more expensive. In principle, it is possible to adapt a method proposed for structure calculation with distances from ISPA to our purposes: Behling et al. periodically updated distance constraints (calculated with the anisotropic model) during energy minimization [229]. It is also unknown how large the effect of internal motion is on rendering the anisotropic more isotropic.

12. Can we detect allosteric mechanisms? Efficient propagation of local perturbations through the protein must be mechanically mediated by coupled elements. In taking one extreme end of the point of view, a model has been proposed that bases allostery solely on the redistribution of atomic fluctuations about mean coordinates [230], and several examples have been reported since then [231-233]. In principle, such motion should be detectable with the eNOE method.

13. Is fully automated software possible? We are currently working on a software solution that integrates as many steps in the entire procedure as possible. Ultimately, it is desirable to have an automated streamline encompassing peak fitting, buildup fitting, correction for spin diffusion and structure calculation.

14. What do intermolecular eNOEs offer? Lastly, it is tempting to contemplate the NOE phenomenon mediated between different molecules, for example, the transferred NOE or INPHARMA. Very interesting prospects offer RNA-protein and protein-protein complexes and binding of small ligands. It is clear that the underlying mathematics is complex, but in principle it

is the same as presented in this work. For example, pharmacophore applications may benefit from the use of exact NOEs.

6. Appendix

The Master equation

The stochastic Hamiltonians are expressed in terms of irreducible tensor operators of rank 2, T_m , and stationary random functions given by second order spherical harmonics, F_m :

$$H_1(t) = \sum_{m=-2}^2 T_m F_m(t) \quad (\text{A1.1})$$

Transformation of $H_1(t)$ into the interaction frame gives:

$$H_1^{\text{int}}(t) = \sum_{m,n} T_m^n F_m(t) e^{i\omega_m^n t} \quad (\text{A1.2})$$

with

$$[H_0, T_m^n] = \omega_m^n T_m^n \quad (\text{A2})$$

T_m^n and ω_m^n are the eigenfunctions and the eigenvalues of $[H_0, \cdot]$. Note that many different conventions are used throughout the literature. Here, the conventions of reference [41] are chosen with the exception that the r dependence is absorbed into the stationary random function in order to maintain a time-dependence of r . The physical constants are collected into the irreducible tensor operators by introducing the following two factors for chemical shift anisotropy (CSA) and dipolar interactions:

$$A_{\text{CSA}(i)} = -\sqrt{\frac{1}{30}} \gamma \Delta \sigma_i \quad (\text{A3.1})$$

$$A_{\text{D}(i,j)} = \sqrt{\frac{3}{10}} \frac{\mu_0}{4\pi} \frac{\gamma^2 \hbar}{(r_{ij}^{\text{rigid}})^3} \quad (\text{A3.2})$$

$\Delta\sigma_i$ is the difference between the parallel and perpendicular main components of Ω_i^a of nucleus i . The expression is exact if the CSA tensor is symmetric. An anisotropic tensor can be constructed by the sum of two symmetric tensors [A1]. Since the polarizing magnetic field is directed along the z axis, \vec{B}_0 reduces to $(0, 0, B_0)^T$. Transverse operators are expressed with the raising and lowering operators defined as:

$$I_{i,\pm} = I_{i,x} \pm iI_{i,y} \quad (\text{A4})$$

For the CSA Hamiltonian of spin i ($a = \text{CSA}(i)$), T_m and F_m are

$$T_0^{\text{CSA}(i)} = -\frac{4A_{\text{CSA}(i)}}{\sqrt{6}} B_0 I_{i,z} \quad (\text{A5.1})$$

$$T_{\pm 1}^{\text{CSA}(i)} = \pm A_{\text{CSA}(i)} B_0 I_{i,\pm} \quad (\text{A5.2})$$

$$T_{\pm 2}^{\text{CSA}(i)} = 0 \quad (\text{A5.3})$$

$$F_m^{\text{CSA}(i)}(t) = \sqrt{4\pi} Y_{2m}^*(\theta_i(t), \varphi_i(t)) \quad (\text{A6})$$

θ_i and φ_i are the polar angles defining the orientation of the tensor main axis of nucleus i . Y_{2m} are the spherical harmonics of rank 2:

$$Y_{20}(\theta, \varphi) = \sqrt{\frac{5}{16\pi}} (3\cos^2\theta - 1) \quad (\text{A7.1})$$

$$Y_{2\pm 1}(\theta, \varphi) = \mp \sqrt{\frac{15}{8\pi}} e^{\pm i\varphi} \sin \theta \cos \theta \quad (\text{A7.2})$$

$$Y_{2\pm 2}(\theta, \varphi) = \sqrt{\frac{15}{32\pi}} e^{\pm 2i\varphi} \sin^2 \theta \quad (\text{A7.3})$$

The asterisk designates the complex conjugate. The addition theorem for spherical harmonics of rank 2 is

$$\frac{4\pi}{5} \sum_{m=-2}^2 Y_{2m}^*(\theta_{a'}, \varphi_{a'}) Y_{2m}(\theta_a, \varphi_a) = P_2(\cos \Theta_{aa'}) \quad (\text{A8})$$

$\Theta_{aa'}$ is the projection angle between the axes of interactions a and a' .

Transformation of $T_m^{\text{CSA}(i)}$ into the interaction frame yields only terms with $n = 0$:

$$T_m^{0, \text{CSA}(i)} = T_m^{\text{CSA}(i)} \quad (\text{A9})$$

and

$$\omega_0^{0, \text{CSA}(i)} = 0 \quad (\text{A10.1})$$

$$\omega_{\pm 1}^{0, \text{CSA}(i)} = \pm \omega_i \quad (\text{A10.2})$$

For the dipolar Hamiltonian of spins i and j , T_m and F_m are ($a = \text{D}(i, j)$)

$$T_0^{\text{D}(i, j)} = -\frac{A_{\text{D}}}{\sqrt{6}} \left(4I_{i,z} I_{j,z} - (I_{i,+} I_{j,-} + I_{i,-} I_{j,+}) \right) \quad (\text{A11.1})$$

$$T_{\pm 1}^{\text{D}(i, j)} = \pm A_{\text{D}} \left(I_{i,z} I_{j,\pm} + I_{i,\pm} I_{j,z} \right) \quad (\text{A11.2})$$

$$T_{\pm 2}^{\text{D}(i, j)} = -A_{\text{D}} I_{i,\pm} I_{j,\pm} \quad (\text{A11.3})$$

$$F_m^{\text{D}(i,j)}(t) = \frac{(r_{ij}^{\text{rigid}})^3}{r_{ij}^3(t)} \sqrt{4\pi} Y_{2m}^*(\theta_i(t), \varphi_i(t)) \quad (\text{A12})$$

θ_i and φ_i are the polar angles defining the orientation of the r vector connecting spins i and j .

Transformation of $T_m^{\text{D}(i,j)}$ into the interaction frame gives terms with $n = 1, 2, 3$:

$$T_0^{1,\text{D}(i,j)} = -\frac{A_D}{\sqrt{6}} 4I_{i,z} I_{j,z} \quad (\text{A13.1})$$

$$T_0^{2,\text{D}(i,j)} = \frac{A_D}{\sqrt{6}} I_{i,+} I_{j,-} \quad (\text{A13.2})$$

$$T_0^{3,\text{D}(i,j)} = \frac{A_D}{\sqrt{6}} I_{i,-} I_{j,+} \quad (\text{A13.3})$$

$$T_{\pm 1}^{1,\text{D}(i,j)} = \pm A_D I_{i,\pm} I_{j,z} \quad (\text{A13.4})$$

$$T_{\pm 1}^{2,\text{D}(i,j)} = \pm A_D I_{i,z} I_{j,\pm} \quad (\text{A13.5})$$

$$T_{\pm 2}^{1,\text{D}(i,j)} = A_D I_{i,\pm} I_{j,\pm} \quad (\text{A13.6})$$

and

$$\omega_0^{1,\text{D}(i,j)} = 0 \quad (\text{A14.1})$$

$$\omega_0^{2,\text{D}(i,j)} = \omega_i - \omega_j \quad (\text{A14.2})$$

$$\omega_0^{3,\text{D}(i,j)} = -(\omega_i - \omega_j) \quad (\text{A14.3})$$

$$\omega_{\pm 1}^{1,\text{D}(i,j)} = \pm \omega_i \quad (\text{A14.4})$$

$$\omega_{\pm 1}^{2,D(i,j)} = \pm \omega_j \quad (\text{A14.5})$$

$$\omega_{\pm 2}^{1,D(i,j)} = \pm (\omega_i + \omega_j) \quad (\text{A14.6})$$

In the derivation of equation 5, the following properties are used:

$$F_m^a(t) \sim Y_{2m}^*(\theta_a(t), \varphi_a(t)) = (-1)^m Y_{2-m}(\theta_a(t), \varphi_a(t)) \sim (-1)^m F_{-m}^{a*}(t) \quad (\text{A15})$$

Hubbard has shown the following useful properties of spherical harmonics Y_{lm} [A2]:

$$\langle Y_{lm}(0) Y_{l'm'}(t) \rangle = \langle Y_{lm}(-t) Y_{l'm'}(0) \rangle \quad (\text{A16})$$

$$\langle Y_{lm}(\tau) Y_{l'm'}(0) \rangle = \delta_{l,l'} \delta_{-m,m'} (-1)^m \langle Y_{l0}(\tau) Y_{l0}(0) \rangle \quad (\text{A17})$$

where $\delta_{l,l'}$ is Kronecker's delta function. These properties imply the drastic simplifications for the correlation function used to derive equation 29. Equation A16 is a mathematical motivation for replacing t by 0 in the correlation function. From equations A15 and A17 follows

$$\begin{aligned} \langle F_{-m}^{a*}(t+\tau) F_m^a(t) \rangle &\sim \langle Y_{2-m}(\theta_{a'}, \varphi_{a'}) Y_{2m}^*(\theta_a, \varphi_a) \rangle \\ &= (-1)^{-m'} \langle Y_{2m'}^*(\theta_{a'}, \varphi_{a'}) Y_{2m}^*(\theta_a, \varphi_a) \rangle = \delta_{m',-m} \langle Y_{20}^*(\theta_{a'}, \varphi_{a'}) Y_{20}^*(\theta_a, \varphi_a) \rangle \\ &\sim \delta_{m',-m} \langle F_0^{a'}(t+\tau) F_0^a(t) \rangle \end{aligned} \quad (\text{A18})$$

As pointed out in the literature, equation A17 is true if the stochastic processes described by F_m are statistically independent [37,41,A3]. In the present case, perhaps a better argument for $\delta_{m,-m'}$ is the fact that $\omega_m^{n,a} \approx -\omega_{m'}^{n',a'}$ cannot be fulfilled for $m \neq -m'$ if $\omega_{i,j}$ is in the range typically obtained for protons in high-field NMR. Thus, such contributions to the Master equation are non-secular and averaged out independently from the exact nature of the correlation function.

In the derivation of equation 6, the following property is used:

$$\text{Trace}(A[B,C]) = \text{Trace}([A,B]C) \quad \text{for any operators } A, B, C \quad (\text{A19})$$

Non-degenerate and degenerate transitions in NOESY

In the following, some explicit calculations are shown for the evaluation of the relaxation matrix R in equation 9. First, some useful spin operator commutation rules are recalled.

$$[I_{i,z}, I_{i,\pm}] = \pm I_{i,\pm} \quad (\text{A20})$$

$$[I_{i,+}, I_{i,-}] = 2I_{i,z} \quad (\text{A21})$$

$$[I_{i,\mu}, I_{j,\mu}] = 0 \quad \mu = x, y, z, +, - \quad (\text{A22})$$

$$[AB,C] = [A,C]B + A[B,C] \quad \text{for any operators } A, B, C \quad (\text{A23})$$

The following relationships can easily be verified (for example, by means of the Pauli matrices).

$$I_{i,\pm} I_{i,\mp} = \pm \frac{1}{2} I_{i,z} \quad (\text{A24})$$

$$I_{i,z} I_{i,z} = \frac{1}{4} \quad (\text{A25})$$

$$I_{i,z} I_{i,\pm} = \pm \frac{1}{2} I_{i,\pm} \quad (\text{A26})$$

$$I_{i,\pm}I_{i,z} = \mp \frac{1}{2}I_{i,\pm} \quad (\text{A27})$$

A complete evaluation of equations 7.1 and 7.2 for $\langle b \rangle = \langle I_{i,z} \rangle$ is provided in Tables A1-A8. Some examples for $\langle b \rangle = \langle 2I_{i,z}I_{j,z} \rangle$ are shown in Tables A9 and A10. It is assumed that the high-temperature approximation holds and $\rho_0 \sim H_0$ nulls all double commutators. Dipolar interaction with $a = D(i,j)$ and $a' = D(i,j)$ induces the non-degenerate and the additional degenerate auto-correlated relaxation pathways listed in Tables A1 and A2, respectively. CSA auto-correlated relaxation is caused by $a = \text{CSA}(i)$ and $a' = \text{CSA}(i)$ from the non-degenerate relaxation pathways as listed in Table A3. There are no additional degenerate relaxation pathways. Pathways induced by cross-correlated relaxation between $a = D(i,j)$ and $a' = \text{CSA}(i)$ and vice versa for non-degenerate and degenerate transitions are listed in Tables A4 and A5, respectively. Dipolar cross-correlated relaxation between $a = D(i,j)$ and $a' = D(i,k)$ and vice versa for non-degenerate transition is treated in Table A6, and for degenerate transitions in Tables A7 ($\omega_j = \omega_k$) and A8 ($\omega_i = \omega_j$). For $\langle b \rangle = \langle 2I_{i,z}I_{j,z} \rangle$, the non-degenerate transition cases for dipolar and CSA auto-correlated relaxation are shown in Tables A9 and A10. Generalization to all other cases is trivial. Summation of all terms in Tables A1 and A3 whose double commutator yields $I_{i,z}$ produces the auto-relaxation rate constants R_{ij}^D and R_i^{CSA} , respectively. The same procedure produces the cross-relaxation rate constant σ_{ij} when the double commutators yield $I_{j,z}$. Inspection of Table A2 shows that dipolar auto-correlated relaxation is identical if non-degenerate transitions are included. Similar considerations with Tables A4 and A6 demonstrate that cross-correlated relaxation creates two- and three-spin order. Non-degenerate transitions add pathways to zero-

quantum transitions (see Tables A5, A7 and A8). It is noted that this effect cannot be represented with the basis chosen in equation 11.

Table A1. Evaluation of the relaxation pathways with $a = D(i,j)$ and $a' = D(i,j)$ for non-degenerate transitions and $\langle b \rangle = \langle I_{i,z} \rangle$.

$\omega_m^{n,a}$	$(-1)^m$	factor	commutator
0	1	$\frac{8}{3} A_{D(i,j)}^2$	$[I_{i,z} I_{j,z}, [I_{i,z} I_{j,z}, I_{i,z}]] = [I_{i,z} I_{j,z}, 0] = 0$
ω_i	-1	$-A_{D(i,j)}^2$	$[I_{i,+} I_{j,z}, [I_{i,-} I_{j,z}, I_{i,z}]] = [I_{i,+} I_{j,z}, I_{i,-} I_{j,z}]$ $= [I_{i,+}, I_{i,-} I_{j,z}] I_{j,z} + I_{i,+} [I_{j,z}, I_{i,-} I_{j,z}] = 2I_{i,z} I_{j,z} I_{j,z} = \frac{1}{2} I_{i,z}$
ω_i	-1	$-A_{D(i,j)}^2$	$[I_{i,-} I_{j,z}, [I_{i,+} I_{j,z}, I_{i,z}]] = [I_{i,-} I_{j,z}, -I_{i,+} I_{j,z}]$ $= [I_{i,-}, -I_{i,+} I_{j,z}] I_{j,z} + I_{i,-} [I_{j,z}, -I_{i,+} I_{j,z}] = 2I_{i,z} I_{j,z} I_{j,z} = \frac{1}{2} I_{i,z}$
ω_j	-1	$-A_{D(i,j)}^2$	$[I_{i,z} I_{j,+}, [I_{i,z} I_{j,-}, I_{i,z}]] = [I_{i,z} I_{j,+}, 0] = 0$
ω_j	-1	$-A_{D(i,j)}^2$	$[I_{i,z} I_{j,-}, [I_{i,z} I_{j,+}, I_{i,z}]] = [I_{i,z} I_{j,-}, 0] = 0$
$\omega_i + \omega_j$	1	$A_{D(i,j)}^2$	$[I_{i,+} I_{j,+}, [I_{i,-} I_{j,-}, I_{i,z}]] = [I_{i,+} I_{j,+}, I_{i,-} I_{j,-}]$ $= [I_{i,+}, I_{i,-} I_{j,-}] I_{j,+} + I_{i,+} [I_{j,+}, I_{i,-} I_{j,-}]$ $= 2I_{i,z} I_{j,-} I_{j,+} + 2I_{i,+} I_{j,z} I_{i,-}$ $= 2I_{i,z} (\frac{1}{2} - I_{j,z}) + 2(\frac{1}{2} + I_{i,z}) I_{j,z} = I_{i,z} + I_{j,z}$
$\omega_i + \omega_j$	1	$A_{D(i,j)}^2$	$[I_{i,-} I_{j,-}, [I_{i,+} I_{j,+}, I_{i,z}]] = [I_{i,-} I_{j,-}, -I_{i,+} I_{j,+}]$ $= [I_{i,-}, -I_{i,+} I_{j,+}] I_{j,-} + I_{i,-} [I_{j,-}, -I_{i,+} I_{j,+}]$ $= 2I_{i,z} I_{j,+} I_{j,-} + 2I_{i,-} I_{j,z} I_{i,+}$ $= 2I_{i,z} (\frac{1}{2} + I_{j,z}) + 2(\frac{1}{2} - I_{i,z}) I_{j,z} = I_{i,z} + I_{j,z}$
$\omega_i - \omega_j$	1	$\frac{1}{6} A_{D(i,j)}^2$	$[I_{i,+} I_{j,-}, [I_{i,-} I_{j,+}, I_{i,z}]] = [I_{i,+} I_{j,-}, I_{i,-} I_{j,+}]$ $= [I_{i,+}, I_{i,-} I_{j,+}] I_{j,-} + I_{i,+} [I_{j,-}, I_{i,-} I_{j,+}]$ $= 2I_{i,z} I_{j,+} I_{j,-} - 2I_{i,+} I_{j,z} I_{i,-}$ $= 2I_{i,z} (\frac{1}{2} + I_{j,z}) - 2(\frac{1}{2} + I_{i,z}) I_{j,z} = I_{i,z} - I_{j,z}$
$\omega_i - \omega_j$	1	$\frac{1}{6} A_{D(i,j)}^2$	$[I_{i,-} I_{j,+}, [I_{i,+} I_{j,-}, I_{i,z}]] = [I_{i,-} I_{j,+}, -I_{i,+} I_{j,-}]$ $= [I_{i,-}, -I_{i,+} I_{j,-}] I_{j,+} + I_{i,-} [I_{j,+}, -I_{i,+} I_{j,-}]$ $= 2I_{i,z} I_{j,-} I_{j,+} - 2I_{i,-} I_{j,z} I_{i,+}$ $= 2I_{i,z} (\frac{1}{2} - I_{j,z}) - 2(\frac{1}{2} - I_{i,z}) I_{j,z} = I_{i,z} - I_{j,z}$

Table A2. Evaluation of the additional relaxation pathways with $a = D(i,j)$ and $a' = D(i,j)$ for degenerate transitions and $\langle b \rangle = \langle I_{i,z} \rangle$.

$\omega_m^{n,a}$	$(-1)^m$	factor	commutator
0	1	$-\frac{2}{3} A_{D(i,j)}^2$	$\begin{aligned} & [I_{i,z} I_{j,z}, [I_{i,+} I_{j,-}, I_{i,z}]] = [I_{i,z} I_{j,z}, -I_{i,+} I_{j,-}] = \\ & [I_{i,z}, -I_{i,+} I_{j,-}] I_{j,z} + I_{i,z} [I_{j,z}, -I_{i,+} I_{j,-}] = \\ & -I_{i,+} I_{j,-} I_{j,z} + I_{i,z} I_{i,+} I_{j,-} = -\frac{1}{2} I_{i,+} I_{j,-} + \frac{1}{2} I_{i,+} I_{j,-} = 0 \end{aligned}$
0	1	$-\frac{2}{3} A_{D(i,j)}^2$	$[I_{i,+} I_{j,-}, [I_{i,z} I_{j,z}, I_{i,z}]] = [I_{i,+} I_{j,-}, 0] = 0$
0	1	$-\frac{2}{3} A_{D(i,j)}^2$	$\begin{aligned} & [I_{i,z} I_{j,z}, [I_{i,-} I_{j,+}, I_{i,z}]] = [I_{i,z} I_{j,z}, I_{i,-} I_{j,+}] = \\ & [I_{i,z}, I_{i,-} I_{j,+}] I_{j,z} + I_{i,z} [I_{j,z}, I_{i,-} I_{j,+}] = \\ & -I_{i,-} I_{j,+} I_{j,z} + I_{i,z} I_{i,-} I_{j,+} = \frac{1}{2} I_{i,-} I_{j,+} - \frac{1}{2} I_{i,-} I_{j,+} = 0 \end{aligned}$
0	1	$-\frac{2}{3} A_{D(i,j)}^2$	$[I_{i,-} I_{j,+}, [I_{i,z} I_{j,z}, I_{i,z}]] = [I_{i,-} I_{j,+}, 0] = 0$
$\omega_i = \omega_j$	-1	$-A_{D(i,j)}^2$	$[I_{i,+} I_{j,z}, [I_{i,z} I_{j,-}, I_{i,z}]] = [I_{i,+} I_{j,z}, 0] = 0$
$\omega_i = \omega_j$	-1	$-A_{D(i,j)}^2$	$[I_{i,-} I_{j,z}, [I_{i,z} I_{j,+}, I_{i,z}]] = [I_{i,-} I_{j,z}, 0] = 0$
$\omega_i = \omega_j$	-1	$-A_{D(i,j)}^2$	$\begin{aligned} & [I_{i,z} I_{j,-}, [I_{i,+} I_{j,z}, I_{i,z}]] = [I_{i,z} I_{j,-}, -I_{i,+} I_{j,z}] = \\ & [I_{i,z}, -I_{i,+} I_{j,z}] I_{j,-} + I_{i,z} [I_{j,-}, -I_{i,+} I_{j,z}] = \\ & = -2I_{i,+} I_{j,z} I_{j,-} - 2I_{i,z} I_{j,-} I_{i,+} \\ & = 2I_{i,+} (\frac{1}{2} I_{j,-}) - 2(\frac{1}{2} I_{i,+}) I_{j,-} = 0 \end{aligned}$
$\omega_i = \omega_j$	-1	$-A_{D(i,j)}^2$	$\begin{aligned} & [I_{i,z} I_{j,+}, [I_{i,-} I_{j,z}, I_{i,z}]] = [I_{i,z} I_{j,+}, I_{i,-} I_{j,z}] = \\ & [I_{i,z}, I_{i,-} I_{j,z}] I_{j,+} + I_{i,z} [I_{j,+}, I_{i,-} I_{j,z}] = \\ & = -2I_{i,-} I_{j,z} I_{j,+} - 2I_{i,z} I_{j,+} I_{i,-} \\ & = -2I_{i,-} (\frac{1}{2} I_{j,+}) + 2(\frac{1}{2} I_{i,-}) I_{j,+} = 0 \end{aligned}$

Table A3. Evaluation of the relaxation pathways with $a = \text{CSA}(i)$ and $a' = \text{CSA}(i)$ for $\langle b \rangle = \langle I_{i,z} \rangle$.

$\omega_m^{n,a}$	$(-1)^m$	factor	commutator
0	1	$\frac{8}{3} A_{\text{CSA}(i)}^2 B_0^2$	$[I_{i,z}, [I_{i,z}, I_{i,z}]] = [I_{i,z}, 0] = 0$
ω_i	-1	$-A_{\text{CSA}(i)}^2 B_0^2$	$[I_{i,+}, [I_{i,-}, I_{i,z}]] = [I_{i,+}, I_{i,-}] = 2I_{i,z}$
ω_i	-1	$-A_{\text{CSA}(i)}^2 B_0^2$	$[I_{i,-}, [I_{i,+}, I_{i,z}]] = [I_{i,-}, -I_{i,+}] = 2I_{i,z}$

Table A4. Evaluation of the relaxation pathways with $a = \text{D}(i,j)$ and $a' = \text{CSA}(i)$ and vice versa for non-degenerate transitions and $\langle b \rangle = \langle I_{i,z} \rangle$.

$\omega_m^{n,a}$	$(-1)^m$	factor	commutator
0	1	$\frac{8}{3} A_{\text{D}(i,j)} A_{\text{CSA}(i)} B_0$	$[I_{i,z} I_{j,z}, [I_{i,z}, I_{i,z}]] = [I_{i,z} I_{j,z}, 0] = 0$
0	1	$\frac{8}{3} A_{\text{D}(i,j)} A_{\text{CSA}(i)} B_0$	$[I_{i,z}, [I_{i,z} I_{j,z}, I_{i,z}]] = [I_{i,z}, 0] = 0$
ω_i	-1	$-A_{\text{CSA}(i)} A_{\text{D}(i,j)} B_0$	$[I_{i,+} I_{j,z}, [I_{i,-}, I_{i,z}]] = [I_{i,+} I_{j,z}, I_{i,-}] = 2I_{i,z} I_{j,z}$
ω_i	-1	$-A_{\text{CSA}(i)} A_{\text{D}(i,j)} B_0$	$[I_{i,-}, [I_{i,+} I_{j,z}, I_{i,z}]] = [I_{i,-}, -I_{i,+} I_{j,z}] = 2I_{i,z} I_{j,z}$
ω_i	-1	$-A_{\text{CSA}(i)} A_{\text{D}(i,j)} B_0$	$[I_{i,-} I_{j,z}, [I_{i,+}, I_{i,z}]] = [I_{i,-} I_{j,z}, -I_{i,+}] = 2I_{i,z} I_{j,z}$
ω_i	-1	$-A_{\text{CSA}(i)} A_{\text{D}(i,j)} B_0$	$[I_{i,+}, [I_{i,-} I_{j,z}, I_{i,z}]] = [I_{i,+}, I_{i,-} I_{j,z}] = 2I_{i,z} I_{j,z}$

Table A5. Evaluation of the additional relaxation pathways with $a = \text{D}(i,j)$ and $a' = \text{CSA}(i)$ and vice versa for degenerate transitions and $\langle b \rangle = \langle I_{i,z} \rangle$.

$\omega_m^{n,a}$	$(-1)^m$	factor	commutator
0	1	$-\frac{2}{3} A_{\text{CSA}(i)} A_{\text{D}(i,j)} B_0$	$[I_{i,+} I_{j,-}, [I_{i,z}, I_{i,z}]] = [I_{i,+} I_{j,-}, 0] = 0$
0	1	$-\frac{2}{3} A_{\text{CSA}(i)} A_{\text{D}(i,j)} B_0$	$[I_{i,z}, [I_{i,+} I_{j,-}, I_{i,z}]] = [I_{i,z}, -I_{i,+} I_{j,-}] = -2I_{i,+} I_{j,-}$
0	1	$-\frac{2}{3} A_{\text{CSA}(i)} A_{\text{D}(i,j)} B_0$	$[I_{i,-} I_{j,+}, [I_{i,z}, I_{i,z}]] = [I_{i,-} I_{j,+}, 0] = 0$
0	1	$-\frac{2}{3} A_{\text{CSA}(i)} A_{\text{D}(i,j)} B_0$	$[I_{i,z}, [I_{i,-} I_{j,+}, I_{i,z}]] = [I_{i,z}, I_{i,-} I_{j,+}] = -2I_{i,-} I_{j,+}$

Table A6. Evaluation of the cross-correlated relaxation pathways with $a = D(i,j)$ and $a' = D(i,k)$ and vice versa for non-degenerate transitions and $\langle b \rangle = \langle I_{i,z} \rangle$.

$\omega_m^{n,a}$	$(-1)^m$	factor	commutator
0	1	$\frac{8}{3} A_{D(i,j)} A_{D(i,k)}$	$[I_{i,z} I_{j,z}, [I_{i,z} I_{k,z}, I_{i,z}]] = [I_{i,z} I_{j,z}, 0] = 0$
0	1	$\frac{8}{3} A_{D(i,j)} A_{D(i,k)}$	$[I_{i,z} I_{k,z}, [I_{i,z} I_{j,z}, I_{i,z}]] = [I_{i,z} I_{k,z}, 0] = 0$
ω_i	-1	$-A_{D(i,j)} A_{D(i,k)}$	$[I_{i,+} I_{j,z}, [I_{i,-} I_{k,z}, I_{i,z}]] = [I_{i,+} I_{j,z}, I_{i,-} I_{k,z}]$ $= 2I_{i,z} I_{j,z} I_{k,z} = \frac{1}{2} 4I_{i,z} I_{j,z} I_{k,z}$
ω_i	-1	$-A_{D(i,j)} A_{D(i,k)}$	$[I_{i,-} I_{j,z}, [I_{i,+} I_{k,z}, I_{i,z}]] = [I_{i,-} I_{j,z}, -I_{i,+} I_{k,z}]$ $= 2I_{i,z} I_{j,z} I_{k,z} = \frac{1}{2} 4I_{i,z} I_{j,z} I_{k,z}$
ω_i	-1	$-A_{D(i,j)} A_{D(i,k)}$	$[I_{i,+} I_{k,z}, [I_{i,-} I_{j,z}, I_{i,z}]] = [I_{i,+} I_{k,z}, I_{i,-} I_{j,z}]$ $= 2I_{i,z} I_{j,z} I_{k,z} = \frac{1}{2} 4I_{i,z} I_{j,z} I_{k,z}$
ω_i	-1	$-A_{D(i,j)} A_{D(i,k)}$	$[I_{i,-} I_{k,z}, [I_{i,+} I_{j,z}, I_{i,z}]] = [I_{i,-} I_{k,z}, -I_{i,+} I_{j,z}]$ $= 2I_{i,z} I_{j,z} I_{k,z} = \frac{1}{2} 4I_{i,z} I_{j,z} I_{k,z}$

Table A7. Evaluation of the additional cross-correlated relaxation pathways with $a = D(i,j)$ and $a' = D(i,k)$ and vice versa for degenerate transitions with $\omega_j = \omega_k$ and $\langle b \rangle = \langle I_{i,z} \rangle$.

$\omega_m^{n,a}$	$(-1)^m$	factor	commutator
$\omega_j = \omega_k$	-1	$-A_{D(i,j)}A_{D(i,k)}$	$\left[I_{i,z}I_{j,+}, \left[I_{i,z}I_{k,-}, I_{i,z} \right] \right] = \left[I_{i,z}I_{j,+}, 0 \right] = 0$
$\omega_j = \omega_k$	-1	$-A_{D(i,j)}A_{D(i,k)}$	$\left[I_{i,z}I_{k,-}, \left[I_{i,z}I_{j,+}, I_{i,z} \right] \right] = \left[I_{i,z}I_{k,-}, 0 \right] = 0$
$\omega_j = \omega_k$	-1	$-A_{D(i,j)}A_{D(i,k)}$	$\left[I_{i,z}I_{j,-}, \left[I_{i,z}I_{k,+}, I_{i,z} \right] \right] = \left[I_{i,z}I_{j,-}, 0 \right] = 0$
$\omega_j = \omega_k$	-1	$-A_{D(i,j)}A_{D(i,k)}$	$\left[I_{i,z}I_{k,+}, \left[I_{i,z}I_{j,-}, I_{i,z} \right] \right] = \left[I_{i,z}I_{k,+}, 0 \right] = 0$
$\omega_i + \omega_j$ $= \omega_i + \omega_k$	1	$A_{D(i,j)}A_{D(i,k)}$	$\left[I_{i,+}I_{j,+}, \left[I_{i,-}I_{k,-}, I_{i,z} \right] \right] = \left[I_{i,+}I_{j,+}, I_{i,-}I_{k,-} \right] = 2I_{i,z}I_{j,+}I_{k,-}$
$\omega_i + \omega_j$ $= \omega_i + \omega_k$	1	$A_{D(i,j)}A_{D(i,k)}$	$\left[I_{i,-}I_{k,-}, \left[I_{i,+}I_{j,+}, I_{i,z} \right] \right] = \left[I_{i,-}I_{k,-}, -I_{i,+}I_{j,+} \right] = 2I_{i,z}I_{j,+}I_{k,-}$
$\omega_i + \omega_j$ $= \omega_i + \omega_k$	1	$A_{D(i,j)}A_{D(i,k)}$	$\left[I_{i,+}I_{k,+}, \left[I_{i,-}I_{j,-}, I_{i,z} \right] \right] = \left[I_{i,+}I_{k,+}, I_{i,-}I_{j,-} \right] = 2I_{i,z}I_{j,-}I_{k,+}$
$\omega_i + \omega_j$ $= \omega_i + \omega_k$	1	$A_{D(i,j)}A_{D(i,k)}$	$\left[I_{i,-}I_{j,-}, \left[I_{i,+}I_{k,+}, I_{i,z} \right] \right] = \left[I_{i,-}I_{j,-}, -I_{i,+}I_{k,+} \right] = 2I_{i,z}I_{j,-}I_{k,+}$
$\omega_i - \omega_j$ $= \omega_i - \omega_k$	1	$\frac{1}{6}A_{D(i,j)}A_{D(i,k)}$	$\left[I_{i,+}I_{j,-}, \left[I_{i,-}I_{k,+}, I_{i,z} \right] \right] = \left[I_{i,+}I_{j,-}, I_{i,-}I_{k,+} \right] = 2I_{i,z}I_{j,-}I_{k,+}$
$\omega_i - \omega_j$ $= \omega_i - \omega_k$	1	$\frac{1}{6}A_{D(i,j)}A_{D(i,k)}$	$\left[I_{i,-}I_{j,+}, \left[I_{i,+}I_{k,-}, I_{i,z} \right] \right] = \left[I_{i,-}I_{j,+}, -I_{i,+}I_{k,-} \right] = 2I_{i,z}I_{j,+}I_{k,-}$
$\omega_i - \omega_j$ $= \omega_i - \omega_k$	1	$\frac{1}{6}A_{D(i,j)}A_{D(i,k)}$	$\left[I_{i,+}I_{j,-}, \left[I_{i,-}I_{k,+}, I_{i,z} \right] \right] = \left[I_{i,+}I_{j,-}, I_{i,-}I_{k,+} \right] = 2I_{i,z}I_{j,-}I_{k,+}$
$\omega_i - \omega_j$ $= \omega_i - \omega_k$	1	$\frac{1}{6}A_{D(i,j)}A_{D(i,k)}$	$\left[I_{i,+}I_{k,-}, \left[I_{i,-}I_{j,+}, I_{i,z} \right] \right] = \left[I_{i,+}I_{k,-}, I_{i,-}I_{j,+} \right] = 2I_{i,z}I_{j,+}I_{k,-}$

Table A8. Evaluation of the additional cross-correlated relaxation pathways with $a = D(i,j)$ and $a' = D(i,k)$ and vice versa for degenerate transitions with $\omega_i = \omega_j$ and $\langle b \rangle = \langle I_{i,z} \rangle$.

$\omega_m^{n,a}$	$(-1)^m$	factor	commutator
0	1	$-\frac{2}{3} A_{D(i,j)} A_{D(i,k)}$	$\left[I_{i,z} I_{j,z}, \left[I_{i,+} I_{k,-}, I_{i,z} \right] \right] = \left[I_{i,z} I_{j,z}, -I_{i,+} I_{k,-} \right] = I_{i,+} I_{j,z} I_{k,-}$
0	1	$-\frac{2}{3} A_{D(i,j)} A_{D(i,k)}$	$\left[I_{i,+} I_{k,-}, \left[I_{i,z} I_{j,z}, I_{i,z} \right] \right] = \left[I_{i,+} I_{k,-}, 0 \right] = 0$
0	1	$-\frac{2}{3} A_{D(i,j)} A_{D(i,k)}$	$\left[I_{i,z} I_{j,z}, \left[I_{i,-} I_{k,+}, I_{i,z} \right] \right] = \left[I_{i,z} I_{j,z}, I_{i,-} I_{k,+} \right] = -I_{i,-} I_{j,z} I_{k,+}$
0	1	$-\frac{2}{3} A_{D(i,j)} A_{D(i,k)}$	$\left[I_{i,-} I_{k,+}, \left[I_{i,z} I_{j,z}, I_{i,z} \right] \right] = \left[I_{i,-} I_{k,+}, 0 \right] = 0$

Table A9. Evaluation of the relaxation pathways with $a = D(i,j)$ and $a' = D(i,j)$ for non-degenerate transitions and $\langle b \rangle = \langle 2I_{i,z} I_{j,z} \rangle$.

$\omega_m^{n,a}$	$(-1)^m$	factor	commutator
0	1	$\frac{8}{3} A_{D(i,j)}^2$	$\left[I_{i,z} I_{j,z}, \left[I_{i,z} I_{j,z}, I_{i,z} I_{j,z} \right] \right] = \left[I_{i,z} I_{j,z}, 0 \right] = 0$
ω_i	-1	$-A_{D(i,j)}^2$	$\begin{aligned} & \left[I_{i,+} I_{j,z}, \left[I_{i,-} I_{j,z}, 2I_{i,z} I_{j,z} \right] \right] = \\ & \left[I_{i,+} I_{j,z}, \left(\left[I_{i,-}, 2I_{i,z} I_{j,z} \right] I_{j,z} + I_{i,-} \left[I_{j,z}, 2I_{i,z} I_{j,z} \right] \right) \right] \\ & = \left[I_{i,+} I_{j,z}, \left(2I_{i,-} I_{j,z} I_{j,z} + 0 \right) \right] = \left[2I_{i,+} I_{j,z}, \frac{1}{4} I_{i,-} \right] \\ & = I_{i,z} I_{j,z} = \frac{1}{2} 2I_{i,z} I_{j,z} \end{aligned}$
ω_i	-1	$-A_{D(i,j)}^2$	$\begin{aligned} & \left[I_{i,-} I_{j,z}, \left[I_{i,+} I_{j,z}, 2I_{i,z} I_{j,z} \right] \right] \\ & = \left[I_{i,-} I_{j,z}, \left(\left[I_{i,+}, 2I_{i,z} I_{j,z} \right] I_{j,z} + I_{i,+} \left[I_{j,z}, 2I_{i,z} I_{j,z} \right] \right) \right] \\ & = \left[I_{i,-} I_{j,z}, \left(-2I_{i,+} I_{j,z} I_{j,z} + 0 \right) \right] = \left[I_{i,-} I_{j,z}, -\frac{1}{2} I_{i,+} \right] \\ & = I_{i,z} I_{j,z} = \frac{1}{2} 2I_{i,z} I_{j,z} \end{aligned}$
ω_j	-1	$-A_{D(i,j)}^2$	$\begin{aligned} & \left[I_{i,z} I_{j,+}, \left[I_{i,z} I_{j,-}, 2I_{i,z} I_{j,z} \right] \right] \\ & = \left[I_{i,z} I_{j,+}, \left(\left[I_{i,z}, 2I_{i,z} I_{j,z} \right] I_{j,-} + I_{i,z} \left[I_{j,-}, 2I_{i,z} I_{j,z} \right] \right) \right] \\ & = \left[I_{i,z} I_{j,+}, \left(0 + 2I_{i,z} I_{j,-} I_{i,z} \right) \right] = \left[I_{i,z} I_{j,+}, \frac{1}{2} I_{j,-} \right] \\ & = I_{i,z} I_{j,z} = \frac{1}{2} 2I_{i,z} I_{j,z} \end{aligned}$
ω_j	-1	$-A_{D(i,j)}^2$	$\begin{aligned} & \left[I_{i,z} I_{j,-}, \left[I_{i,z} I_{j,+}, 2I_{i,z} I_{j,z} \right] \right] \\ & = \left[I_{i,z} I_{j,-}, \left(\left[I_{i,z}, 2I_{i,z} I_{j,z} \right] I_{j,+} + I_{i,z} \left[I_{j,+}, 2I_{i,z} I_{j,z} \right] \right) \right] \\ & = \left[I_{i,z} I_{j,-}, \left(0 - 2I_{i,z} I_{j,+} I_{i,z} \right) \right] = \left[I_{i,z} I_{j,-}, -\frac{1}{2} I_{j,+} \right] \\ & = I_{i,z} I_{j,z} = \frac{1}{2} 2I_{i,z} I_{j,z} \end{aligned}$
$\omega_i + \omega_j$	1	$A_{D(i,j)}^2$	$\begin{aligned} & \left[I_{i,+} I_{j,+}, \left[I_{i,-} I_{j,-}, 2I_{i,z} I_{j,z} \right] \right] \\ & = \left[I_{i,+} I_{j,+}, \left(\left[I_{i,-}, 2I_{i,z} I_{j,z} \right] I_{j,-} + I_{i,-} \left[I_{j,-}, 2I_{i,z} I_{j,z} \right] \right) \right] \\ & = \left[I_{i,+} I_{j,+}, \left(2I_{i,-} I_{j,z} I_{j,-} + 2I_{i,-} I_{j,-} I_{i,z} \right) \right] \\ & = \left[I_{i,+} I_{j,+}, \left(-I_{i,-} I_{j,-} + I_{i,-} I_{j,-} \right) \right] = \left[I_{i,+} I_{j,+}, 0 \right] = 0 \end{aligned}$

$\omega_i + \omega_j$	1	$A_{D(i,j)}^2$	$\begin{aligned} & [I_{i,-}I_{j,-}, [I_{i,+}I_{j,+}, 2I_{i,z}I_{j,z}]] \\ &= [I_{i,-}I_{j,-}, ([I_{i,+}, 2I_{i,z}I_{j,z}]I_{j,+} + I_{i,+}[I_{j,+}, 2I_{i,z}I_{j,z}])] \\ &= [I_{i,-}I_{j,-}, (-2I_{i,+}I_{j,z}I_{j,+} - 2I_{i,+}I_{i,z}I_{j,+})] \\ &= [I_{i,-}I_{j,-}, (-I_{i,+}I_{j,+} + I_{i,+}I_{j,+})] = [I_{i,-}I_{j,-}, 0] = 0 \end{aligned}$
$\omega_i - \omega_j$	1	$\frac{1}{6}A_{D(i,j)}^2$	$\begin{aligned} & [I_{i,+}I_{j,-}, [I_{i,-}I_{j,+}, 2I_{i,z}I_{j,z}]] \\ &= [I_{i,+}I_{j,-}, ([I_{i,-}, 2I_{i,z}I_{j,z}]I_{j,+} + I_{i,-}[I_{j,+}, 2I_{i,z}I_{j,z}])] \\ &= [I_{i,+}I_{j,-}, (2I_{i,-}I_{j,z}I_{j,+} - 2I_{i,-}I_{i,z}I_{j,+})] \\ &= [I_{i,+}I_{j,-}, (I_{i,-}I_{j,+} - I_{i,-}I_{j,+})] = [I_{i,+}I_{j,-}, 0] = 0 \end{aligned}$
$\omega_i - \omega_j$	1	$\frac{1}{6}A_{D(i,j)}^2$	$\begin{aligned} & [I_{i,-}I_{j,+}, [I_{i,+}I_{j,-}, 2I_{i,z}I_{j,z}]] \\ &= [I_{i,-}I_{j,+}, ([I_{i,+}, 2I_{i,z}I_{j,z}]I_{j,-} + I_{i,+}[I_{j,-}, 2I_{i,z}I_{j,z}])] \\ &= [I_{i,-}I_{j,+}, (-2I_{i,+}I_{j,z}I_{j,-} + 2I_{i,+}I_{i,z}I_{j,-})] \\ &= [I_{i,-}I_{j,+}, (I_{i,+}I_{j,-} - I_{i,+}I_{j,-})] = [I_{i,-}I_{j,+}, 0] = 0 \end{aligned}$

Table A10. Evaluation of the relaxation pathways with $a = \text{CSA}(i)$, $\text{CSA}(j)$ and $a' = \text{CSA}(i)$, $\text{CSA}(j)$ for non-degenerate transitions and $\langle b \rangle = \langle 2I_{i,z}I_{j,z} \rangle$.

$\omega_m^{n,a}$	$(-1)^m$	factor	commutator
0	1	$\frac{8}{3}A_{\text{CSA}(i)}^2B_0^2$	$[I_{i,z}, [I_{i,z}, 2I_{i,z}I_{j,z}]] = [I_{i,z}, 0] = 0$
ω_i	-1	$-A_{\text{CSA}(i)}^2B_0^2$	$[I_{i,+}, [I_{i,-}, 2I_{i,z}I_{j,z}]] = [I_{i,+}, 2I_{i,-}I_{j,z}] = 2(2I_{i,z}I_{j,z})$
ω_i	-1	$-A_{\text{CSA}(i)}^2B_0^2$	$[I_{i,-}, [I_{i,+}, 2I_{i,z}I_{j,z}]] = [I_{i,-}, -2I_{i,+}I_{j,z}] = 2(2I_{i,z}I_{j,z})$
ω_j	-1	$-A_{\text{CSA}(i)}^2B_0^2$	$[I_{j,+}, [I_{j,-}, 2I_{i,z}I_{j,z}]] = [I_{j,+}, 2I_{i,z}I_{j,-}] = 2(2I_{i,z}I_{j,z})$
ω_j	-1	$-A_{\text{CSA}(i)}^2B_0^2$	$[I_{j,-}, [I_{j,+}, 2I_{i,z}I_{j,z}]] = [I_{j,-}, -2I_{i,z}I_{j,+}] = 2(2I_{i,z}I_{j,z})$

Strong scalar coupling

The derivation follows the formalism used in references [53,54]. The basis chosen in equation 11 is not appropriate anymore if the scalar coupling constant becomes comparable to the difference of the Larmor frequencies of spins i and j . In what follows, the Master equation is derived for a two-spin system under neglect of CSA interaction and as a consequence, also of cross-correlated relaxation. Using the full expression for H_0 as written in equation 10.1, equation A2 produces modified eigenfunctions and eigenvalues. The eigenvalues determine the frequencies at which the peaks are observed in a NOESY spectrum. Diagonalization of the matrix representation of H_0 gives the following observable transition frequencies:

$$\begin{aligned}
 \omega(12) &= \frac{\omega_i + \omega_j}{2} + \pi J_{ij} - \sqrt{\left(\frac{\omega_i - \omega_j}{2}\right)^2 + (\pi J_{ij})^2} \\
 \omega(13) &= \frac{\omega_i + \omega_j}{2} + \pi J_{ij} + \sqrt{\left(\frac{\omega_i - \omega_j}{2}\right)^2 + (\pi J_{ij})^2} \\
 \omega(24) &= \frac{\omega_i + \omega_j}{2} - \pi J_{ij} + \sqrt{\left(\frac{\omega_i - \omega_j}{2}\right)^2 + (\pi J_{ij})^2} \\
 \omega(34) &= \frac{\omega_i + \omega_j}{2} - \pi J_{ij} - \sqrt{\left(\frac{\omega_i - \omega_j}{2}\right)^2 + (\pi J_{ij})^2}
 \end{aligned}
 \tag{A28.1-4}$$

The eigenbasis of H_0 is spanned by

$$\begin{aligned}
 |1\rangle &= |\alpha\alpha\rangle \\
 |2\rangle &= \cos \theta_{ij}^J |\alpha\beta\rangle + \sin \theta_{ij}^J |\beta\alpha\rangle \\
 |3\rangle &= -\sin \theta_{ij}^J |\alpha\beta\rangle + \cos \theta_{ij}^J |\beta\alpha\rangle \\
 |4\rangle &= |\beta\beta\rangle
 \end{aligned}
 \tag{A29.1-4}$$

where $|\alpha\alpha\rangle, |\alpha\beta\rangle, |\beta\alpha\rangle, |\beta\beta\rangle$ are the basis functions of the Hilbert space with α and β being the spin states of spin i and j , respectively, and θ_{ij}^J is defined as

$$\tan(2\theta_{ij}^J) = \frac{2\pi J_{ij}}{\omega_i - \omega_j} \quad (\text{A30})$$

From A28 it can be seen that in the weak coupling limit ($2\pi J_{ij} \ll |\omega_i - \omega_j|$) the frequencies correspond to the Larmor frequencies of spins i and j , respectively, each split by $2\pi J_{ij}$. However, as the coupling becomes stronger, the frequencies shift towards the center. If it is assumed that the multiplets due to scalar coupling are not resolved, but the peaks still are (that is, $2\pi J_{ij} < \text{linewidth} < |\omega_i - \omega_j|$), the spectra can be analyzed by using equation 12 with modified expressions. The basis that is introduced in equation 11 used to solve the Master is then replaced by operators referred to as magnetization modes, $\tilde{I}_{i,z}$ and $\tilde{I}_{j,z}$, which have predominantly i and j spin character, respectively, and $2\tilde{I}_{i,z}\tilde{I}_{j,z}$:

$$\begin{aligned} \tilde{I}_{i,z} &= +P_1 + P_2 - P_3 - P_4 \\ \tilde{I}_{j,z} &= +P_1 - P_2 + P_3 - P_4 \\ 2\tilde{I}_{i,z}\tilde{I}_{j,z} &= +P_1 - P_2 - P_3 + P_4 \end{aligned} \quad (\text{A31.1-3})$$

P_x is the population of the state x given in A29. The Master equation is:

$$\frac{d}{dt} \begin{pmatrix} \langle \tilde{I}_{i,z} \rangle - \tilde{I}_{i,0} \\ \langle \tilde{I}_{j,z} \rangle - \tilde{I}_{j,0} \\ \langle 2\tilde{I}_{i,z}\tilde{I}_{j,z} \rangle \end{pmatrix} = - \begin{pmatrix} \rho_i^{\text{D,Jstrong}} & \sigma_{ij}^{\text{Jstrong}} & \xi_{ij}^{\text{Jstrong}} \\ \sigma_{ij}^{\text{Jstrong}} & \rho_j^{\text{D,Jstrong}} & \xi_{ij}^{\text{Jstrong}} \\ \xi_{ij}^{\text{Jstrong}} & \xi_{ij}^{\text{Jstrong}} & \rho_{ij}^{\text{D,Jstrong}} \end{pmatrix} \begin{pmatrix} \langle \tilde{I}_{i,z} \rangle - \tilde{I}_{i,0} \\ \langle \tilde{I}_{j,z} \rangle - \tilde{I}_{j,0} \\ \langle 2\tilde{I}_{i,z}\tilde{I}_{j,z} \rangle \end{pmatrix} \quad (\text{A32})$$

with

$$\rho_i^{\text{D,Jstrong}} = R_{ij}^{\text{D,Jstrong}} + R_i^{\text{leak}} = R_{ij}^{\text{D}} - \Delta_{ij}^{\text{D,Jstrong}} - \varepsilon_{ij}^{\text{D,Jstrong}} + R_i^{\text{leak}} \quad (\text{A33.1})$$

$$\rho_{ij}^{\text{D,Jstrong}} = \lambda_{ij}^{\text{D}} \quad (\text{A33.2})$$

$$\sigma_{ij}^{\text{Jstrong}} = \sigma_{ij} + \varepsilon_{ij}^{\text{D,Jstrong}} \quad (\text{A33.3})$$

$$\xi_{ij}^{\text{D,Jstrong}} = -\frac{1}{2} \sin(2\theta_{ij}^{\text{J}}) \lambda_{ij}^{\text{D}} \quad (\text{A33.4})$$

with

$$\Delta_{ij}^{\text{D,Jstrong}} = \left(1 - \cos(2\theta_{ij}^{\text{J}})\right) \left(\frac{\mu_0}{4\pi}\right)^2 \frac{\gamma^4 \hbar^2}{20} \frac{3}{(r_{ij}^{\text{rigid}})^6} \left[J_{ij}^{\text{D}}(\omega_i) - J_{ij}^{\text{D}}(\omega_j) \right] \quad (\text{A34.1})$$

$$\varepsilon_{ij}^{\text{D,Jstrong}} = \sin^2(2\theta_{ij}^{\text{J}}) \left(\frac{\mu_0}{4\pi}\right)^2 \frac{\gamma^4 \hbar^2}{10} \frac{1}{(r_{ij}^{\text{rigid}})^6} J_{ij}^{\text{D}}(\omega_i - \omega_j) \quad (\text{A34.2})$$

Note that there is a magnetization transfer pathway from single- to two-spin order even in the absence of cross-correlated relaxation. If only the contributions are retained that contain the spectral density function sampled at $|\omega_i - \omega_j|$, the following modification to the case in the weak coupling limit are obtained:

$$R_{ij}^{\text{D}} \rightarrow R_{ij}^{\text{D,Jstrong}} = R_{ij}^{\text{D}} - \varepsilon_{ij}^{\text{D,Jstrong}} = \left(1 - \sin^2(2\theta_{ij}^{\text{J}})\right) R_{ij}^{\text{D}} \quad (\text{A35.1})$$

$$\sigma_{ij} \rightarrow \sigma_{ij}^{\text{Jstrong}} = \sigma_{ij} + \sin^2(2\theta_{ij}^{\text{J}}) \varepsilon_{ij}^{\text{D,Jstrong}} = \left(1 - \sin^2(2\theta_{ij}^{\text{J}})\right) \sigma_{ij} \quad (\text{A35.2})$$

The Wigner rotation element

The Wigner element is

$$D_{m'm}^l(\alpha, \beta, \gamma) = e^{-im'\alpha} d_{m'm}^l(\beta) e^{-im'\gamma} \quad (\text{A36})$$

where Wigner's small d-matrix is

$$d_{m'm}^l(\beta) = \sum_s \frac{(-1)^{m'-m+s} \sqrt{(l+m)!(l-m)!(l+m')!(l-m')!}}{(l-m'-s)!(l+m-s)!(s+m'-m)!s!} \left(\cos \frac{\beta}{2}\right)^{2l+m-m'-2s} \left(\sin \frac{\beta}{2}\right)^{m'-m+2s} \quad (\text{A37})$$

The Wigner rotation elements are related to the spherical harmonics as:

$$D_{m0}^l(\alpha, \beta, \gamma) = \left(\frac{4\pi}{2l+1}\right)^{1/2} Y_{lm}^*(\beta, \alpha) \quad (\text{A38})$$

$$D_{0m}^l(\alpha, \beta, \gamma) = (-1)^m \left(\frac{4\pi}{2l+1}\right)^{1/2} Y_{lm}^*(\beta, \gamma) \quad (\text{A39})$$

$$D_{mm'}^l(-\gamma, -\beta, -\alpha) = D_{m'm}^{l*}(\alpha, \beta, \gamma) \quad (\text{A40})$$

Simplified spectral density function for methyl groups

$J_{\bar{ij}}^{\text{D,methyl}}(\omega)$ can be treated by separation of the rotation around the c3 symmetry axis from the fluctuation of the c3 axis *per se*.

$$J_{\bar{i}}^{\text{D,methyl}}(\omega_{\bar{i}}) = \int_0^{t_{\text{mix}}} C^{\text{D}(\bar{i}),\text{methyl}}(\tau) \cos(\omega\tau) d\tau \quad (\text{A41})$$

with the correlation function

$$\begin{aligned}
& C^{D(\vec{i}),\text{methyl}}(\tau) \\
&= \sum_{\kappa < 1} \frac{1}{3} \sum_{l,l'=-2}^2 \langle D_{0l'}^2(\Theta^{\text{mol}}(\tau)) D_{0l}^{2*}(\Theta^{\text{mol}}(0)) \rangle \langle D_{l'q'}^2(\tilde{\Theta}_{i_{\kappa i_1}}^{c3}(\tau)) D_{lq}^{2*}(\tilde{\Theta}_{i_{\kappa i_1}}^{c3}(0)) F_{2q'}^*(\Theta_{i_{\kappa i_1}}^{\text{prot}}(\tau)) F_{2q}(\Theta_{i_{\kappa i_1}}^{\text{prot}}(0)) \rangle \\
&= \sum_{\kappa < 1} \frac{1}{3} \sum_{l,l'=-2}^2 \langle D_{0l'}^2(\Theta^{\text{mol}}(\tau)) D_{0l}^{2*}(\Theta^{\text{mol}}(0)) \rangle 4\pi \langle D_{l'q'}^2(\tilde{\Theta}_{i_{\kappa i_1}}^{c3}(\tau)) D_{lq}^{2*}(\tilde{\Theta}_{i_{\kappa i_1}}^{c3}(0)) Y_{2q'}(\Theta_{i_{\kappa i_1}}^{\text{prot}}(\tau)) Y_{2q}^*(\Theta_{i_{\kappa i_1}}^{\text{prot}}(0)) \rangle
\end{aligned} \tag{A42}$$

In analogy to equation 30, the proton coordinates are transformed into the molecule-fixed frame and the according Wigner rotation elements are averaged independently. A second transformation (expressed by $\tilde{\Theta}_{i_{\kappa i_1}}^{c3}$) brings the polar coordinates of the proton-proton vectors into a frame fixed to the c3 axis. $r_{i_{\kappa j_1}}(t) = r_{\text{methyl}}$ is rigid and can be separated from the averaging, which gives

$$F_{2q} = \sqrt{4\pi} Y_{2q}^*.$$

Now, it is assumed that the methyl rotation happens instantaneously. The Lipari-Szabo approximation then employs an internal correlation time for the fluctuation of the c3 axis. This fluctuation can be on a similar timescale as the methyl rotation (picoseconds) and effectively would absorb the correlation time of the methyl rotation. Due to the three-fold symmetry, only $Y_{20}(\Theta_{i_{\kappa i_1}}^{\text{prot}}(\tau)) Y_{20}^*(\Theta_{i_{\kappa i_1}}^{\text{prot}}(0))$ has nonzero values upon averaging.

$$\begin{aligned}
& C^{D(\vec{i}),\text{methyl}}(\tau) \\
&\approx \sum_{\kappa < 1} \frac{1}{3} \sum_{l,l'=-2}^2 \langle D_{0l'}^2(\Theta^{\text{mol}}(\tau)) D_{0l}^{2*}(\Theta^{\text{mol}}(0)) \rangle 4\pi \langle D_{0l'}^{2*}(\Theta_{i_{\kappa i_1}}^{c3}(\tau)) D_{0l}^2(\Theta_{i_{\kappa i_1}}^{c3}(0)) \rangle \langle Y_{20}(\Theta_{i_{\kappa i_1}}^{\text{prot}}) Y_{20}^*(\Theta_{i_{\kappa i_1}}^{\text{prot}}) \rangle \\
&= \sum_{\kappa < 1} \frac{1}{3} \sum_{l,l'=-2}^2 \langle D_{0l'}^2(\Theta^{\text{mol}}(\tau)) D_{0l}^{2*}(\Theta^{\text{mol}}(0)) \rangle 4\pi \frac{4\pi}{5} \langle Y_{2l'}(\Theta_{i_{\kappa i_1}}^{c3}(\tau)) Y_{2l}^*(\Theta_{i_{\kappa i_1}}^{c3}(0)) \rangle \langle Y_{20}(\Theta_{i_{\kappa i_1}}^{\text{prot}}) Y_{20}^*(\Theta_{i_{\kappa i_1}}^{\text{prot}}) \rangle \\
&= \sum_{l,l'=-2}^2 \langle D_{0l'}^2(\Theta^{\text{mol}}(\tau)) D_{0l}^{2*}(\Theta^{\text{mol}}(0)) \rangle \langle F_{l'}^*(\Theta_{\vec{i}}^{c3}(\tau)) F_l(\Theta_{\vec{i}}^{c3}(0)) \rangle \sum_{\kappa < 1} \frac{1}{3} \frac{4\pi}{5} \langle Y_{20}(\Theta_{i_{\kappa i_1}}^{\text{prot}}) Y_{20}^*(\Theta_{i_{\kappa i_1}}^{\text{prot}}) \rangle \\
&= \sum_{l,l'=-2}^2 \langle D_{0l'}^2(\Theta^{\text{mol}}(\tau)) D_{0l}^{2*}(\Theta^{\text{mol}}(0)) \rangle \langle F_{l'}^*(\Theta_{\vec{i}}^{c3}(\tau)) F_l(\Theta_{\vec{i}}^{c3}(0)) \rangle \sum_{\kappa < 1} \frac{1}{3} \langle P_2(\Theta_{i_{\kappa i_1}}^{\text{prot}}) P_2(\Theta_{i_{\kappa i_1}}^{\text{prot}}) \rangle
\end{aligned} \tag{A43}$$

In the second line, equation A40 is used to replace $D_{0l}^2(\tilde{\Theta}_{i_k i_l}^{c3})$ by $D_{l0}^{2*}(\Theta_{i_k i_l}^{c3})$. As the proton-proton vectors lie in the x-y plane of the c3 frame at all times, $\theta_{i_k i_l}^{\text{prot}} = 90^\circ$. In the fourth line, $\Theta_{i_k i_l}^{c3}$ is replaced by $\Theta_{\tilde{i}}^{c3}$, as the frame is the same for all three protons. The methyl axis rotation order parameter is defined as

$$\left(S^{\text{methyl,prot}}\right)^2 = \sum_{\kappa < \iota} \frac{1}{3} \left\langle P_2(\theta_{i_\kappa i_\iota}^{\text{prot}}) P_2(\theta_{i_\kappa i_\iota}^{\text{prot}}) \right\rangle = \frac{1}{4} \quad (\text{A44})$$

The correlation function is now in the same form as the one for a single proton with an additional factor:

$$C^{\text{D}(\tilde{i}),\text{methyl}}(\tau) = \left(S^{\text{methyl,prot}}\right)^2 \sum_{p=-2}^2 e^{-\tau/\tau_p} C_{\text{int},p}^{\text{D}(\tilde{i}),\text{methyl,c3}}(\tau) \quad (\text{A45})$$

7. References

- [1] A.W. Overhauser, Polarization of nuclei in metals, *Phys. Rev.* 92 (1953) 411-415.
- [2] J.H. Noggle, R.E. Schirmer, *The nuclear Overhauser effect: Chemical applications*. Academic Press, New York, 1971.
- [3] K. Wüthrich, *NMR of Proteins and Nucleic Acid*. Wiley, New York, 1986.
- [4] B.A. Borgias, M. Gochin, D.J. Kerwood, T.L. James, Relaxation matrix analysis of 2D NMR data, *Prog. Nucl. Magn. Reson. Spectrosc.* 22 (1990) 83-100.
- [5] R. Brüschweiler, D.A. Case, Characterization of biomolecular structure and dynamics by NMR cross relaxation, *Prog. Nucl. Magn. Reson. Spectrosc.* 26 (1994) 27-58.
- [6] F. Ni, Recent developments in transferred NOE methods, *Prog. Nucl. Magn. Reson. Spectrosc.* 26 (1994) 517-606.
- [7] H. Mo, T.C. Pochapsky, Intermolecular interactions characterized by nuclear Overhauser effects, *Prog. Nucl. Magn. Reson. Spectrosc.* 30 (1997) 1-38.
- [8] R. Brüschweiler, Dipolar averaging in NMR spectroscopy: From polarization transfer to cross relaxation, *Prog. Nucl. Magn. Reson. Spectrosc.* 32 (1998) 1-19.
- [9] M. Nilges, S.I. O'Donoghue, Ambiguous NOEs and automated NOE assignment, *Prog. Nucl. Magn. Reson. Spectrosc.* 32 (1998) 107-139.
- [10] T. Brand, E.J. Cabrita, S. Berger, Intermolecular interaction as investigated by NOE and diffusion studies, *Prog. Nucl. Magn. Reson. Spectrosc.* 46 (2005) 159-196.
- [11] N. Rama Krishna, V. Jayalakshmi, Complete relaxation and conformational exchange matrix analysis of STD-NMR spectra of ligand-receptor complexes, *Prog. Nucl. Magn. Reson. Spectrosc.* 49 (2006) 1-25.
- [12] A.W. Overhauser, Polarization of nuclei in metals, *Phys. Rev.* 91 (1953) 476.
- [13] T.R. Carver, C.P. Slichter, Polarization of nuclear spins in metals, *Phys. Rev.* 92 (1953) 212-213.
- [14] I. Solomon, Relaxation processes in a system of two spins, *Phys. Rev.* 99 (1955) 559-565.
- [15] F.A.L. Anet, A.J.R. Bourn, Nuclear magnetic resonance spectral assignments from nuclear overhauser effects, *J. Am. Chem. Soc.* 87 (1965) 5250-5251.
- [16] A.A. Bothner-By, R. Gassend, Binding of small molecules to proteins, *Ann. NY Acad. Sci.* 222 (1972) 668-676.
- [17] J.P. Albrand, B. Birdsall, J. Feeney, G.C.K. Roberts, A.S.V. Burgen, The use of transferred nuclear overhauser effects in the study of the conformations of small molecules bound to proteins, *Int. J. Biol. Macromol.* 1 (1979) 37-41.
- [18] A. Kumar, G. R.R. Ernst, K. Wüthrich, A two-dimensional nuclear Overhauser enhancement (2D NOE) experiment for the elucidation of complete proton-proton cross-relaxation networks in biological macromolecules, *Biochem. Biophys. Res. Commun.* 96 (1980) 1-6.
- [19] S. Macura, R.R. Ernst, Elucidation of cross relaxation in liquids by two-dimensional N.M.R. spectroscopy, *Mol. Phys.* 41 (1980) 95-117.
- [20] A. Kumar, G. Wagner, R.R. Ernst, K. Wüthrich, Buildup rates of the nuclear Overhauser effect measured by two-dimensional proton magnetic resonance spectroscopy: Implication for studies of protein conformation, *J. Am. Chem. Soc.* 103 (1981) 3654-3658.

- [21] R. Kaptein, R. Boelens, R.M. Scheek, W.F. van Gunsteren, Protein structures from NMR, *Biochemistry* 27 (1988) 5389-5395.
- [22] K. Wüthrich, Protein structure determination in solution by nuclear magnetic resonance spectroscopy, *Science* 243 (1989) 45-50. [H] S.P. Edmondson, NOE R factors and structural refinement using FIRM, an iterative relaxation matrix program, *J. Magn. Reson.* 98 (1992) 283-298.
- [23] C.M. Dobson, E.T. Olejniczak, F.M. Poulsen, R.G. Ratcliffe, Time development of proton nuclear Overhauser effects in proteins, *J. Magn. Reson.* 48 (1982) 97-110.
- [24] E.T. Olejniczak, F.M. Poulsen, C.M. Dobson, Distance dependence of proton nuclear Overhauser effects in proteins, *J. Magn. Reson.* 59 (1984) 518-523.
- [25] G.M. Clore, A.M. Gronenborn, Theory of the time dependent transferred nuclear Overhauser effect: Applications to structural analysis of ligand-protein complexes in solution *J. Magn. Reson.* 84 (1983) 423-442.
- [26] C.B. Post, Exchange-transferred NOE spectroscopy and bound ligand structure determination, *Curr. Opin. Struct. Biol.* 13 (2003) 581-588.
- [27] J.W. Keepers, T.L. James, A theoretical study of distance determinations from NMR. Two-dimensional nuclear Overhauser effect spectra, *J. Magn. Reson.* 57 (1984) 404-426.
- [28] G.M. Clore, A.M. Gronenborn, Assessment of errors involved in the determination of interproton distance ratios and distances by means of one- and two-dimensional NOE measurements, *J. Magn. Reson.* 61 (1985) 158-164.
- [29] E.T. Olejniczak, F.M. Poulsen, C.M. Dobson, Proton nuclear Overhauser effects and protein dynamics, *J. Am. Chem. Soc.* 103 (1981) 6574-6580.
- [30] B. Vögeli, S. Kazemi, P. Güntert, R. Riek, Spatial elucidation of motion in proteins by ensemble-based structure calculation using exact NOEs, *Nat. Struct. Mol. Biol.* 19 (2012) 1053-1057.
- [31] B. Vögeli, P. Güntert, R. Riek, Multiple-state ensemble structure determination from eNOE spectroscopy, *Mol. Phys.* 111 (2013) 437-454.
- [32] B. Vögeli, J. Orts, D. Strotz, P. Güntert, R. Riek, Discrete three-dimensional representation of macromolecular motion from eNOE-based ensemble calculation, *Chimia* 66 (2012) 787-790.
- [33] B. Vögeli, T.F. Segawa, D. Leitz, A. Sobol, A. Choutko, D. Trzesniak, W. van Gunsteren, R. Riek, Exact distances and internal dynamics of perdeuterated ubiquitin from NOE buildups, *J. Am. Chem. Soc.* 131 (2009) 17215-17225.
- [34] B. Vögeli, M. Friedmann, D. Leitz, A. Sobol, R. Riek, Quantitative determination of NOE rates in perdeuterated and protonated proteins: practical and theoretical aspects, *J. Magn. Reson.* 204 (2010) 290-302.
- [35] D. Neuhaus, M.P. Williamson, *The Nuclear Overhauser Effect in Structural and Conformational Analysis*. Wiley, New York, 2000.
- [36] A. Abragam, *Principles of nuclear magnetism*. Clarendon Press, Oxford, 1961.
- [37] R.R. Ernst, G. Bodenhausen, A. Wokaun, *Principles of nuclear magnetic resonance in one and two dimensions*, Clarendon Press, Oxford, 1987.
- [38] A.G. Redfield, On the theory of relaxation processes, *IBM. J. Res. Develop.* 1 (1957) 19-31.
- [39] M. Goldman, Advances in magnetic resonance: Formal theory of spin-lattice relaxation. *J. Magn. Reson.* 149 (2001) 160-187.
- [40] J. Cavanagh, W.J. Fairbrother, A.G. Palmer, M. Rance, N.J. Sklepton, *Protein NMR spectroscopy. Principles and practice*, Academic Press, San Diego, 2007.

- [41] D.M. Korzhnev, M. Billeter, A.S. Arseniev, V.Y. Orekhov, NMR studies of Brownian tumbling and internal motions in proteins, *Prog. Nucl. Magn. Reson. Spectrosc.* 38 (2001) 197-266.
- [42] C. Dalvit, G. Bodenhausen, Evidence for dipolar cross-correlation from triple-quantum-filtered two-dimensional exchange NMR spectroscopy, *J. Am. Chem. Soc.* 110 (1988) 7924-7926.
- [43] A. Kumar, R.C.R. Grace, P.K. Madhu, Cross-correlations in NMR, *Prog. Nucl. Magn. Reson. Spectrosc.* 37 (2000) 191-319.
- [44] J. Tropp, Dipolar relaxation and nuclear Overhauser effects in nonrigid molecules: The effect of fluctuating internuclear distances. *J. Chem. Phys.* 72 (1980) 6035-6043.
- [45] T.M.G. Koning, R. Boelens, R. Kaptein, Calculation of the nuclear Overhauser effect and the determination of proton-proton distances in the presence of internal motions. *J. Magn. Reson.* 90 (1990) 111-123.
- [46] K. Wüthrich, M. Billeter, W. Braun, Pseudo-structures for the 20 common amino acids for use in studies of protein conformations by measurements of intramolecular proton-proton distance constraints with nuclear magnetic resonance. *J. Mol. Biol.* 169 (1983) 949-961.
- [47] N. Müller, G. Bodenhausen, Cross correlation of chemical shift anisotropy and dipolar interactions in methyl protons investigated by selective nuclear magnetic resonance spectroscopy. *J. Chem. Phys.* 98 (1993) 6062-6069.
- [48] L.G. Werbelow, A.G. Marshall, Internal rotation and nonexponential methyl nuclear relaxation for macromolecules. *J. Magn. Reson.* 11 (1973) 299-313.
- [49] E.T. Olejniczak, Including methyl rotation in simulations of spin-lattice relaxation experiments. *J. Magn. Reson.* 81 (1989) 392-394.
- [50] S.B. Landy, B.D.N. Rao, Dynamical NOE in multiple-spin systems undergoing chemical exchange. *J. Magn. Reson.* 81 (1989) 371-377.
- [51] F. Ni, Complete relaxation matrix analysis of transferred nuclear Overhauser effects, *J. Magn. Reson.* 96 (1992) 651-656.
- [52] L.E. Kay, J.N. Scarsdale, D.R. Hare, J.H. Prestegard, Simulation of two-dimensional cross-relaxation spectra in strongly coupled spin systems, *J. Magn. Reson.* 68 (1986) 515-525.
- [53] J. Keeler, D. Neuhaus, M.P. Williamson, The nuclear Overhauser effect in strongly coupled spin systems. *J. Magn. Reson.* 73 (1987) 45-68.
- [54] V.V. Krishnan, A. Kumar, Dipolar cross-correlation effects in the nuclear Overhauser experiments of weakly and strongly coupled spins. *J. Magn. Reson.* 92 (1991) 293-311.
- [55] R.C.R. Grace, A. Kumar, Cross peaks in the standard 2D NOE experiment induced by strong coupling even in the absence of relaxation, *J. Magn. Reson.* 97 (1992) 184-191.
- [56] L.E. Kay, T.A. Holak, B.A. Johnson, I.M. Armitage, J.H. Prestegard, Second-order effects in two-dimensional cross-relaxation spectra of proteins: Investigation of glycine spin systems, *J. Am. Chem. Soc.* 108 (1986) 4242-4244.
- [57] S. Macura, Y. Huang, D. Suter, R.R. Ernst, Two-dimensional chemical exchange and cross-relaxation spectroscopy of coupled nuclear spins, *J. Magn. Reson.* 43 (1981) 259-281.
- [58] T.E. Bull, Cross-correlation and 2D NOE spectra, *J. Magn. Reson.* 72 (1987) 397-413.
- [59] H.M. McConnell, Reaction rates by nuclear magnetic resonance. *J. Chem. Phys.* 28 (1958) 430-431.
- [60] B.H. Meier, R.R. Ernst, Elucidation of chemical exchange networks by two-dimensional NMR spectroscopy: The heptamethylbenzenonium ion, *J. Am. Chem. Soc.* 101 (1979) 6441-6442.

- [61] J. Jeener, B.H. Meier, P. Bachmann, R.R. Ernst, Investigation of exchange processes by two-dimensional NMR spectroscopy, *J. Chem. Phys.* 71 (1979) 4546-4553.
- [62] M. Zerbetto, A. Polimeno, E. Meirovitch, General theoretical/computational tool for interpreting NMR spin relaxation in proteins. *J. Phys. Chem. B* 113 (2009) 13613-13625.
- [63] E. Meirovitch, Y.E. Shapiro, A. Polimeno, J.H. Freed, Structural dynamics of biomacromolecules by NMR: The slowly relaxing local structure approach. *Prog. Nucl. Magn. Reson. Spectrosc.* 56 (2010) 360-405.
- [64] L.D. Favro, Theory of the rotational Brownian motion of a free rigid body, *Phys. Rev.* 119 (1953) 53-62.
- [65] B. Vögeli, L. Yao, Correlated dynamics between HN and HC bonds observed by NMR cross relaxation, *J. Am. Chem. Soc.* 131 (2009) 3668-3678.
- [66] B. Vögeli, Comprehensive description of NMR cross-correlated relaxation under anisotropic molecular tumbling and correlated local dynamics on all timescales, *J. Chem. Phys.* 133 (2010) 014501.
- [67] R. Brüschweiler, B. Roux, M. Blackledge, C. Griesinger, M. Karplus, R.R. Ernst, Influence of rapid intramolecular motions on NMR cross-relaxation rates. A molecular dynamics study of antamanide in solution. *J. Am. Chem. Soc.* 114 (1992) 2289-2302.
- [68] V. Tugarinov, L.E. Kay, Relaxation rates of degenerate ^1H transitions in methyl groups of proteins as reporters of side-chain dynamics. *J. Am. Chem. Soc.* 128 (2006) 7299-7308.
- [69] N.R. Skrynnikov, O. Millet, L.E. Kay, Deuterium spin probes of side-chain-dynamics in proteins. 2. Spectral density mapping and identification of nanosecond time-scale side-chain motions. *J. Am. Chem. Soc.* 124 (2002) 6449-6460.
- [70] G.M. Clore, A. Szabo, A. Bax, L.E. Kay, P.C. Driscoll, A.M. Gronenborn, Deviations from the simple two parameter model free approach to the interpretation of ^{15}N nuclear magnetic relaxation of proteins. *J. Am. Chem. Soc.* 112 (1990) 4989-4991.
- [71] G. Lipari, A. Szabo, Model-free approach to the interpretation of nuclear magnetic resonance relaxation in macromolecules. 1. Theory and range of validity, *J. Am. Chem. Soc.* 104 (1982) 4546-4559.
- [72] G. Lipari, A. Szabo, Model-free approach to the interpretation of nuclear magnetic resonance relaxation in macromolecules. 2. Analysis of experimental results, *J. Am. Chem. Soc.* 104 (1982) 4559-4570.
- [73] S.W. Fesik, T.J. O'Donnell, R.T. Gampe, E.T. Olejniczak, Determining the structure of a glycopeptide-Ac₂-Lys-D-Ala-D-Ala complex using NMR parameters and molecular modeling, *J. Am. Chem. Soc.* 108 (1986) 3165-3170.
- [74] E.T. Olejniczak, R.T. Gampe, S.W. Fesik, Accounting for spin diffusion in the analysis of 2D NOE data, *J. Magn. Reson.* 67 (1986) 28-41.
- [75] A.N. Lane, The influence of spin diffusion and internal motions on NOE intensities in proteins. *J. Magn. Reson.* 78 (1988) 425-439.
- [76] R. Boelens, T.M.G. Koning, R. Kaptein, Determination of biomolecular structures from proton-proton NOEs using a relaxation matrix approach, *J. Mol. Biol.* 173 (1988) 299-311.
- [77] N.H. Andersen, H.L. Eaton, X. Lai, Quantitative small molecule NOESY. A practical guide for derivation of cross-relaxation rates and internuclear distances, *Magn. Reson. Chem.* 27 (1989) 515-528.
- [78] M. Nilges, G.M. Clore, A.M. Gronenborn, N. Piel, L.W. McLaughlin, Refinement of the solution structure of the DNA decamer 5'd(CTGGATCCAG)₂. *Biochemistry* 26 (1987) 3734-3744.

- [79] B.A. Borgias, T.L. Lames, Two-dimensional nuclear Overhauser effect: Complete relaxation matrix analysis, *Methods Enzymol.* 176 (1989) 169-183.
- [80] J.D. Baleja, J. Moulton, B.D. Sykes, Distance measurement and structure refinement with NOE data. *J. Magn. Reson.* 87 (1990) 375-384.
- [81] C.B. Post, R.P. Meadows, D.G. Gorenstein, On the evaluation of interproton distances for three-dimensional structure determination by NMR using a relaxation rate matrix analysis. *J. Am. Chem. Soc.* 112 (1990) 6796-6803.
- [82] T.L. James, Relaxation matrix analysis of two-dimensional nuclear Overhauser effect spectra, *Curr. Opin. Struct. Biol.* 1 (1991) 1042-1053.
- [83] P.D. Thomas, V.J. Basus, T.L. James, Protein solution structure determination using distances from two-dimensional nuclear Overhauser effect experiments: Effect of approximations on the accuracy of derived structures, *Proc. Natl. Acad. Sci. USA* 88 (1991) 1237-1241.
- [84] C.B. Post, Internal motional averaging and three-dimensional structure determination by nuclear magnetic resonance. *J. Mol. Biol.* 224 (1992) 1087-1101.
- [85] S.P. Edmondson, NOE R factors and structural refinement using FIRM, an iterative relaxation matrix program, *J. Magn. Reson.* 98 (1992) 283-298.
- [86] C.M. Fletcher, D.N.M. Jones, R. Diamond, D. Neuhaus, Treatment of NOE constraints involving equivalent or nonstereoassigned protons in calculations of biomolecular structures. *J. Biomol. NMR* 8 (1996) 292-310.
- [87] H. Liu, P.D. Thomas, T.L. James, Averaging of cross-relaxation rates and distances for methyl, methylene, and aromatic ring protons due to motion or overlap. Extraction of accurate distances iteratively via relaxation matrix analysis of 2D NOE spectra. *J. Magn. Reson.* 98 (1992) 163-175.
- [88] Z. Dzakula, W.M. Westler, A.S. Edison, J.L. Markley, The "CUPID" method for calculating the continuous probability distribution of rotamers from NMR data, *J. Am. Chem. Soc.* 114 (1992) 6195-6199.
- [89] Z. Dzakula, A.S. Edison, W.M. Westler, J.L. Markley, Analysis of χ_1 rotamer populations from NMR data by the CUPID method, *J. Am. Chem. Soc.* 114 (1992) 6200-6207.
- [90] J. Iwahara, G.M. Clore, Structure-independent analysis of the breadth of the positional distribution of disordered groups in macromolecules from order parameters for long, variable-length vectors using NMR paramagnetic relaxation enhancement, *J. Am. Chem. Soc.* 132 (2010) 13346-13356.
- [91] J. Fennen, A.E. Torda, W.F. van Gunsteren, Structure refinement with molecular dynamics and a Boltzmann-weighted ensemble, *J. Biomol. NMR* 6 (1995) 163-170.
- [92] A.E. Torda, R.M. Scheek, W.F. van Gunsteren, Time-averaged nuclear Overhauser effect distance restraints applied to tendamistat, *J. Mol. Biol.* 214 (1990) 223-235.
- [93] K. Lindorff-Larsen, R.B. Best, M.A. DePristo, C.M. Dobson, M. Vendruscolo, Simultaneous determination of protein structure and dynamics, *Nature* 433 (2005) 128-132.
- [94] B. Richter, J. Gsponer, P. Varnai, X. Salvatella, M. Vendruscolo, The MUMO (minimal under-restraining minimal over-restraining) method for the determination of native state ensembles of proteins, *J. Biomol. NMR* 37 (2007) 117-135.
- [95] A.E. Torda, R.M. Scheek, W.F. Van Gunsteren, Time-dependent distance restraints in molecular dynamics simulations, *Chem. Phys. Lett.* 157 (1989) 289-294.
- [96] D.A. Pearlman, How is an NMR structure best defined? An analysis of molecular dynamics distance-based approaches, *J. Biomol. NMR* 4 (1994) 1-16.

- [97] J. Kemmink, C.P.M. van Mierlo, R.M. Scheek, T.E. Creighton, Local structure due to an aromatic-amide interaction observed by ^1H -nuclear magnetic resonance spectroscopy in peptides related to the N terminus of bovine pancreatic trypsin inhibitor, *J. Mol. Biol.* 230 (1993) 312-322.
- [98] D.F. Mierke, R.M. Scheek, H. Kessler, Coupling constants as restraints in ensemble distance driven dynamics, *Biopolymers* 34 (1994) 559-563.
- [99] A.M.J.J. Bonvin, R. Boelens, R. Kaptain, Time- and ensemble-averaged direct NOE restraints, *J. Biomol. NMR* 4 (1994) 143-149.
- [100] C. Peters, X. Daura, W.F. van Gunsteren, Calculation of NMR-relaxation parameters for flexible molecules from molecular dynamics simulations, *J. Biomol. NMR* 20 (2001) 297-310.
- [101] A. Kalk, H.J.C. Berendsen, Proton magnetic relaxation and spin diffusion in protein. *J. Magn. Reson.* 24 (1976) 343-366.
- [102] R. Boelens, G.W. Vuister, T.M.G. Koning, R. Kaptein, Observation of spin diffusion in biomolecules by three-dimensional NOE-NOE spectroscopy, *J. Am. Chem. Soc.* 111 (1989) 8525-8526.
- [103] J.N. Berg, R. Boelens, G.W. Vuister, R. Kaptein, 3D NOE-NOE spectroscopy of proteins. Observation of sequential 3D NOE cross peaks in arc repressor, *J. Magn. Reson.* 87 (1990) 646-651.
- [104] G.W. Vuister, R. Boelens, A. Padilla, R. Kaptein, Statistical analysis of double NOE transfer pathways in proteins as measured in 3D NOE-NOE spectroscopy, *J. Biomol. NMR* 1 (1991) 421-438.
- [105] M. Madrid, J.E. Mace, O. Jardetzky, Consequences of magnetization transfer on the determination of solution structures of proteins, *J. Magn. Reson.* 83 (1989) 267-278.
- [106] G.M. Clore, A.M. Gronenborn, How accurately can interproton distances in macromolecules really be determined by full relaxation matrix analysis of nuclear Overhauser enhancement data? *J. Magn. Reson.* 84 (1989) 398-409.
- [107] X.N. Lai, C.P. Chen, N.H. Andersen, The DISCON algorithm, an accurate and robust alternative to an eigenvalue solution for extracting experimental distances from NOESY data. *J. Magn. Reson. B* 101 (1993) 271-288.
- [108] W. Masefski, P.H. Bolton, Quantitative analysis of nuclear Overhauser effects, *J. Magn. Reson.* 65 (1985) 526-530.
- [109] D. Marion, M. Genest, M. Ptak, Reconstruction of NOESY maps. A requirement for a reliable conformational analysis of biomolecules using 2D NMR, *Biophys. Chem.* 28 (1987) 235-244.
- [110] J.F. Lefevre, A.N. Lane, O. Jardetzky, Solution structure of the trp operator of *escherichia coli* determined by NMR, *Biochemistry* 26 (1987) 5076-5090.
- [111] M.J. Forster, Comparison of computational methods for simulating nuclear Overhauser effects in NMR spectroscopy, *J. Comput. Chem.* 12 (1991) 292-300.
- [112] J. Orts, B. Vögeli, R. Riek, Relaxation matrix analysis of spin diffusion for the NMR structure calculation with eNOEs, *J. Chem. Theory Comput.* 8 (2012) 3483-3492.
- [113] J.P. Linge, M. Habeck, W. Rieping, M. Nilges, Correction of spin diffusion during iterative automated NOE assignment, *J. Magn. Reson.* 167 (2004) 334-342.
- [114] R. Boelens, T.M.G. Koning, G.A. Van der Marel, J.H. Van Boom, R. Kaptein, Iterative procedure for structure determination from proton-proton NOEs using a full relaxation matrix approach. Application to a DNA octamer, *J. Magn. Reson.* 82 (1989) 290-308.

- [115] A.M.J.J. Bonvin, J.A.C. Rullmann, R.M.J.N. Lamerichs, R. Boelens, R. Kaptain, "Ensemble" iterative relaxation matrix approach: A new NMR refinement protocol applied to the solution structure of crambin, *Proteins Struct. Func. Genet.* 15 (1993) 385-400.
- [116] B.A. Borgias, T.L. James, MARDIGRAS - a procedure for matrix analysis of relaxation for discerning geometry of an aqueous structure. *J. Magn. Reson.* 87 (1990) 475-487.
- [117] M.F. Summers, T.L. South, B. Kim, D.R. Hare, High-resolution structure of an HIV zinc fingerlike domain via a new NMR-based distance geometry approach, *Biochemistry* 29 (1990) 329-340.
- [118] C.B. Post, R.P. Meadows, D.G. Gorenstein, MORASS program, (1989).
- [119] E.P. Nikonowicz, R.P. Meadows, D.G. Gorenstein, NMR structural refinement of an extrahelical adenosine tridecamer d(CGCAGAATTTCGCG)₂ via a hybrid relaxation matrix procedure, *Biochemistry* 29 (1990) 4193-4204.
- [120] B.R. Leeftang, L.M.J. Kroon-Batenburg, CROSREL: Full relaxation matrix analysis for NOESY and ROESY NMR spectroscopy, *J. Biomol. NMR* 2 (1992) 495-518.
- [121] M. Madrid, E. Llinas, M. Llinas, Model-independent refinement of interproton distances generated from ¹H-NMR Overhauser intensities, *J. Magn. Reson.* 93 (1991) 329-346.
- [122] K.L. Constantine, L. Mueller, N.H. Andersen, H. Tong, C.F. Wandler, M.S. Friederichs, R.E. Bruccoleri, Structural and dynamic properties of a β-hairpin-forming linear peptide. 1. Modeling using ensemble-averaged constraints, *J. Am. Chem. Soc.* 117 (1995) 10841-10854.
- [123] N.R. Nirmala, G.M. Lippens, K. Hallenga, Theory and experimental results of transfer NOE experiments. II. The influence of residual mobility and relaxation centers inside the protein on the size of transfer NOEs, *J. Magn. Reson.* 100 (1992) 25-42.
- [124] R.E. London, M.E. Perlman, D.G. Davis, Relaxation-matrix analysis of the transferred nuclear Overhauser effect for finite exchange rates. *J. Magn. Reson.* 97 (1992) 79-98.
- [125] R.E. London, Theoretical analysis of the inter-ligand overhauser effect: A new approach for mapping structural relationships of macromolecular ligands, *J. Magn. Reson.* 141 (1999) 301-311.
- [126] M. Mayer, B. Meyer, Mapping the active site of angiotensin-converting enzyme by transferred NOE spectroscopy, *J. Med. Chem.* 43 (2000) 2093-2099.
- [127] J. Orts, J. Tuma, M. Reese, S.K. Grimm, P. Monecke, S. Bartoschek, A. Schiffer, K.U. Wendt, C. Griesinger, T. Carlomagno, Crystallography-independent determination of ligand binding modes, *Angew. Chem. Int. Ed. Engl.* 47 (2008) 7736-7740.
- [128] J. Orts, C. Griesinger, T. Carlomagno, The INPHARMA technique for pharmacophore mapping: A theoretical guide to the method, *J. Magn. Reson.* 200 (2009) 64-73.
- [129] B. Stauch, J. Orts, T. Carlomagno, The description of protein internal motions aids selection of ligand binding poses by the INPHARMA method, *J. Biomol. NMR* 54 (2012) 1-12.
- [130] H.N.B. Moseley, E.V. Curto, N.R. Krishna, Complete relaxation and conformational exchange matrix (CORCEMA) analysis of NOESY spectra of interacting systems; Two-dimensional transferred NOESY, *J. Magn. Reson. B* 108 (1995) 243-261.
- [131] E.V. Curto, H.N.B. Moseley, N.R. Krishna, CORCEMA evaluation of the potential role of intermolecular transferred NOESY in the characterization of ligand-receptor complexes, *J. Comput. Aided Mol. Des.* 10 (1996) 361-371.

- [132] V. Jayalakshmi, N.R. Krishna, CORCEMA refinement of the bound ligand conformation within the protein binding pocket in reversibly forming weak complexes using STD-NMR intensities, *J. Magn. Reson.* 168 (2004) 36-45.
- [133] E.Z. Eisenmesser, A.P.R. Zbell, C.B. Post, Accuracy of bound peptide structures determined by exchange transferred nuclear Overhauser data: A simulation study, *J. Biomol. NMR* 17 (2000) 17-32.
- [134] B.A. Borgias, T.L. James, COMATOSE: A method for constrained refinement of macromolecular structure based on two-dimensional nuclear Overhauser effect spectra. *J. Magn. Reson.* 79 (1988) 493-512.
- [135] P. Yip, D.A. Case, A new method for refinement of macromolecular structures based on nuclear Overhauser effect spectra, *J. Magn. Reson.* 83 (1989) 643-648.
- [136] M. Nilges, J. Habbazettl, A. Brunger, T.A. Holak, Relaxation matrix refinement of the solution structure of squash trypsin inhibitor, *J. Mol. Biol.* 219 (1991) 499-510.
- [137] P.F. Yip, A computationally efficient method for evaluating the gradient of 2D NOESY intensities, *J. Biomol. NMR* 3 (1993) 361-365.
- [138] M.J. Dellwo, J. Wand, Computationally efficient gradients for relaxation matrix-based structure refinement including the accommodation of internal motions, *J. Biomol. NMR* 3 (1993) 205-214.
- [139] J.E. Mertz, P. Güntert, K. Wüthrich, W. Braun, Complete relaxation matrix refinement of NMR structures of proteins using analytically calculated dihedral angle derivatives of NOE intensities, *J. Biomol. NMR* 1 (1991) 257-269.
- [140] S. Macura, B.T. Farmer, L.R. Brown, An improved method for the determination of cross-relaxation rates from NOE data. *J. Magn. Reson.* 70 (1986) 493-499.
- [141] S.G. Hyberts, G. Wagner, Taylor transformation of 2D NMR τ_m series from time dimension to polynomial dimension. *J. Magn. Reson.* 81 (1989) 418-422.
- [142] T.S. Ulmer, B.E. Ramirez, F. Delaglio, A. Bax, Evaluation of backbone proton positions and dynamics in a small protein by liquid crystal NMR spectroscopy, *J. Am. Chem. Soc.* 125 (2003) 9179-9191.
- [143] L. Yao, B. Vögeli, D.A. Torchia, A. Bax, Simultaneous NMR study of protein structure and dynamics using conservative mutagenesis, *J. Phys. Chem. B* 112 (2008) 6045-6056.
- [144] L.S. Yao, B. Vögeli, J. Ying, A. Bax, NMR determination of amide N-H equilibrium bond length from concerted dipolar coupling measurements, *J. Am. Chem. Soc.* 130 (2008) 16518-16520.
- [145] M. Takeda, T. Terauchi, M. Kainosho, Conformational analysis by quantitative NOE measurements of the β -proton pairs across individual disulfide bonds in proteins, *J. Biomol. NMR* 52 (2012) 127-139.
- [146] S. Macura, J. Fejzo, W.M. Westler, J.L. Markley, Influence of slow internal motion in proteins on cross-relaxation rates determined by two-dimensional exchange spectroscopy, *Bull. Magn. Reson.* 16 (1994) 73-93.
- [147] S.W. Fesik, E.R.P. Zuiderweg, Heteronuclear three-dimensional NMR spectroscopy. A strategy for the simplification of homonuclear two-dimensional NMR spectra, *J. Magn. Reson.* 78 (1988) 588-593.
- [148] B.T. Farmer, Simultaneous [^{13}C , ^{15}N]-HMQC, a pseudo-triple-resonance experiment, *J. Magn. Reson.* 93 (1991) 635-641.
- [149] S.M. Pascal, D.R. Muhandiram, T. Yamazaki, J.D. Forman-Kay, L.E. Kay, $^1\text{H}_\text{C}$ and $^1\text{H}_\text{N}$ total NOE correlations in a single 3D NMR experiment. ^{15}N and ^{13}C time-sharing in t_1

- and t_2 dimensions for simultaneous data acquisition, *J. Magn. Reson. Ser. B* 103 (1994) 197-201.
- [150] A. Bax, D.G. Davies, MLEV-17-based two-dimensional homonuclear magnetization transfer spectroscopy, *J. Magn. Reson.* 65 (1985) 355-360.
- [151] D. Marion, M. Ikura, R. Tschudin, A. Bax, Rapid recording of 2D NMR-spectra without phase cycling - Application to the study of hydrogen-exchange in proteins, *J. Magn. Reson.* 85 (1989) 393-399.
- [152] L. Zhu, H.J. Dyson, P.E. Wright, A NOESY-HSQC simulation program, SPIRIT, *J. Biomol. NMR* 11 (1998) 17-29.
- [153] L.E. Kay, P. Keifer, T. Saarinen, Pure absorption gradient enhanced heteronuclear single quantum correlation spectroscopy with improved sensitivity, *J. Am. Chem. Soc.* 114 (1992) 10663-10665.
- [154] A.J. Shaka, P.B. Barker, R. Freeman, Computer-optimized decoupling scheme for wideband applications and low-level operation, *J. Magn. Reson.* 194 (1985) 547-552.
- [155] R. Tycko, A. Pines, J. Guckenheimer, Fixed point theory of iterative excitation schemes in NMR, *J. Chem. Phys.* 83 (1985) 2775-2802.
- [156] T. Fujiwara, K. Nagayama, Composite inversion pulses with frequency switching and their application to broadband decoupling, *J. Magn. Reson.* 77 (1988) 53-63.
- [157] J.M. Böhlen, G. Bodenhausen, Experimental aspects of chirp NMR spectroscopy, *J. Magn. Reson. Ser. A* 102 (1993) 293-301.
- [158] R. Baumann, G. Wider, R.R. Ernst, K. Wüthrich, Improvement of 2D NOE and 2D correlated spectra by symmetrization, *J. Magn. Reson.* 44 (1981) 402-406.
- [159] A.F. Mehlkopf, D. Korbee, T.A. Tiggelman, R. Freeman, Sources of t_1 noise in two-dimensional NMR, *J. Magn. Reson.* 58 (1984) 315-323.
- [160] R.E. Klevit, Improving two-dimensional NMR spectra by t_1 ridge subtraction, *J. Magn. Reson.* 62 (1985) 551-555.
- [161] W. Denk, G. Wagner, M. Rance, K. Wüthrich, Combined suppression of diagonal peaks and t_1 ridges in two-dimensional nuclear Overhauser enhancement spectra, *J. Magn. Reson.* 62 (1985) 350-355.
- [162] J.M. Withka, S. Swaminathan, P.H. Bolton, NOEs in duplex DNA depend on orientations of internuclear vectors to the symmetry axis. *J. Magn. Reson.* 89 (1990) 386-390.
- [163] A.J. Duben, W.C. Hutton, Spatial aspects of homonuclear, proton NMR cross-relaxation. 1. The effects of molecular shape and internal motion. *J. Magn. Reson.* 112 (1990) 5917-5924.
- [164] K. Kaluarachchi, R.P. Meadows, D.G. Gorenstein, How accurately can oligonucleotide structures be determined from the hybrid relaxation rate matrix/NOESY distance restrained molecular dynamics approach? *Biochemistry* 30 (1991) 8785-8797.
- [165] D. Leitz, B. Vögeli, J. Greenwald, R. Riek, Temperature dependence of $^1\text{H}_\text{N}$ - $^1\text{H}_\text{N}$ distances in ubiquitin as studied by exact measurements of NOEs, *J. Phys. Chem. B* 115 (2011) 7648-7660.
- [166] S.L. Chang, N. Tjandra, Temperature dependence of protein backbone motion from carbonyl ^{13}C and amide ^{15}N NMR relaxation, *J. Magn. Reson.* 174 (2005) 43-53.
- [167] O.F. Lange, N.A. Lakomek, C. Farès, G.F. Schröder, K.F.A. Walter, S. Becker, J. Meiler, H. Grubmüller, C. Griesinger, B.L. de Groot, Recognition dynamics up to microseconds revealed from an RDC-derived ubiquitin ensemble in solution, *Science* 320 (2008) 1471-1475.

- [168] E.T. Olejniczak, C.M. Dobson, M. Karplus, R.M. Levy, Motional averaging of proton nuclear Overhauser effects in proteins. Predictions from a molecular dynamics simulation of lysozyme, *J. Am. Chem. Soc.* 106 (1984) 1923-1930.
- [169] T.M.G. Koning, R. Boelens, G.A. van der Marel, J.H. van Boom, R. Kaptein, Structure determination of a DNA octamer in solution by NMR spectroscopy. Effect of fast local motions, *Biochemistry* 30 (1991) 3787-3797.
- [170] J.B. Hall, D. Fushman, Characterization of the overall and local dynamics of a protein with intermediate rotational anisotropy: Differentiating between conformational exchange and anisotropic diffusion in the B3 domain of protein G, *J. Biomol. NMR* 27 (2003) 261-275.
- [171] S. Vijay-Kumar, C.E. Bugg, W.J. Cook, Structure of ubiquitin refined at 1.8 Å resolution, *J. Mol. Biol.* 194 (1987) 531-544.
- [172] C.P. Butts, C.R. Jones, E.C. Towers, J.L. Flynn, L. Appleby, N.J. Barron, Interproton distance determination by NOE - surprising accuracy and precision in a rigid organic molecule, *Org. Biomol. Chem.* 9 (2011) 177-184.
- [173] G.B. Young, T.L. James, Determination of molecular structure in solution via two-dimensional nuclear Overhauser effect experiments: Proflavine as a rigid molecule test case, *J. Am. Chem. Soc.* 106 (1984) 7986-7988.
- [174] M.S. Broido, T.L. James, G. Zon, J.W. Keepers, Investigation of the solution structure of a DNA octamer [d(GGAATTCC)]₂ using two-dimensional nuclear Overhauser enhancement spectroscopy, *Eur. J. Biochem.* 150 (1985) 117-128.
- [175] N. Jamin, T.L. James, G. Zon, Two-dimensional nuclear Overhauser enhancement investigation of the solution structure and dynamics of the DNA octamer [d(GGTATACC)]₂, *Eur. J. Biochem.* 152 (1985) 157-166.
- [176] E. Suzuki, N. Pattabiraman, G. Zon, T.L. James, Solution structure of [d(A-T)₅]₂ via complete relaxation matrix analysis of two-dimensional nuclear Overhauser effect spectra and molecular mechanics calculations: Evidence for a hydration tunnel, *Biochemistry* 25 (1986) 6854-6865.
- [177] E.P. Nikonowicz, R.P. Meadows, D.G. Gorenstein, A hybrid complete relaxation matrix structural refinement of an extra-helical adenosine tridecamer d(CGCAGAATTCGCG)₂ from 2D ¹H NMR, *Bull. Magn. Reson.* 11 (1989) 226-229.
- [178] S.W. Fesik, G. Bolis, H.L. Sham, E.T. Olejniczak, Structure refinement of a cyclic peptide from two-dimensional NMR data and molecular modeling, *Biochemistry* 26 (1987) 1851-1859.
- [179] C.D. Schwieters, J.J. Kuszewski, G.M. Clore, Using Xplor-NIH for NMR molecular structure determination, *Prog. Nucl. Magn. Reson. Spectrosc.* 48 (2006) 47-62.
- [180] L.E. Kay, D.A. Torchia, A. Bax, Backbone dynamics of proteins as studied by ¹⁵N inverse detected heteronuclear NMR spectroscopy: Application to staphylococcal nuclease, *Biochemistry* 28 (1989) 8972-8979.
- [181] D. Lee, C. Hilty, G. Wider, K. Wüthrich, Effective rotational correlation times of proteins from NMR relaxation interference, *J. Magn. Reson.* 178 (2006) 72-76.
- [182] O. Jardetzky, On the nature of molecular conformations inferred from high-resolution NMR, *Biochim. Biophys. Acta* 621(1980) 227-232.
- [183] H. Kessler, C. Griesinger, J. Lutz, A. Müller, W.F. van Gunsteren, H.J.C. Berendsen, Conformational dynamics detected by nuclear magnetic resonance NOE values and *J* coupling constants, *J. Am. Chem. Soc.* 110 (1988) 3393-3396.

- [184] U. Schmitz, A. Kumar, T.L. James, Dynamic interpretation of NMR data: Molecular dynamics with weighted time-averaged restraints and ensemble R-factor, *J. Am. Chem. Soc.* 114 (1992) 10654-10656.
- [185] A.E. Torda, R.M. Brunne, T. Huber, H. Kessler, W.F. van Gunsteren, Structure refinement using time-averaged J-coupling constant restraints, *J. Biomol. NMR* 3 (1993) 55-66.
- [186] R. Brüschweiler, M. Blackledge, R.R. Ernst, Multi-conformational peptide dynamics derived from NMR data: A new search algorithm and its application to antamanide, *J. Biomol. NMR* 1 (1991) 3-11.
- [187] A.M.J.J. Bonvin, A.T. Brünger, Conformational variability of solution nuclear magnetic resonance structures, *J. Mol. Biol.* 250 (1995) 80-93.
- [188] A.T. Brünger, G.M. Clore, A.M. Gronenborn, R. Saffrich, M. Nilges, Assessing the quality of solution nuclear magnetic resonance structures by complete cross-validation, *Science* 261 (1993) 328-331.
- [189] A.M.J.J. Bonvin, A.T. Brünger, Do NOE distances contain enough information to assess the relative populations of multi-conformer structures? *J. Biomol. NMR* 7 (1996) 72-76.
- [190] M.S. Friederichs, T.R. Stouch, R.E. Bruccoleri, L. Mueller, K.L. Constantine, Structural and dynamic properties of a β -hairpin-forming linear peptide. 2. ^{13}C NMR relaxation analysis, *J. Am. Chem. Soc.* 117 (1995) 10855-10864.
- [191] A. Donati, C. Rossi, S. Martini, N.B. Ulyanov, T.L. James, NOE intensities from multiple conformations in solution analyzed by the complete relaxation matrix approach, *Appl. Magn. Reson.* 15 (1998) 401-406.
- [192] G.M. Clore, C.D. Schwieters, How much backbone motion in ubiquitin is required to account for dipolar coupling data measured in multiple alignment media as assessed by independent cross-validation? *J. Am. Chem. Soc.* 126 (2004) 2923-2938.
- [193] G.M. Clore, C.D. Schwieters, Amplitudes of protein backbone dynamics and correlated motions in a small α/β protein: Correspondence of dipolar coupling and heteronuclear relaxation measurements, *Biochemistry* 43 (2004) 10678-10691.
- [194] N. Tjandra, A. Bax, Direct measurement of distances and angles in biomolecules by NMR in a dilute liquid crystalline medium, *Science* 278 (1997) 1111-1114.
- [195] G.M. Clore, C.D. Schwieters, Concordance of residual dipolar couplings, backbone order parameters and crystallographic B-factors for a small α/β protein: A unified picture of high probability, fast atomic motions in proteins, *J. Mol. Biol.* 355 (2006) 879-886.
- [196] B. Vögeli, L. Yao, A. Bax, Protein backbone motions viewed by intraresidue and sequential $\text{H}^{\text{N}}-\text{H}^{\alpha}$ residual dipolar couplings, *J. Biomol. NMR* 41 (2008) 17-28.
- [197] B. Vögeli, J.F. Ying, A. Grishaev, A. Bax, Limits on variations in protein backbone dynamics from precise measurements of scalar couplings, *J. Am. Chem. Soc.* 129 (2007) 9377-9385.
- [198] R.B. Fenwick, S. Esteban-Martin, B. Richter, D. Lee, K.F.A. Walter, D. Milovanovic, S. Becker, N.A. Lakomek, C. Griesinger, X. Salvatella, Weak long-range correlated motions in a surface patch of ubiquitin involved in molecular recognition., *J. Am. Chem. Soc.* 133 (2011) 10336-10339.
- [199] P.R.L. Markwick, G. Bouvignies, M. Blackledge, Exploring multiple timescale motions in protein GB3 using accelerated molecular dynamics and NMR spectroscopy, *J. Am. Chem. Soc.* 129 (2007) 4724-4730.
- [200] G. Bouvignies, P. Bernado, S. Meier, K. Cho, S. Grzesiek, R. Brüschweiler, M. Blackledge, Identification of slow correlated motions in proteins using residual dipolar

- and hydrogen-bond scalar couplings, *Proc. Natl. Acad. Sci. USA* 102 (2005) 13885-13890.
- [201] P.R.L. Markwick, S.A. Showalter, G. Bouvignies, R. Brüschweiler, M. Blackledge, Structural dynamics of protein backbone ϕ angles: Extended molecular dynamics simulations versus experimental 3J scalar couplings, *J. Biomol. NMR* 45 (2009) 17-21.
- [202] T. Li, Q. Jing, L. Yao, Dynamics of the GB3 loop regions from MD simulation: How much of it is real? *J. Phys. Chem. B* 115 (2011) 3488-3495.
- [203] B. Zagrovic, W.F. van Gunsteren, Comparing atomistic simulation data with the NMR experiment: How much can NOEs actually tell us? *Proteins Struct. Func. Genet.* 63 (2006) 210-218.
- [204] R. Bürge, J. Pitera, W.F. van Gunsteren, Assessing the effect of conformational averaging on the measured values of observables, *J. Biomol. NMR* 19 (2001) 305-320.
- [205] P. Güntert, C. Mumenthaler, K. Wüthrich, Torsion angle dynamics for NMR structure calculation with the new program DYANA, *J. Mol. Biol.* 273 (1997) 283-298.
- [206] P. Güntert, Automated NMR protein structure calculation, *Prog. Nucl. Magn. Reson. Spectrosc.* 43 (2003) 105-125.
- [207] P. Güntert, Automated structure determination from NMR spectra, *Eur. Biophys. J.* 38 (2009) 129-143.
- [208] J.P. Derrick, D.B. Wigley, The third IgG-binding domain from streptococcal protein G. An analysis by X-ray crystallography of the structure alone and in a complex with Fab, *J. Mol. Biol.* 243 (1994) 906-918.
- [209] A.K. Suri, R.M. Levy, A relaxation-matrix analysis of distance-constraint ranges for NOEs in proteins at long mixing times, *J. Magn. Reson. B* 106 (1995) 24-31.
- [210] R. Sounier, L. Blanchard, Z. Wu, J. Boisbouvier, High-accuracy distance measurement between remote methyls in specifically protonated proteins. *J. Am. Chem. Soc.* 129 (2007) 472-473.
- [211] R. Horst, G. Wider, J. Fiaux, E.B. Bertelson, A.L. Horwich, K. Wüthrich, Proton-proton Overhauser NMR spectroscopy with polypeptide chains in large structures, *Proc. Natl. Acad. Sci. U. S. A.* 103 (2006) 15445-15450.
- [212] L.E. Kay, G.M. Clore, A. Bax, A.M. Gronenborn, Four-dimensional heteronuclear triple resonance NMR spectroscopy of interleukin-1 β in solution, *Science* 249 (1990) 411-414.
- [213] J. Ying, J.H. Chill, J.M. Louis, A. Bax, Mixed-time parallel evolution in multiple quantum NMR experiments: Sensitivity and resolution enhancement in heteronuclear NMR, *J. Biomol. NMR* 37 (2007) 195-204.
- [214] V. Tugarinov, L.E. Kay, I. Ibraghimov, V.Y. Orekhov, High-resolution four-dimensional ^1H - ^{13}C NOE spectroscopy using methyl-TROSY, sparse data acquisition, and multidimensional decomposition, *J. Am. Chem. Soc.* 127 (2005) 2767-2775.
- [215] M.J. Bostock, D.J. Holland, D. Nietlispach, Compressed sensing reconstruction of undersampled 3D NOESY spectra: Application to large membrane proteins, *J. Biomol. NMR* 54 (2012) 15-32.
- [216] P. Schmieder, A.S. Stern, G. Wagner, J.C. Hoch, Improved resolution in triple-resonance spectra by nonlinear sampling in the constant-time domain, *J. Biomol. NMR* 4 (1994) 483-490.
- [217] V.Y. Orekhov, I.V. Ibraghimov, M. Billeter, MUNIN: a new approach to multi-dimensional NMR spectra interpretation, *J. Biomol. NMR* 20 (2001) 49-60.

- [218] S. Hiller, I.V. Ibraghimov, G. Wagner, V.Y. Orekhov, Coupled decomposition of four-dimensional NOESY spectra, *J. Am. Chem. Soc.* 131 (2009) 12970-12978.
- [219] B.E. Coggins, J.W. Werner-Allen, A. Yan, P.Zhou, Rapid protein global fold determination using ultrasparse sampling, high-dynamic range artifact suppression, and time-shared NOESY, *J. Am. Chem. Soc.* DOI: 10.1021/ja307445y.
- [220] E. Kupce, R. Freeman, Projection-reconstruction of three-dimensional NMR spectra, *J. Am. Chem. Soc.* 125 (2003) 13958-13959.
- [221] V. Galius, C. Leontiou, T. Richmond, G. Wider, Projected [$^1\text{H},^{15}\text{N}$]-HMQC- ^1H -NOESY for large molecular systems: Application to a 121 kDa protein-DNA complex, *J. Biomol. NMR* 40 (2008) 175-181.
- [222] S. Hiller, F. Fiorito, K. Wüthrich, G. Wider, Automated projected spectroscopy (APSY), *Proc. Natl. Acad. Sci. USA* 102 (2005) 10876-10881.
- [223] F.A. Kovacs, D.J. Fowler, G.J. Gallagher, L.K. Thompson, A practical guide for solid-state NMR distance measurements in proteins, *Concept. Magn. Reson. A* 30 (2007) 21-39.
- [224] K. Takegoshi, S. Nakamura, T. Terao, ^{13}C - ^1H dipolar-assisted rotational resonance in magic-angle spinning NMR, *Chem. Phys. Lett.* 344 (2001) 631-637.
- [225] A. Lange, S. Luca, M. Baldus, Structural constraints from proton-mediated rare-spin correlation spectroscopy in rotating solids, *J. Am. Chem. Soc.* 124 (2002) 9704-9705.
- [226] M. Veshtort, R.G. Griffin, Proton-driven spin diffusion in rotating solids via reversible and irreversible quantum dynamics, *J. Chem. Phys.* 135 (2011) 134509.
- [227] W. Rieping, M. Habeck, M. Nilges, Inferential structure determination, *Science* 309 (2005) 303-306.
- [228] S. Olsson, J. Frellsen, W. Boomsma, K. V. Mardia, T. Hamelryck, Inference of protein structure ensembles from sparse, averaged data, *submitted*.
- [229] R.W. Behling, S.N. Rao, P.K. Kollman, D.R. Kearns, Molecular mechanics and dynamics calculations on $(\text{dA})_{10}(\text{dT})_{10}$ incorporating distance constraints derived from NMR relaxation measurements, *Biochemistry* 26 (1987) 4674-4681.
- [230] A. Cooper, D.T.F. Dryden, Allostery without conformational change – A plausible model, *Eur. Biophys. J. Biophys. Lett.* 11 (1984) 103-109.
- [231] K. Gunasekaran, B. Ma, R. Nussinov, Is allostery an intrinsic property of all dynamic proteins? *PROTEINS: Struc. Func. Bioinf.* 57 (2004) 433-443.
- [232] C.J. Tsai, A. del Sol, R. Nussinov, Allostery: Absence of a change in shape does not imply that allostery is not at play, *J. Mol. Biol.* 378 (2008) 1-11.
- [233] C.J. Tsai, A. del Sol, R. Nussinov, Protein allostery, signal transmission and dynamics: A classification scheme of allosteric mechanisms, *Mol. Biosyst.* 5 (2009) 207-216.
- [A1] M. Goldman, Interference effects in the relaxation of a pair of unlike spin-1/2 nuclei, *J. Magn. Reson.* 15 (1998) 401-406.
- [A2] P.S. Hubbard, Some properties of correlation functions of irreducible tensor operators, *Phys. Rev.* 180 (1969) 319-326.
- [A3] M. Goldman, Quantum description of high-resolution NMR in liquids. Clarendon Press, Oxford, 1988.

8. Curriculum vitae

Beat Rolf Vögeli

born on May 13 1976

Swiss

married, two sons

Education

Ph. D. in Natural Sciences (Dr. sc. nat.) at the Institut für Physikalische Chemie, ETH Zürich (Swiss Federal Institute of Technology), 2005

Diploma in Physics (Dipl. phys. ETH) at ETH Zürich (Biophysics and Particle Physics), 2001

Employment

Oberassistent (Senior Researcher)

Institut für Physikalische Chemie, ETH Zürich, Switzerland, in the research group of Prof. Roland Riek, 2011-present

Postdoctoral Researcher

Institut für Physikalische Chemie, ETH Zürich, Switzerland, in the research group of Prof. Roland Riek, 2008-2011

Laboratory of Chemical Physics, National Institute of Diabetes, Digestive & Kidney Diseases (NIDDK) of the National Institutes of Health (NIH), Bethesda, Maryland, USA, in the research group of Dr. Ad Bax, 2005-2008

Research Fellow

Institut für Physikalische Chemie, ETH Zürich, Switzerland, in the research group of Prof. Konstantin Pervushin, 2001-2005

Institute of Molecular Biology and Biophysics, ETH Zürich, Switzerland, in the research group of Prof. Kurt Wüthrich, 2000-2001

Teaching

Lectures

Second in charge, script revision, physical chemistry for biologists and pharmacists, ETH Zürich, 2010-2013

Laboratory Supervising

Supervisor of Ph.D. thesis, ETH Zürich, own funding from 2013 on; semester thesis, ETH Zürich, 2009; bachelor thesis, ETH Zürich, 2012

Practical Courses

NMR Praktikum (part physical chemistry), ETH Zürich, 2010

Praktikum Allgemeine Chemie (part physical chemistry), ETH Zürich, 2009-2010

Exercise Assistant

Head of exercise assistants, Physical chemistry for biologists and pharmacists, ETH Zürich, 2011-2012

Magnetic resonance (physical chemistry IV), ETH Zürich, 2011-2012

Physical chemistry for biologists and pharmacists, ETH Zürich, 2009-2010, 2012

Advanced techniques in solution state NMR of biomolecules, ETH Zürich, 2005

Physical chemistry for biologists, chemists and pharmacists, ETH Zürich, 2001-2005

Publications

* equal contributions

** corresponding author

32. Beat Vögeli**, *Full Relaxation Matrix Analysis of Apparent Cross-Correlated Relaxation Rates in Four-Spin Systems*, 2013, **J. Magn. Reson.**, 226, 52-63.
31. Beat Vögeli**, Julien Orts, Dean Strotz, Peter Güntert, and Roland Riek, *Discrete Three-Dimensional Representation of Macromolecular Motion from eNOE-Based Ensemble Calculation*, 2012, **Chimia**, 66, 787-790.
30. Beat Vögeli, Peter Güntert, and Roland Riek, *Multiple-State Ensemble Structure Determination from eNOE Spectroscopy*, 2013, **Mol. Phys.**, 111, 437-454.
29. Beat Vögeli, Sina Kazemi, Peter Güntert, and Roland Riek, *Spatial Elucidation of Motions in Proteins by Ensemble-based Structure Calculation Using Exact NOEs*, 2012, **Nat. Struct. Mol. Biol.**, 19, 1053-1057.
28. Julien Orts, Beat Vögeli, and Roland Riek, *Relaxation Matrix Analysis of Spin Diffusion for the NMR Structure Calculation with eNOEs*, 2012, **J. Chem. Theory Comput.**, 8, 3483-3492.
27. Beat Vögeli**, *How Uniform is the Peptide Plane Geometry? A High-Accuracy NMR Study of Dipolar C^α - C'/H^N - N Cross-Correlated Relaxation*, 2011, **J. Biomol. NMR**, 50, 315-329.
26. Dominik Leitz, Beat Vögeli, Jason Greenwald, and Roland Riek, *Temperature Dependence of $^1H^N$ - $^1H^N$ Distances in Ubiquitin as studied by exact Measurements of NOEs*, 2011, **J. Phys. Chem. B**, 115, 7648-7660.
25. Beat Vögeli**, *Comprehensive Description of NMR Cross-Correlated Relaxation under Anisotropic Molecular Tumbling and Correlated Local Dynamics on All Timescales*, 2010, **J. Chem. Phys.** 133, 014501.
Selected for the **Virt. J. Biol. Phys. Res.**, 2010, 20:1.
24. Beat Vögeli, Michael Friedmann, Dominik Leitz, Alexander Sobol, and Roland Riek, *Quantitative Determination of NOE Rates in Perdeuterated and Protonated Proteins: Practical and Theoretical Aspects*, 2010, **J. Magn. Reson.**, 204, 290-302.
23. Beat Vögeli** and Roland Riek, *Side Chain-Backbone Projections in Aromatic and ASX Residues from NMR Cross-Correlated Relaxation*, 2010, **J. Biomol. NMR**, 46, 135-147.
22. Beat Vögeli, Takuya Segawa, Dominik Leitz, Alexander Sobol, Alexandra Choutko, Daniel Trzesniak, Wilfred Van Gunsteren and Roland Riek, *Exact Distances and Internal Dynamics of Perdeuterated Ubiquitin from NOE Buildups*, 2009, **J. Am. Chem. Soc.**, 131, 17215-17225.
21. Beat Vögeli** and Lishan Yao, *Correlated Dynamics between Protein HN and HC Bonds Observed by NMR Cross Relaxation*, 2009, **J. Am. Chem. Soc.**, 131, 3668-3678.

20. Lishan Yao, Beat Vögeli, Jinfay Ying and Ad Bax, *NMR Determination of Amide N-H Equilibrium Bond Length from Concerted Dipolar Coupling Measurements*, 2008, **J. Am. Chem. Soc.**, 130, 16518-20.
19. Beat Vögeli, Lishan Yao and Ad Bax, *Protein Backbone Motion Viewed by Intraresidue and Sequential H^N - H^α Residual Dipolar Couplings*, 2008, **J. Biomol. NMR**, 41, 17-28.
18. Lishan Yao, Beat Vögeli, Dennis Torchia and Ad Bax, *Simultaneous NMR Study of Protein Structure and Dynamics Using Conservative Mutagenesis*, 2008, **J. Phys. Chem.**, 121, 6045-6056.
17. Konstantin Pervushin, Katherina Vamvaca*, Beat Vögeli* and Donald Hilvert, *Structure and Dynamics of an Enzymatically Active Molten Globule*, 2007, **Nat. Struct. Mol. Biol.**, 14, 1202-1206.
16. Beat Vögeli, Jinfay Ying, Alexander Grishaev, and Ad Bax, *Limits on Variations in Protein Backbone Dynamics from Precise Measurements of Scalar Couplings*, 2007, **J. Am. Chem. Soc.**, 129, 9377-9385.
15. Kaifeng Hu, Beat Vögeli and G. Marius Clore, *Spin-State Selective Carbon-Detected HNC0 with TROSY Optimization in All Dimensions and Double Echo-Antiecho Sensitivity Enhancement in Both Indirect Dimensions*, 2007, **J. Am. Chem. Soc.**, 129, 5484-5491.
14. Kaifeng Hu*, Beat Vögeli* and G. Marius Clore, *^{13}C -Detected HN(CA)C and HMCNC Experiments Using a Single Methyl-Reprotonated Sample for Unambiguous Methyl Resonance Assignment*, 2006, **J. Biomol. NMR**, 36, 259-266.
13. Kaifeng Hu*, Beat Vögeli* and G. Marius Clore, *Interference between Transverse Cross-Correlated Relaxation and Longitudinal Relaxation Affects Apparent J-Coupling and Transverse Cross-Correlated Relaxation*, 2006, **Chem. Phys. Lett.**, 423, 123-125.
12. Donghan Lee, Beat Vögeli and Konstantin Pervushin, *Detection of C' , C^α Correlations in Proteins Using a New Time- and Sensitivity-Optimal Experiment*, 2005, **J. Biomol. NMR**, 31, 273-278.
11. Beat Vögeli, Konstantin Pervushin (Supervisor), *Towards Structure and Dynamics of Large and Dynamically Disordered Biomacromolecules: New Methods in Solution NMR Spectroscopy*, 2005, **Ph.D. Thesis ETH Zürich**, Diss. ETH No. 15993, <http://e-collection.ethbib.ethz.ch/show?type=diss&nr=15993>.
10. Kaifeng Hu, Beat Vögeli and Konstantin Pervushin, *Side-Chain H and C Resonance Assignment in Protonated / Partially Deuterated Proteins Using a New 3D ^{13}C -Detected HCC-TOCSY*, 2005, **J. Magn. Reson.**, 174, 200-208.
9. Beat Vögeli, Helena Kovacs and Konstantin Pervushin, *Simultaneous ^1H - or ^2H -, ^{15}N - and Multiple-Band-Selective ^{13}C -Decoupling during Acquisition in ^{13}C -Detected Experiments with Proteins and Oligonucleotides*, 2005, **J. Biomol. NMR**, 31, 1-9.

8. Konstantin Pervushin, Beat Vögeli, Tim Heinz and Philippe Hünenberger, *Measuring ^1H - ^1H and ^1H - ^{13}C RDCs in Methyl Groups: Example of Pulse Sequences with Numerically Optimized Coherence Transfer Schemes*, 2005, **J. Magn. Reson.**, 172, 36-47.
7. Katherina Vamvaca, Beat Vögeli, Peter Kast, Konstantin Pervushin and Donald Hilvert, *An Enzymatic Molten Globule: Efficient Coupling of Folding and Catalysis*, 2004, **Proc. Natl. Acad. Sci. USA**, 101, 12860-12864.

Selected for Editors' Choice: Highlights of the Recent Literature, Biochemistry: *One Size Fits Many*, 2004, **Science**, 305, 5691-5691.
6. Katherina Vamvaca, Beat Vögeli, Peter Kast, Konstantin Pervushin and Donald Hilvert, *Enzymatic Catalysis: Taking "Induced Fit" to Extremes*, 2004, **Protein Sci.**, 13, 106-106 Suppl. 1, Meeting Abstract 170.
5. Beat Vögeli, Helena Kovacs and Konstantin Pervushin, *Measurements of Side-Chain ^{13}C - ^{13}C Residual Dipolar Couplings in Uniformly Deuterated Proteins*, 2004, **J. Am. Chem. Soc.**, 126, 2414-2420.
4. Konstantin Pervushin and Beat Vögeli, *Observation of Individual Transitions in Magnetically Equivalent Spin Systems*, 2003, **J. Am. Chem. Soc.**, 125, 9566-9567.
3. Beat Vögeli and Konstantin Pervushin, *TROSY Experiment for Refinement of Backbone ψ and ϕ by Simultaneous Measurements of Cross-Correlated Relaxation Rates and $^{3,4}J_{\text{H}\alpha\text{HN}}$ Coupling Constants*, 2002, **J. Biomol. NMR**, 24, 291-300.
2. Konstantin Pervushin, Beat Vögeli and Alexander Eletsy, *Longitudinal ^1H Relaxation Optimization in TROSY NMR Spectroscopy*, 2002, **J. Am. Chem. Soc.**, 124, 12898-12902.
1. Beat Vögeli, Roland Riek (Supervisor) and Kurt Wüthrich (Supervisor), *NMR Solution Structure of the Fragments of the Human Prion Protein hPrP(121-226) and hPrP(130-230)*, 2001, **Diploma Thesis**, ETH Zürich.

Project Grants

Project funding by the Swiss National Science Foundation, "NMR Methodology for Description of Motional Networks in Proteins", 3 years, 220'000 Swiss Fr. (ca. 250'000 US\$), 2012

Awards and Fellowships

Visiting Fellow Award by the National Institutes of Health, U.S.A., 2007

Visiting Fellow Award by the National Institutes of Health, U.S.A., 2006

Competitive Fellowship by the Swiss National Science Foundation, 2005

Service

Peer review for Journal of Biomolecular NMR

Peer review for Journal of Magnetic Resonance

Peer review for Journal of Physical Chemistry

Talks

54th ENC Experimental Nuclear Magnetic Resonance Conference, Asilomar Conference Center, Pacific Grove, CA, USA, 2013 to be given

Department of Molecular Pharmacology, Physiology & Biotechnology (MPPB), Brown University, Providence, RI, USA, 2012

Indo-Swiss Symposium on Recent Trends in NMR of Biomolecules and Advanced Materials, National Chemical Laboratory, Pune, India, 2012

Colloquium of the Institut für Physikalische Chemie, ETH Zürich, Switzerland, 2012

Institute of Molecular Biology and Biophysics, ETH Zürich, Switzerland, 2010

Helmholtz Centre for Infection Research, Braunschweig, Germany, 2010

18th Swiss NMR Symposium, Geneva, Switzerland, 2009

Schweizerische NMR Benutzertagung, Basel, Switzerland, 2009

Physikalisch-Chemisches Institut, Universität Zürich, Switzerland, 2008

Institut für Physikalische Chemie, ETH Zürich, Switzerland, 2007

Group representative for evaluation committee, ETH Zürich, Switzerland, 2004

Colloquium of the Institut für Physikalische Chemie, ETH Zürich, Switzerland, 2004

Lecture Summer School Otocec, Slovenia, 2003

EENC European Experimental Nuclear Magnetic Resonance Conference, Prague, Czech Republic, 2002